

QATAR UNIVERSITY

COLLEGE OF ARTS AND SCIENCES

ENHANCING THE FOULING RESISTANCE AND  
REJECTION OF CELLULOSE ACETATE [CA] /MXENE  
[ $Ti_3C_2Tx$ ] NANOCOMPOSITE MEMBRANES

BY

REEM SAMIR BASHIR AZAM

A Thesis Submitted to  
the College of Arts and Sciences  
in Partial Fulfillment of the Requirements for the Degree of  
Masters of Science in Material Science and Technology

January 2021

© 2021 REEM SAMIR AZAM. All Rights Reserved.

## COMMITTEE PAGE

The members of the Committee approve the Thesis of  
Reem Azam defended on 28/11/2020.

---

Dr. Ahmed Abdelfattah Elzatahry  
Thesis/Dissertation Supervisor

---

Dr. Khaled Mahmoud  
Co-Supervisor

---

Dr. Khaled Youssef  
Committee Member

---

Dr. Mohamed Hassan  
Committee Member

Approved:

---

Ibrahim AlKaabi, Dean, College of Arts and Sciences

## ABSTRACT

AZAM, REEM,S., Masters : January : [2021], Material Science and Technology

Title: Enhancing the Fouling Resistance and Rejection of Cellulose Acetate [CA]/MXene [ $Ti_3C_2Tx$ ] Nanocomposite Membranes

Supervisor of Thesis: Ahmed Elzatahry.

Obstacles in the membrane-based separation field are mainly related to membrane fouling. This study synthesized a pioneering covalently crosslinked cellulose acetate anti-fouling mixed matrix membrane containing between 0 wt.% and 12 wt.% MXene (CCAM-0% to CCAM-12%) via the phase inversion process prior to formaldehyde crosslinking for ultrafiltration/nanofiltration membrane applications. The membranes' water flux and salt, dye, and protein rejection performances were tested using DE filtration and CF filtration. The physiochemical properties of the fabricated membranes were tested using various characterization tools, including SEM, EDS, XRD, TGA, AFM, BET, and water contact angle techniques. The fabricated membranes, especially CCAM-10%, showed excellent hydrophilicity (with a contact angle of  $48.06^\circ$ ), good surface roughness (with  $R_a=47.4$  nm and  $R_q=60.2$  nm), offering admirable permeation flux, a high surface area ( $124.3$  m<sup>2</sup>/g), good thermal stability, with an enhanced decomposition temperature reaching  $\sim 310^\circ\text{C}$ , and high water uptake (125.3%) and porosity (72.35%). The average pore diameter and molecular weight cut-off of the CCAM-10% were  $\sim 1.73$  nm and 435 Dalton, respectively.

The fabricated membranes' performances were also evaluated based on the fouling resistance ratios and separation performance, including the water flux and rejection rate. The CCAM-10% had the highest pure water flux of  $522.25$  L m<sup>2</sup> bar<sup>-1</sup> h

<sup>-1</sup> due to a CF tangential flow that had a shearing impact on the surface of the membrane, thereby inhibiting cake buildup on the membrane surface. In contrast, the DE filtration configuration endured more stress.

The CCAM-10% exhibited a more than 85% rejection of methyl green and a ~96.6% rejection of BSA as well as the highest hydrophilicity, leading to increased fouling resistance performance. During the antifouling evaluation, the novel CCAM-10% showed the highest flux recovery ratio of 67.3% and the lowest irreversible fouling ratio of 32.7%. These are excellent fouling resistance ratios, evidencing the good antifouling property of the membrane. In particular, the low irreversible fouling resistance ratio ( $R_{ir}$ ) of 32.7% showed that the fouling was caused by the elimination of BSA on the membrane surface, further underscoring the good antifouling performance. Hence, based on its excellent physicochemical properties as well as its separation and fouling resistance performance, CCAM-10% is highly recommended for ultrafiltration water purification applications.

## DEDICATION

*“This thesis is dedicated to my darling parents, husband, and beloved friends, who provided me with continuous care, support, and motivation during the two years of my master’s study. The achievement of this thesis would not have been probable without their prayers and patience”.*

## ACKNOWLEDGMENTS

I owe my gratitude to Prof. Ahmed El Zatahry, my co-supervisor, Dr. Khaled Mahmoud, and Dr. Mohamed Hassan for their guidance and assistance during the master's thesis education. Their feedback was consistently helpful and filled the gaps in my thesis to achieve the level it has.

I have a special thanks for my co-supervisor Dr. Khaled Mahmoud who initiated the work of this thesis and paved the path for me to work with Qatar Environment and Energy Research Institute (QEERI) and their water and air quality team. They provided continuous assistance finding necessary information and gave valuable comments on the project outputs.

Also, I would like to thank Dr. Alaa Al Hawari, Radwan Alfahel and MhdAmmar Hafiz from Department of Civil and Architectural Engineering from Qatar University for enabling me to perform my study using advanced lab facilities.

Last but most importantly, I must thank my parents, my husband and loved ones supporting me in completing my master's degree and encouraging me to stay focused and provide emotional support at crucial times.

## TABLE OF CONTENTS

DEDICATION .....	V
ACKNOWLEDGMENTS .....	VI
LIST OF TABLES .....	XI
LIST OF FIGURES .....	XII
LIST OF ABBREVIATION .....	XVIII
LIST OF ABBREVIATION .....	XIX
CHAPTER 1: INTRODUCTION AND LITERATURE REVIEW .....	1
1.1 Thesis Outline .....	1
1.2 Thesis Main Objectives .....	2
1.3 Desalination and Wastewater Treatment Technologies .....	3
1.3.1 Membrane Material Selections .....	9
1.3.2 Membrane Fabrication Method .....	14
1.4 Mixed Matrix Membranes .....	15
1.5 CA MMMs .....	16
1.6 Membrane Modification .....	21
<i>MXene Structures</i> .....	26
1.6.1 <i>MXenes' Unique Combination of Properties</i> .....	28
1.6.2 <i>MXene Membrane Applications</i> .....	28
1.7 Membranes' Chemical Crosslinking .....	42

1.8	MXene Composite Membranes and Their Fabrication Techniques.....	43
1.9	A Gap in The Literature .....	46
CHAPTER 2: MATERIALS AND METHODOLOGY .....		49
2.1	Materials.....	49
2.2	Equipment .....	49
2.3	Methods.....	50
2.3.1	Preparation of Delaminated MXene .....	50
2.3.2	Preparation of The Chemically Crosslinked MXene At CA Mixed Matrix Nanoporous Membrane .....	51
2.4	Material and Membrane Characterization.....	56
2.4.1	<i>Fourier-Transform Infrared (FTIR)</i> .....	56
2.4.2	<i>Scanning Electron Microscopy</i> .....	57
2.4.3	<i>Energy-Dispersive X-ray Spectroscopy</i> .....	59
2.4.4	<i>X-ray Diffractometry</i> .....	61
2.4.5	<i>Zeta Potential Analysis</i> .....	63
2.4.6	<i>Brunauer-Emmett-Teller (BET) Accelerated Surface Area and Porosimeter Analysis ASAP 2420</i> .....	64
2.4.7	<i>Water Contact Angle Analysis</i> .....	65
2.4.8	<i>Atomic Force Microscope (AFM)</i> .....	67
2.4.9	<i>Thermogravimetric Analysis</i> .....	68



2.4.10	<i>Differential Scanning Calorimetry</i> .....	69
2.5	Dead-end and Crossflow Filtration .....	70
2.5.1	<i>Water Uptake and Membrane Porosity Studies</i> .....	73
2.5.2	<i>Membrane Flux, Rejection Rate, Pore Radius Measurements, and MWCO</i>	74
2.5.3	<i>Antifouling Performance Evaluation</i> .....	75
CHAPTER 3: RESULTS AND DISCUSSION.....		77
3.1	Structural Characterization and Surface Morphology of Chemically Cross-linked MXene At CA Mixed Matrix Nanoporous Membranes.....	77
3.2	Contact Angle Measurements and Surface Topology of MXene At CA MMMs	86
3.3	Membrane Thermal Stability .....	90
3.4	Membrane Water Uptake, Porosity, MWCO, and BET Analysis.....	91
3.5	Membrane Separation Performance .....	94
3.6	Impact of Operating Conditions on The Separation Performance .....	100
3.7	Membrane Antifouling Performance Evaluation .....	103
CHAPTER 4: CONCLUSIONS AND RECOMMENDATIONS.....		106
REFERENCES .....		110
APPENDIXES .....		156
Appendix A: Poster Awards and Presentation .....		156
A.	A snapshot of the poster award is shown below.....	156

.....	157
Appendix B: Research Outcomes (Publications) .....	158
A. A snapshot of the first page of the first published paper is shown below. ....	158
B. A snapshot of the first page of the second published paper is shown below.	159

## LIST OF TABLES

Table 1. Summary of membrane types based on filtration class; extracted from Ref [11] .....	4
Table 2. Summary of reported data for NF CA membranes with various additives listed with their values of flux, salt rejection and membrane porosity.....	18
Table 3. Separation performance of stated CA, MXene and GO membranes; adapted from [6] .....	24
Table 4. MMM filler types, polymer types, fabrication methods used, and the filler advantages; adapted from Ref [11] .....	44
Table 5. Surface roughness parameters of CCAM-0% and CCAM-10%. .....	89
Table 6. BET surface area, mean pore diameter, and pore volume of CCAM-0%, and CCAM-10%. .....	93

## LIST OF FIGURES

Figure 1. Filtration bands of MF, UF, NF and RO. Sourced from Ref [3].	4
Figure 2. Schematic representation of the transportation of various molecules in 2D NF (silver/MXene nanosheets) membrane between the layers. Adapted from [5].	13
Figure 3. Fundamental parameters for membrane selection; extracted from Ref [97]	16
Figure 4. Process flow representation of the $Ti_3AlC_2$ exfoliation process. (a) Assembly of $Ti_3AlC_2$ ; (b) exchange process between the hydroxyl (OH) group and the aluminum atoms after the acid etching process; (c) delamination process through sonication of ML-MXene, which leads to detached nanosheets and results in hydrogen bond breakage [146].	27
Figure 5. Principal components of the MAX phase and MXenes, including their intercalation ions. The elements in the blue boxes exhibit reports exclusively in the MAX phase and have not been produced in MXenes. The elements in the red boxes are the A element of the MAX phase and can be selectively etched to make MXenes. Yellow boxes represents cations that have been implanted in MXenes to date. Retrieved from [4]	27
Figure 6. MXene ( $Ti_3C_2T_x$ ) and 21%Ag@MXene membrane performances, including filtration of RhB, MG and BSA species at ambient temperature. (a) Membrane water flux, and (b) membrane rejection rate. Retrieved from [5].	30
Figure 7. PVDF (control membrane), MXene ( $Ti_3C_2T_x$ ), and 21%Ag@MXene membrane antibacterial activities. (a) Photos of bacteria ( <i>E. coli</i> ) cells growing at 35°C . (b) Values for the cell viability of <i>E. coli</i> . Retrieved from [5].	31
Figure 8. FT-IR spectra fo: (i) DL-MXene, (ii) CA and (iii) CCAM-10%; retrieved	

from [6] .....	36
Figure 9. (a) Pure water flux of non-crosslinked and crosslinked membranes; (b) rejection performance rate of the fabricated CCAM-10%; (c) rejection performance comparison among CAM-0%, CCAM-0% , CAM-10%, and CCAM-10% for various salts, different dyes and proteins; (d) rejection performance comparison among CAM-0%, CCAM-0%, CAM-10%, and CCAM-10% for various dyes and proteins; retrieved from [6]. .....	37
Figure 10. Zeta potential values of CAM, CCAM, CCAM-10% at pH 7; retrieved from [6].....	38
Figure 11. The effect of membrane thickness on the water flux and Na <sub>2</sub> SO <sub>4</sub> rejection (CCAM-10%). Aqueous solution of Na <sub>2</sub> SO <sub>4</sub> (2000 ppm) were used as feed; retrieved from [6]. .....	38
Figure 12. Impact of crosslinking duration on the pure water flux of CCAM, CCAM-2%, CCAM-4%, CCAM-6%,CCAM-8% and CCAM-10% composite membranes; retrieved from [6]......	39
Figure 13. Crosslinking time impacts on the rejection performance of different MXene@CA hybrid membranes crosslinked for 30, 60, 90, and 120 min. Aqueous solution of Na <sub>2</sub> SO <sub>4</sub> (2000 ppm) was used as feed; retrieved from [6]. .....	39
Figure 14. Durability and flux recovery test of the 10%MXene@CA membrane during three cycles filtration of RhB (0.1g/L) solution at pressure of 1 bar; retrieved from [6]. .....	40
Figure 15. The oxidative stability of the fabricated mixed matrix membranes after curing in NaOCl (0.1%) aqueous solution at temperature of 70 <sup>0</sup> C with various intervals (0–70 h); retrieved from [6]. .....	40

Figure 16. Antibacterial activity of prepared membranes (CCAM-0-10%): (a) Pictures of bacterial (*E. coli* and *B. subtilis*) growth on various CCAM-X% membranes incubated for 24 h at temperature of 35°C. (b) Bacterial cell viability amounts of *E. coli* and *B. subtilis* on various prepared membranes after 24 h. ....41

Figure 17. DL-MXene preparation procedures: 1) Acid (LiF/HCL) etching of aluminium layer from MAX ( $Ti_3AlC_2$ ) using a Teflon bottle for 24hr. 2) Centrifugation. 3) Washing with DI water. 4) Measuring the pH value using a voltmeter. 5) Neutral supernatant with pH ~6 is collected in an empty bottle. 6) The frozen bottle is kept in a freeze-drier. 7) Ultrasonication process of the ML-MXene to produce DL-MXene. 8) VAF of DL-MXene solution in PVDF filter paper. 8) the PVDF filter paper with a MXene layer.....53

Figure 18. Preparation of the MXene at CA solution and membrane casting procedure: 10) Dried DL-MXene sheet is collected from the oven. 11) The sheet is crushed into a powder and the weight of the DL-MXene is measured. 12) Bath sonication to dissolve the MXene content into the solution and obtain a homogenous mixture. 13) Homogenous membrane solution. 14) The membrane in solution is kept for stirring for 24 hours. 15) The mixture is covered with foil and a small hole is made on the top of the glass to allow for degassing. 16) Degassing the mixture using a vacuum desiccator attached to a pump. 17) The viscous membrane solution is poured onto a glass plate. 18) By using a Casting Knife Film Applicator (Elcometer 3580) and a Labcoat Master casting system (PHILOS, Gyeonggi-do, Korea), a thin film is formed on a clean glass plate with a thickness of 280  $\mu m$ . 19) The thin-film membranes are kept drying for half an hour at room temperature. ....54

Figure 19. 20) The casted thin film membranes are submerged in a cold DI water (~15

°C) coagulation bath for 2 h. 21) The membranes are splashed with DI water several times and kept in glass containers. 22) CH<sub>2</sub>O crosslinking 23) The prepared membranes are dried using a glass plate inside an oven at 30 °C for 24 h prior to physicochemical characterization. ....55

Figure 20. Schematic representation of the phase inversion of MXene at cellulose acetate membrane.....55

Figure 21. Nicolet™ iS50 FTIR Spectrometer .....57

Figure 22. Schematic representation of SEM; adapted from Ref [282]. .....60

Figure 23. FEI Quanta 650 FEG SEM instrument with a Bruker Flat Quad 5060F energy dispersive X-ray detector (EDS). ....60

Figure 24. Bruker D8 Advance: Powder X-ray Diffractometer (XRD) .....62

Figure 25. Diffraction schismatic in solid crystals as stated by Bragg’s law for constructive interference; adapted from Ref [285]. .....62

Figure 26. SurPASS Electro Kinetic Analyzer (Anton Paar KG, Austria).....63

Figure 27. Micromeritics ASAP® 2420 Accelerated Surface Area and Porosimetry System.....65

Figure 28. KRUSS Drop Shape Analyzer DSA25 equipped with a camera and photo analysis system.....66

Figure 29. Asylum Research MFP-3D Origin+ Atomic Force Microscope .....67

Figure 30. Thermogravimetric analyzer (TGA 4000 – Perkin Elmer) .....69

Figure 31. Differential scanning calorimetry: (DSC 8500 - Perkin Elmer).....70

Figure 32. Dead-end filtration process setup. ....72

Figure 33. Cross flow filtration process setup. ....72

Figure 34. Schematic representation of (a) the dead-end filtration principle and (b) the

CF principle; taken from Ref [291]. .....	73
Figure 35. (a) SEM image of the ML-MXene surface morphology; (b) XRD ML-MXene spectrum; (c) SEM image of the DL-MXene surface morphology; and (d) XRD DL-MXene spectrum .....	79
Figure 36. XRD model of CA, DL-Ti <sub>3</sub> C <sub>2</sub> Tx and CCAM-10% .....	79
Figure 37. FT-IR spectra for the CCAM-10% membrane .....	81
Figure 38. SEM pictures of the prepared membranes: (a) Surface CCAM-0% showing a dense structure; (b) surface CCAM-2%; (c) surface CCAM-8%; (d) surface CCAM-10% presenting a reduction in pore size after introducing MXene into the CA matrix; (e) cross-section of CCAM-0% displaying a dense structure; (f) cross-section of CCAM-2%; (g) cross-section of CCAM-8%; and (h) CCAM-10% cross-section showing a dense structure. ....	84
Figure 39. XRD of crosslinked cellulose acetate MXene membranes .....	85
Figure 40. EDS cross-section mapping analysis images for (a) CCAM-0%, (b) CCAM-2%, (c) CCAM-8%, and (d) CCAM-10% .....	86
Figure 41. Water contact angle of cross-linked CCAM-X% with MXene contents (X) from 0% to 10%. ....	88
Figure 42. Atomic force microscopy (AFM) 2D and 3D images for (a) CCAM-0% and (b) CCAM-10%. ....	89
Figure 43. TGA of CAM-0%, CCAM-0%, CAM-10% and CCAM-10%. ....	91
Figure 44. (a) Water uptake and (b) porosity of CCAM at different MXene contents (0-10 wt.%). ....	93
Figure 45. Molecular weight cut-off (MWCO) trend of CCAM-10% .....	94
Figure 46. (a) Permeation flux of CMCA and CCAMs with various MXene contents	



(0-12%) using DE and CF filtration; (b) rejection of various salts, MG and BSA by CACM, CCAM-0%, CCAM-8%, CCAM-10% and CCAM-12% using DE filtration; (c) rejection of MG and BSA by CCAM-0%, CCAM-8%, CCAM-10% using CF filtration.....99

Figure 47. (a) Rejection of different salts, MG and BSA by CCAM-10% using DE filtration; (b) comparison between DE and CF filtration using CCAM-10% for the rejection of MG and BSA. .... 100

Figure 48. (a) Effects of operating pressure (0.5-2 bar) on water flux using DE filtration; (b) operating pressure impacts on the rejection of Na<sub>2</sub>SO<sub>4</sub> (2000 ppm) using DE filtration; (C) operating pressure impacts on the rejection of MG and BSA using a pressure range (1-2 bar) using DE (blue symbol) and CF (red symbol) filtration; (d) effect of Na<sub>2</sub>SO<sub>4</sub> concentration (1000-4000 ppm) on the rejection performance of CCAM-0% and CCAM-10% tested by DE filtration. .... 102

Figure 49. (a) Water recovery ratio of CCAM-0%, CCAM-8%, and CCAM-10% after fouling using 500 ppm BSA protein solution using CF filtration; (b) fouling resistance ratios of CCAM-0%, CCAM-8%, and CCAM-10% using CF filtration..... 105

## LIST OF ABBREVIATION

Delaminated MXene	DL-MXene
Multi-layered MXene	ML-MXene
Cellulose Acetate	CA
Two Dimensional	2D
Crosslinked Cellulose Acetate	CCAM-X%
Membrane with MXene content	
Pristine Crosslinked Cellulose	CCAM-0%
Acetate Membrane	
Crosslinked Cellulose Acetate	CCAM-10%
Membrane with 10% MXene Content	
Cellulose Acetate Commercial	CACM
Membrane	
Dead-End filtration	DE-filtration
Crossflow filtration	CF-filtration
Ultra-filtration	UF
Deionized Water	DI-water
Phase Inversion	PI
Mixed Matrix Membranes	MMMs
Membrane Water Uptake	WU
Membrane Porosity	P
Molecular Weight Cutoff	MWCO
Formaldehyde	CH <sub>2</sub> O

## LIST OF ABBREVIATION

Lithium Fluoride	LiF
Sodium Chloride	NaCl
Hydrogen Chloride	HCL
Sodium Sulfate	Na <sub>2</sub> SO <sub>4</sub>
Sulfuric Acid	H <sub>2</sub> SO <sub>4</sub>
Magnesium Chloride	MgCl <sub>2</sub>
Bovine Serum Albumin	BSA
Methyl Green	MG
Silver-Nanoparticles	AgNPs
Vacuum-Assisted Filtration	VAF
Scanning Electron Microscopy	SEM
X-ray Diffractometer	XRD
Energy Dispersive X-Ray Spectroscopy	EDS
Fourier-Transform Infrared	FTIR
Thermo-Gravimetric Analysis	TGA
Atomic Force Microscope	AFM
Brunauer-Emmett-Teller	BET
Flux Recovery Ratio	FRR
Reversible Fouling	R <sub>r</sub>
Resistance Ratio	
Irreversible Fouling	R <sub>ir</sub>
Resistance Ratio	

## CHAPTER 1: INTRODUCTION AND LITERATURE REVIEW

### 1.1 Thesis Outline

This thesis has the following organization:

➤ **Chapter 1: Introduction and Literature Review:**

Chapter 1 describes the importance of nanofiltration membranes and their effective role in water treatment applications. Furthermore, it reveals the importance of cellulose acetate composite membranes and the various potential enforcing agents that can be used to improve membrane properties. It also demonstrates the achievements and weaknesses in the previous literature. The chapter reveals which additive the researcher used for the specific purpose and applications, and a table is provided to facilitate a comparison with the work results. The significance of the novel MXene material is also explained, as is its role in improving the anti-fouling properties of the membrane. The chapter concludes with an overview of what was done in previous work in relation to cellulose acetate composite membranes and their limitations.

➤ **Chapter 2: Materials and Methodology:**

The chapter presents a list of the supplies used to synthesize the MXene material, along with the materials used in the preparation of the cellulose acetate membrane and in the crossflow filtration process. This is followed by a description of the devices and operating parameters used to control and optimize the membrane performance as well as the underlying theory. The chapter also reveals the characterization tools, namely FTIR, SEM cross-section-EDS mapping, SEM surface morphology, TGA, BET, XRD, DSC, contact angle and AFM, for the six prepared samples, before running a crossflow filtration to verify the expected causes of problems that can emerge in the process, such as membrane fouling. Also, this chapter reviews the appropriateness of the membrane preparation (mechanical properties) for this

specific application or whether enhancement is required in addition to how the mechanical properties of the membrane change after filtration.

➤ **Chapter 3: Results and Discussion:**

This chapter reports and analyzes the results obtained using different characterization tools before and after conducting dead-end and crossflow filtration. It also discusses the effects of adding MXene with a content from 0 wt.% to 12 wt.% in terms of membrane performance and fouling resistance. It clarifies the relationships and trends among the operational parameters and reveals the calculated values for flux and rejection. This demonstrates the membrane performance, enabling a comparison between the obtained results and the values reported by previous work to demonstrate the strength of the proposed membrane and show how it can overcome the limitations found in previous studies.

➤ **Chapter 4: Conclusion and Recommendations for Future Work:**

This chapter sums up the overall achievements and results and reports the possible applications and enhancements of the optimized MXene/cellulose acetate membrane.

## 1.2 Thesis Main Objectives

The research aims to synthesize an efficient antifouling and high-performance chemically crosslinked MXene/cellulose acetate mixed matrix membrane. The main goal is to study the effect of adding MXene to the cellulose acetate composite in improving the antifouling, flux, and rejection performances of the membrane. Herein, the objectives of this research are:

- To improve the antifouling properties of membranes for wastewater treatment.
- To maintain a good flux and improve the foulant rejection performance of the membrane.
- To examine the antifouling properties of the membrane with the addition of

different MXene contents to a cellulose acetate membrane.

- To test the impacts of pressure and feed concentration on the separation performance of the membrane, including the pure water flux and rejection rate, using the DE and CF filtration processes.

### 1.3 Desalination and Wastewater Treatment Technologies

Limited water resources and the steady growth in the global population have led to burgeoning demand for fresh water and clean energy [9]. Thus, the researcher is motivated to explore and develop high-quality water purification and desalination technologies. Water treatment technologies include coagulation, adsorption, distillation, media filtration, disinfection, and membrane filtration. These are categorized and presented in Figure 1 and Table 1, showing the typical contaminations removed and operating pressure for each membrane type. Among all these technologies, membrane filtration processes are preferred due to their superior advantages of lower overall energy cost and easy operation [10].

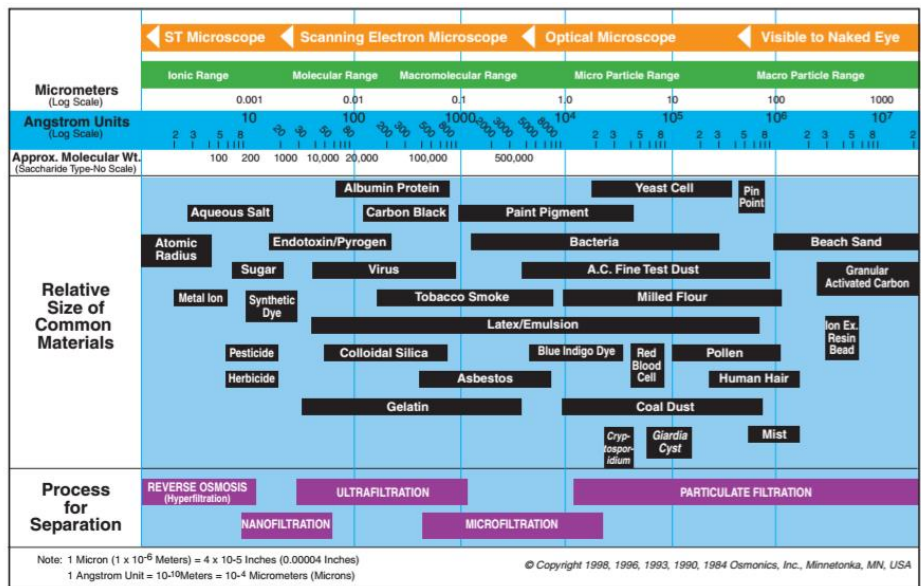


Figure 1. Filtration bands of MF, UF, NF and RO. Sourced from Ref [3].

Table 1. Summary of membrane types based on filtration class; extracted from Ref [11]

Membrane type	Pore size	Standard contaminants eliminated	Standard pressure
Microfiltration (MF)	0.1-10 $\mu\text{m}$	Suspended solids, protozoa, bacteria	0.1-2 bar
Ultrafiltration (UF)	3-100 nm (1-100 kDa)	Colloidal or molecular particles, partially viruses, proteins, most bacteria	Cross flow: 1-5 bar Dead end :0.2-0.3bar
Nanofiltration (NF)	1-5 nm (250-400 Da)	Natural organic matter (NOM), viruses, divalent or multivalent ions	5-20 bar
Reverse osmosis (RO)	< 125 Da	Contaminations comprising monovalent ions.	10-100 bar
FO	< 125 Da	Contaminations comprising monovalent ions.	Osmotic pressure

MF, UF, RO, and NF are pressure-driven membrane filtration processes that offer promising solutions for clean water production [12]. These membrane processes have attracted significant attention from researchers over the last few decades [13-15]. MF is a membrane separation process. It uses membranes that have pore sizes ranging from 0.1 and 10  $\mu\text{m}$  and a comparatively low operating pressure of feed water ranging from 100 to 400 kPa (15 to 60psi). It is mostly used for the removal of large particles, such as in treating wastewater in the food and beverage industry [14]. The UF process system is similar to the MF process, although this membrane process type has lower pore sizes varying between 0.01 and 0.1  $\mu\text{m}$ . In addition to the ability to remove all the microbiological species removed by MF, UF membranes can also eliminate other species, such as viruses, and are thus used widely in wastewater treatment. Both UF and MF require lower operating pressures compared to RO and NF. However, fouling is a chronic issue in membranes, which leads to the shortening of membranes' lifespan and increases the operational costs [15]. Fouling commonly encompasses the buildup of undesired deposits either on the surface of the membrane (in the case of RO and NF, due to their non-porous nature) or on the internal side of the membrane pores (in the case of MF and UF), causing a reduction in permeation flux and molecule rejection [16]. Several studies have confirmed that fouling resistance is enhanced by dissolved organic matter in the feed. To preserve membrane permeability, maintaining and replacing membranes is necessary, but this factor , increases operational costs [17].

Another obstacle in the membrane application field is biofouling, which is due to bacteria adhering to and growing on the membrane surface. Membrane processes are mostly affected by biofouling because microorganisms continue to reproduce, and so even if most of them have been eliminated, enough cells remain to grow and multiply due to the biodegradable matter in the feed water. Previous work reported that



biofouling is a major issue in various filtration processes, including NF and RO, and is considered to be the cause of more than 45% of membrane fouling [18, 19]. Biofouling has numerous impacts on membrane systems, including the formation of biofilms with low permeability, causing a decline in the membrane flux rate and requiring higher feeds and differential pressures to maintain a good production rate. Furthermore, biofouled membranes are susceptible to acidic by-products, which adhere to and concentrate on the membrane surface and lead to membrane biodegradation. Biofilms also lead to a reduction in product water quality due to increased salt passage through the membrane as dissolved ions accumulate in the biofilm at the membrane surface. Finally, biofouling causes higher energy consumption due to increased differential and feed pressures required to compensate for the flux decay and biofilm resistance [18].

Numerous studies that have made substantial achievements in inhibiting biofouling and enhancing membrane anti-biofouling properties. Pandey et al. [5] fabricated an Ag@MXene composite membrane via silver nitrite self-reduction on the MXene sheet surface, followed by coating the solution in PVDF substrate using the VAF method. This membrane exhibited around 99% inhibition of bacteria (*E. coli*). However, a MXene membrane with only the PVDF substrate showed only 60% *E. coli* inhibition, highlighting the excellent antibacterial activity of Ag-NPs. Another study by Shameli et al. [20] examined a silver/polylactic acid (Ag/PLA) nanocomposite sheet. The results confirmed that by increasing the Ag nanoparticle loading, the antibacterial activity against bacteria (positive and negative) was enhanced.

Lin et al. [21] fabricated cerium-replaced hydroxyapatite nanoparticles with various atomic ratios of cerium ( $C_e$ ) / [cerium ( $C_e$ ) + calcium ( $C_a$ )] ( $X_{ce}$ ) using the sol-gel superficial fluid drying method. The authors found that when calcium was partially substituted by cerium for a  $X_{ce}$  above 0.08, the antibacterial activity was enhanced. Meanwhile, Lu et al. [22] prepared an antibacterial film by blending konjac glucomannan (KGM) and poly(diallyldimethyl ammonium chloride) (PDADMAC) in an aqueous medium, attaining excellent antibacterial performance against *B. subtilis* and *S. aureus*. Liao et al. [23] fabricated an UF membrane made of polyvinylidene fluoride (PVDF) with silver ion exchange NaY zeolite particles (AgNaY) using the phase inversion method. AgNaY mixed matrix PVDF membranes revealed novel and durable antibacterial properties against *E. coli*, and the authors found that increasing Ag<sup>+</sup> content enhanced the antibacterial performance. Chen et al. [24] fabricated an UF composite membrane of polyether sulfone and halloysite nanotubes filled with Cu<sup>+2</sup> and Cu<sup>+2</sup>-HNTs, which acted as antibacterial agents. The antibacterial experiment confirmed the favorable antibacterial action of the composite against *S. aureus* and *E. coli*.

The NF process is like an RO membrane in that it is designed to eliminate dissolved chemical impurities involving salts. NF and RO both contain a thin-film composite layer. The pore size of NF membranes is around 1 to 5 nm, while RO membranes are much tighter. Both involve high operating pressures and use similar membrane materials. However, RO [15-17, 25, 26] requires higher capital and operational costs and is more prone to fouling than NF. RO yields the most wastewater, at between 25 and 50% of the feed [12]. In addition, NF eliminates many of the same solutes as RO, but to a smaller degree (see Figure 1). NF membranes can also operate at lower pressures than RO membranes and are thus considered ideal for attaining an

optimal combination of flux and salt rejection [14]. Although NF is infrequently used in the potable water reuse process, water purification plants are considering it as an efficient alternative to RO in terms of energy [14]. NF membranes combine the properties of UF and RO membranes, making them attractive due to the novel benefits for water sanitization and the elimination of organic matter, multivalent ions, and industrial deposits [5]. Nanoporous membranes are presently a vital part of NF technologies [5].

Of the advanced pressure-driven membrane separation processes presented above, NF has become one of the most commonly used techniques in wastewater treatment, water softening, and the chemical and pharmaceutical industries [27-30]. The NF technique controls numerous processes, including the selective separation of multivalent ions and organic molecules, because it uses a special separation technique based on steric hindrance, low operation pressure, electrostatic repulsion, and Donnan exclusion [29, 31, 32]. There are several vital criteria for enhancing the function of NF membranes, such as high selectivity, fouling resistance, and mechanical stability [27, 33-37]. Numerous strategies are used to mitigate the problems of membrane fouling and enhance NF membrane properties, including the modification with hydrophilic polymers [37-39] and nanomaterials [40, 41]. The most effective strategy is imbuing hydrophilic nanomaterials into polymeric matrix membranes [42], thereby developing stability and hydrophilicity and improving the fouling resistance of the membrane [43-46].

### *1.3.1 Membrane Material Selections*

Separation membranes include polymer membranes, ceramic membranes, nanotube membranes, porous carbon membranes, inorganic-organic nanocomposites, biomimetic membranes, and 2D material membranes. According to the previous literature, promising materials for polymeric membranes are cellulose acetate (CA), polypropylene (PP), polyvinylidene (PVDF), polyacrylonitrile (PAN), polysulphone (PSF), polyether sulfone (PES), poly fluoroethylene (PTFE) and thin film composites (TFC) [47]. Of these, CA, one of the first active polymers used to produce a water membrane for MF and RO, is flexible, hydrophilic, and relatively easy to use and has low production cost, a wide range of pore sizes, low fouling propensity, and a smooth surface membrane material [42]. However, CA membranes are not suitable in temperatures above 31 °C and they are also limited to pH levels between 4 and 7.5. Furthermore, CA membranes should be used at the recommended operation pressure to avoid membrane degradation [42].

TFC membranes contain a condensed ultrathin barrier layer that polymerizes in situ above a microporous polymeric support membrane. The advantages of TFC membranes are that they work at lower pressures and higher flux, are not biodegradable, have good chemical stability, high salt rejection, and a good rejection of materials such as silica, nitrate, and organics due to their independent combination of a special selective layer and a porous support layer [48]. Ceramic membranes mainly consist of silica, alumina, zirconia, titanium oxide or any combination of these materials. Ceramic membranes are restricted to use in applications where polymeric membranes are not appropriate, such as under high operating temperatures or in heavily contaminated feed/radioactive environments. However, ceramic membranes are not used frequently due to their high manufacturing cost [49].

Meanwhile, inorganic nanotechnology membranes are typically divided into two types according to the structure and method of separation. Porous carbon membranes involving carbide-derived carbon elements offer superior control in terms of pore size, shape, and consistency [25]. For example, carbon nanotube (CNT) membranes include antifouling properties, higher water flux and superior strength. However, CNT membranes have lower rejection rates for smaller contaminations, such as metal ions, because of the large pore size [50]. Recent studies synthesized 2D material membranes from 2D class nanosheets, such as graphene [51], graphene oxide (GO) and MXene. Unlike other filler morphologies, 2D porous fillers provide a superior surface area to volume ratio, offering greater contact between the porous fillers and the membrane polymer matrix [52]. The transportation of ions and molecules inside the 2D nanosheets among the layers is presented in a schematic representation (Figure 2) [5], whereby the smaller transported materials are filtered out through the membranes. 2D layered membranes are highly adaptable as the water flow rate and particle rejection rate can be controlled by the overall membrane thickness, interlayer distance, and varying flake size. GO is a particularly promising material in the separation membranes field, offering clean treated water with high price efficiency. Also, as mentioned by Lee J et al. [53], the inclusion of only about 1 wt.% of GO in a polymer-based membrane improves its water flow flux and biofouling resistance.

GO membranes reveal high water flow flux and low water friction because of the well-defined 2D nanometer sheets of GO membranes [54-56]. However, only a limited number of 2D materials can be used and processed into membranes and can filter or sieve particles while maintaining the membranes' mechanical cohesion. Although MXene and GO membranes are similarly robust and hydrophilic and both consist of 2D nanochannels, MXene membranes have electrical and ionic conductivity.

Therefore, MXene is a novel and promising membrane material for the rejection of molecules and ions.

There are some basic barriers related to the separation method in that a practical membrane should have the appropriate structure for the anticipated applications, such as pore size, porosity and physicochemical properties, including membrane surface hydrophilicity, chemical, mechanical and thermal stability, and good membrane roughness [11]. The membrane molecular weight cut-off (MWCO) [57] is also an important factor. It is a characterization tool used to measure the membrane pore size and it is estimated as the rejection rate of the spherical shape of a solute that has a particular molecular weight [58]. According to numerous studies, UF/NF membrane performance in pressure-driven methods is impacted by the membrane's MWCO [3,4]. Kadel et al. confirmed that for a given UF/NF membrane, there is a direct relationship between the MWCO, that is the pore size, and the membrane permeability or permeate flux of the membrane. Conversely, there is an inverse proportionality between the size of the pores and the membrane rejection rate. As the membrane pore size increases, the membrane permits the transportation of particles with a wider range of molecular weights; thus, the permeate flux increases and the rejection rate decreases [59].

The permeability and rejection rate of a membrane are generally determined by the surface pore size and membrane porosity [11]. One of the vital issues facing membrane technologies is fouling. Membrane fouling denotes a drop in the performance of the membrane over time as a result of cake formation on the surface of the membrane owing to the adsorption of impurities or membrane pore blocking [60].

The membrane fouling characteristics are controlled by the surface hydrophilicity and roughness of the membrane. Characteristics such as thermal, chemical and mechanical durability affect the stability of the membrane under certain

conditions [11]. Grafting a variety of nanofiller materials onto polymer matrices (mixed matrix membranes) allows the modification of the membrane properties and structure. A previous study showed that surface hydrophilicity can be improved by adding hydrophilic nanomaterials [61]. As membrane biofouling impacts the overall performance of the membrane, including flux, rejection, and membrane lifetime, upgrading membranes' antibacterial activity or fabricating a bacterially resistant membrane is a fundamental task in the water treatment and desalination fields.

The selection of the membrane material is one of the traditional approaches for biofouling control. The selected materials should have certain characteristics, such as being easy to clean and a low bacterial affinity. Membrane surface modification is another technique to control biofouling, such as by providing the membrane surface with a bacteriostatic property to inhibit microorganism growth. The surface modification approach can be attained in several ways, including polymer blending, coating, and grafting using antimicrobial or inorganic additives during membrane fabrication. Polymer blending modifies the characteristics of the membrane surface with only a slight change in the bulk morphology and membrane properties. The grafting approach uses hydrophilic polymers or plasma treatment techniques to fabricate a fouling-resistant membrane surface. While this approach can be employed to any polymeric material, recent research has focused on membrane surface graft polymerization using porous polypropylene or thin-film composite polyamide membranes.

Surface coating is accomplished by using additives that can be easily adapted to existing membrane fabrication processes. The coating of a membrane surface can modify its properties, such as the surface charge, hydrophilicity, roughness, and resistance to biofouling. Numerous studies have used inorganic additives to enhance

the fouling resistance of membranes, such as nano-sized alumina [62], zirconium dioxide [63], nano-sized titanium dioxide [64], lithium perchlorate [65] and silica [66]. There has been substantial work in this field, especially in relation to titanium dioxide, uses UV radiation and photocatalytic degradation of the foulant before it reaches the membrane surface, thus improving the membrane's antifouling properties [67]. Antimicrobial additives that have been used to provide the membrane surface with antimicrobial properties include fabricated antimicrobial polymers, which consist of phosphonium salts or quaternary ammonium, polyethylene oxide, heavy metals, including silver or copper, chitosan, and Ag-NPs. Composite NF and UF membranes with immobilized Ag-NPs have revealed good anti-biofouling features [18].

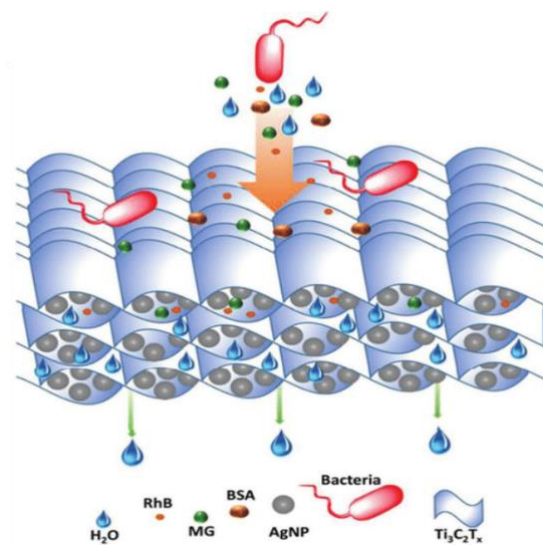


Figure 2. Schematic representation of the transportation of various molecules in 2D NF (silver/MXene nanosheets) membrane between the layers. Adapted from [5].



### *1.3.2 Membrane Fabrication Method*

Recent work has concentrated on improving nanocomposite membranes for sustainable water treatment, targeting the improvement of the antifouling properties, and overcoming the trade-off between the solution rejection rate and permeability.

Recently, polymer-based nanocomposite membranes have attracted a significant awareness among other various nanocomposites [68]. These are produced through the incorporation of NPs, nanofibers, nanosheets/nanotubes into the membrane polymer matrix using different methods, such as phase inversion (PI) [69-73], physical coating [73-76], interfacial polymerization (IP) [77-80], electrospinning and crosslinking [81-83], self-assembly [84-86], layer by layer assembly [84, 87], and the chemical grafting [88, 89] and physical [90] and chemical deposition [91] of NPs on the surface of the membrane. The incorporation of engineered NPs, such as metal oxides (titanium dioxide ( $\text{TiO}_2$ ), alumina ( $\text{Al}_2\text{O}_3$ ), silica ( $\text{SiO}_2$ ), ferric oxide ( $\text{Fe}_2\text{O}_3$ ), zinc oxide ( $\text{ZnO}$ ), magnesium oxide ( $\text{MgO}$ ), zirconium dioxide ( $\text{ZrO}_2$ ) and zeolite) [68, 92, 93], metals (copper, silver), carbon-based materials (CNTs, graphene, nanofiber polymers (polyurethane, polylactic acid, polyethylene oxide) and carbon nanofibers, have been used as efficient enforcing agents in the fabrication of various composite membranes [94].

An example is the elimination of organic foulants by using  $\text{TiO}_2$  nanoparticles to coat the membrane surface prior to using UV radiation; the result is photocatalysis. Hereby, groups of active oxidant detecting agents are revealed on the membrane surface that are responsible for the decomposition of the membrane foulants [95]. However, the advantages of grafting NPs onto membranes are limited by their weak adhesion to the polymeric matrix or by NP aggregation. Furthermore, large NP contents weaken the membrane's mechanical stability [96]. Thus, pursuing a synthesis technique to integrate

NPs into the membrane polymer base while preventing NP accumulation at the membrane surface and maintaining good adhesion between the NP and the membrane polymer matrix has received much research interest.

#### 1.4 Mixed Matrix Membranes

A membrane can be characterized as a thin semi-permeable hindrance that holds effluents and permits clean water to pass. Vital rejection methods for these impurities include mass diffusion, molecule sieving, and charge-charge interaction [97]. The main cause of the separation process is the pressure difference throughout the membrane. Fig.3 illustrates the important factors affecting water membrane fields [97]. Mixed matrix membranes (MMMs) are heterogeneous membranes consisting of advanced inorganic fillers distributed in transmutable polymer mediums. These can enable standard membranes to be used to address manufacturing process concerns [52]. In other words, MMMs denote the introduction of nanomaterials (liquid, solid or both) into a matrix [98]. Each phase contains a type of material, whereby the matrix is a polymeric material phase, while a porous material, such as zeolite, carbon molecular sieve, activated carbon, CNTs and 2D materials, is the dispersed phase [98]. The concept of an MMM derives benefit from the dispersed fillers as these offer high selectivity, whereas the polymer provides an attractive mechanical property as well as cost-effective processability [52].

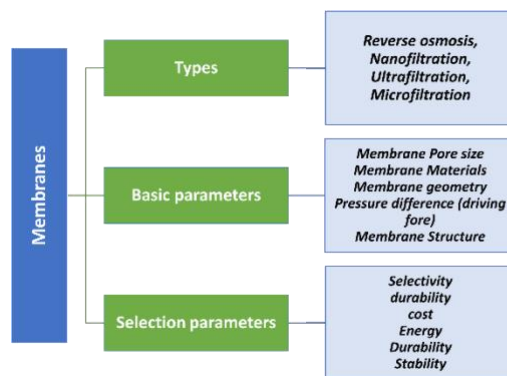


Figure 3. Fundamental parameters for membrane selection; extracted from Ref [97]

### 1.5 CA MMMs

Of the organic materials, cellulose is the most widespread as it is renewable, naturally occurring, biodegradable and inexpensive [99]. Cellulose is considered to represent an almost unlimited source for environmentally friendly raw materials and biocompatible goods [99]. Although cellulose has significant a hydrophilic property, it is insoluble in water and some organic solvents due to the stiff molecule nature and close chain packing structure [99] derived from the numerous inter- and intra-molecular hydrogen bonds among the cellulose molecules [100]. However, cellulose is soluble in many solvents, such as N-methyl morpholine, N-oxide and ionic solutions, although these are unrelated. CA membranes are synthesized from acetylated cellulose [101].

CA membranes were the first commercially developed membranes and are used in a range of applications, from MF to RO [101]. Commercial CA (CMCA) membranes are structurally categorized as asymmetric membranes. CA is an environmentally friendly (i.e. extracted from sustainable resources) and attractive polymer due to its cheap price and good resistance to chlorine. However, CMCA membranes experience poor rejection when hydrolyzed by acids and alkalis. The main hurdle to the extensive usage of CMCA membranes is their exposure to surface fouling and the subsequent

reduction in the permeate flux [102, 103]. For that reason, the researcher focuses on improving the CMCA membranes using different methodologies and techniques to address the fouling issue. Numerous researchers have used CA in their work to fabricate NF water treatment membranes, as shown in Table 2 and Table 4, which present the respective permeation flux and rejection rates of different salts and dyes according to the additive type and membrane fabrication method. In comparison to other hydrophilic polymers, CA is substantially used to fabricate NF membranes [103-106] and is considered a promising substitute due to its outstanding film-forming capability, hydrophilic nature, biodegradability, superior toughness, tremendous biocompatibility, simple chemical modification, and fairly cheap price [107-109]. However, one of the main obstacles in CA membranes is their high sensitivity to fouling by biological and organic foulants, which may cause an overall weakening in CA membranes' separation performance [110, 111]. This has inspired researchers to enhance the fouling resistance of CA membranes via the incorporation of additives such as 2D class materials and NPs to attain enhanced separation performance [110-113]. In this work, CA membranes are fabricated as a promising polymeric membrane for water purification applications.

Table 2. Summary of reported data for NF CA membranes with various additives listed with their values of flux, salt rejection and membrane porosity.

Name of membrane	Type of membrane filtration	Water flux (L $m^{-2} h^{-1}$ )	Membrane porosity/pore size	Application (type of salt/dye rejected)	Salt rejection (%)	References
Original triacetate (CA) hollow fiber membrane		2.32	0.5-2.0nm	Widely utilized in water purification applications, such as wastewater recovery and industrial solutions.		[114]
				NaCl	90.8 %	
				Na <sub>2</sub> SO <sub>4</sub>	91.5%	
Modification of the original triacetate (CA) hollow fiber membrane	Nanofiltration membrane	5.2	0.5-2.0nm	NaCl	66.4 %	[114]
				Na <sub>2</sub> SO <sub>4</sub>	95.4%	

Name of membrane	Type of membrane filtration	Water flux (L $m^{-2} h^{-1}$ )	Membrane porosity/pore size	Application (type of salt/dye rejected)	Salt rejection (%)	References	
PA50/CNC/PES	Nanofiltration membrane	204 at 0.6 MPa	Pore size for CNC coating 60-150nm	Important for saline water desalination and purification of water for consumption	[115]		
						<u>Na<sub>2</sub>SO<sub>4</sub></u>	97.7 %
						<u>MgSO<sub>4</sub></u>	86 %
						<u>MgCl<sub>2</sub></u>	15.5%
						<u>CaCl<sub>2</sub></u>	11%
						<u>NaCl</u>	6.5%
Bamboo cellulose thin film membrane (BCM)		15.6 4	6.2 nm, with BET surface area of 1.1 × 10 $m^2/g$	NaCl	40%	[116]	

Name of membrane	Type of membrane filtration	Water flux (L $m^{-2} h^{-1}$ )	Membrane porosity/pore size	Application (type of salt/dye rejected)	Salt rejection (%)	References
(IP-NF-BCM)	Nano filtration membrane	15.64	1 nm, with BET surface area of $3.2 \times 10^3 (m^2/g)$	Na <sub>2</sub> SO <sub>4</sub>	71.23 %	[117]
NaCl				40.12%		
MgSO <sub>4</sub>				62.33%		
MgCl <sub>2</sub>				24.66 %		
CaCl <sub>2</sub>				29.13%		
Cellulose/AMIMCI solution		128.5 at 0.4 MPa	—	Brilliant blue Congo Red Methyl Orange	99% 98% 28%	[118]

## 1.6 Membrane Modification

Novel materials have been used effectively with CA membranes as well as other polymeric membranes to improve membrane performance with regards to the rejection rate and permeation flux as well as to enhance the membrane hydrophilicity and antifouling properties [119]. Novel materials, such as NPs, is are the most common novel material for CA membranes, 2D materials (graphene, GO and MXene), nanoporous GO, CNTs, zwitterion materials, metal oxides (titanium dioxide, zinc oxide, and aluminum oxides) and AG-NPs, have been combined with polymer membranes to enhance their biofouling and chlorine resistance, permeability, and mechanical strength [5].

The literature shows that, among these materials, 2D GO has significant potential to improve membrane performance because of its large surface area, high mechanical properties and hydrophilicity [16, 120]. NF polyamide membranes have previously been modified with 0.005 wt.% amine-functionalized multiwalled CNTs. The results showed excellent performance comprising 36.71% rejection of  $\text{Na}_2\text{SO}_4$  and 95.72% rejection of  $\text{NaCl}$  as well as enhanced antifouling properties compared to the unmodified polyamide membrane, as reported by Zarrabi et al. [121]. Zinadin et al. used a PES mixed matrix NF membrane modified by GO nanoplates via the PI method. In comparison with an unmodified PES membrane, the results confirmed that membranes filled with GO nanoplates have a better water flux as well as a higher dye rejection rate, while merely 0.5 wt.% of GO was able to enhance the biofouling resistance of the membrane [122]. In another study, Wang et al. blended GO with a PVDF membrane and noted that the hydrophilicity of the membrane was increased through a decline in the membrane contact angle from  $79.2^\circ$  to  $60.7^\circ$ , which led to a better fouling resistance.



Recently, numerous novel materials have appeared as prospective enhancements to, or even replacements for, existing TFC membranes [16]. Several studies have used NF process membranes with additives to enhance the fouling resistance and membrane performance based on the pure water flux and rejection rate, as shown in Table 3 and Table 4.

Abedini et al. [123] suspended titanium dioxide NP into a CA casting solution and discovered that membrane porosity increased, leading to an increase in the mean pore size, resulting in a higher permeation water flux. Ahmed et al. [124] dispersed a different content of silica into CA/polyether glycol (PEG) membranes, which enhanced the membrane's hydrophilicity and the fouling resistance properties. The overall performance of the CA/PEG membrane modified by silica was increased by  $2.11 \text{ L h}^{-1} \text{ m}^2$  and 11.41% for the water flux and salt rejection rate, respectively. A CNT/CA nanocomposite membrane was effectively prepared by Badawi et al. [123] using the PI method. As the CNTs increase, the number of macrovoids in the membrane declines, leading to an enhanced (54%) permeation flux along with a slight decrease (6%) in the salt rejection rate. A GO-CA nanocomposite membrane was prepared by Kabari and Namazi [125]. The authors found that adding GO to the CA membrane leads to an increase in the mechanical parameters, including the Young's modulus (63.88) and tensile strength (61.92%) of the membrane, due to the good mechanical properties of the GO material. A GO-coated polyamide thin layer composite membrane was made by Choi et al., whereby the developed GO coating layer strengthened the membrane's surface hydrophilicity and roughness, leading to enhanced fouling resistance [126].

Sanchuan et al. [114] used a commercial CA hollow fiber membrane and compared it to a CA modified with hydrolysis and carboxymethyl. They found that the water flux was enhanced, as was the  $\text{Na}_2\text{SO}_4$  rejection rate, while the rejection rate of

NaCl worsened. Wang et al. [127] developed triple sheets of a TFC NF membrane through the conventional interfacial polymerization of piperazine and trimesoyl chloride on a cellulose nanocrystal (CNC) interlayer reinforced with a PES MF support (PA50/CNC/PES). The results showed excellent water flux ( $204 \text{ L m}^{-2} \text{ h}^{-1}$ ) with 0.6 MPa and a more than 97% rejection of  $\text{Na}_2\text{SO}_4$ , although the membrane exhibited relatively poor rejection rates for small salt particles, such as NaCl, CaCl and MgCl. Seyedeh et al. [128] synthesized a CA/GO NC membrane via the PI technique. Their results showed that CA/GO nanocomposite membranes offer excellent mechanical strength, good salt rejection and good hydrophilicity. As the authors increased the content of GO from 0 wt.% to 0.01 wt.%, membrane pore size increased. Also, the incorporation of GO decreased the membrane contact angle from  $70.59^\circ$  to  $53.42^\circ$ , indicating better hydrophilicity. In comparison with a neat CA membrane (0 wt.% GO), the CA membrane which contained 0.005 wt.% GO had a permeation rate that was higher by 2.3 times with a slight decrease ( $\sim 15\%$ ) in salt rejection.

A MXene/PES composite membrane was synthesized by Han et al. The membrane outcomes showed admirable flux ( $115 \text{ L m}^{-2} \text{ h}^{-1}$ ). They also rejected Congo red dye with a rejection rate of 92.3% at 0.1 MPa. For inorganic salts, the membrane had a favorable flux of  $432 \text{ L m}^{-2} \text{ h}^{-1}$  but a poor rejection ability –less than 23% [129]. Previous work reported that the incorporation of MXene content into a polyvinyl alcohol (PVA) polymer could enhance the durability and lifetime of MXene composite membranes [130]. Zhang et al. fabricated MXene/UHMWPE nanocomposites and their results indicated that MXene NPs can enhance the mechanical and thermal properties of UHMWPE. The authors noted that the friction-reducing performance, mechanical properties, breaking strengths, and crystallinity of the MXene/UHMWPE nanocomposite membrane improve with the MXene content [131]. A MXene/LLDPE

nanocomposite membrane was fabricated by Cao et al., and the membrane showed a better thermal stability of the composites after MXene loading [132]. Naguib et al. synthesized MXene-polyacrylamide nanocomposite films with the incorporation of 6 wt.% MXene content; thereafter, considerable development in membrane flexibility and conductivity was noted and measured to be  $3.3 \times 10^{-2} \text{ sm}^{-1}$  [133].

Table 3. Separation performance of stated CA, MXene and GO membranes; adapted from [6]

Membrane	Salt/dye/protein	Water flux ( $\text{L m}^{-2} \text{ h}^{-1} \text{ bar}^{-1}$ )	Rejection (%)	Reference
GO at nylon 6-13	MB	11	95	[36]
	MO		99	
	NaCl		27	
	Na <sub>2</sub> SO <sub>4</sub>		56	
PA 6 at GO (120) at PA 6	MB	13	92	[33]
	MO		99	
GO/PDA/PSF	NaCl	81	19	[134]
	Na <sub>2</sub> SO <sub>4</sub>		46	
	MB		66	
	RhB		95	
G-CNTm	NaCl	11	51	[135]
	Na <sub>2</sub> SO <sub>4</sub>		83	
	MO		96	
GO-COOH	NaCl	5	48	[136]
	Na <sub>2</sub> SO <sub>4</sub>		91	
ATP/GO	RhB	41	99	[137]
CA/MOF at GO <sub>0.12</sub>	BSA	122	~92	[107]
CNCs/CDA	BSA	75	90	[138]
CA/GO-0.5	BSA	125	90	[139]

Membrane	Salt/dye/protein	Water flux (L m <sup>-2</sup> h <sup>-1</sup> bar <sup>-1</sup> )	Rejection (%)	Reference
GO-UR/CA	NaCl	20	27	[140]
	MgSO <sub>4</sub>		73	
1.5% CGO	MO	30	53	[141]
	BSA		100	
CA:PA=4:1	BSA	34	60	[109]
MXene membrane	RhB	1000	85	[142]
	BSA		100	
MXene (Ti <sub>3</sub> C <sub>2</sub> T <sub>x</sub> )	RhB	118	81	[143]
	MG		94	
	BSA		100	
21% Ag at MXene	RhB	420	80	[143]
	MG		92	
	BSA		100	

### *MXene Structures*

MXene is one of the most common layered carbide 2D class materials; this family originated in 2011 from the most widely considered layered MAX phases,  $\text{Ti}_3\text{AlC}_2$  [144, 145]. As we published recently [6, 146], “the typical MAX phases formula is  $\text{M}_{n+1}\text{AX}_n$ , where n: 1, 2 or 3 and M: denotes early transition metal elements, while A typically denotes non-metals from group IV A or III A elements; for example, Si and Al and X can be either nitrogen or carbon (Fig.4 & Fig.5). The MAX structure can be described as A sheets acting as a sandwich for both the M and X layers, whereby the X atoms fill the octahedral sites among the M sheets. The sandwich-like structure allows for the etching process of MAX phases into MXenes via the elimination of A element-sheets via either direct HF etching or *in situ* hydrogen chloride/lithium fluoride acid mixture [147, 148]. MXene, known as  $\text{M}_{n+1}\text{X}_n\text{T}_x$ , is terminated by extremely hydrophilic and reactive  $\text{T}_x$  surfaces and T denote functional groups, such as O, OH and/or F groups, while x represents the terminating group total number (Fig.4 & Fig.5) [49].”

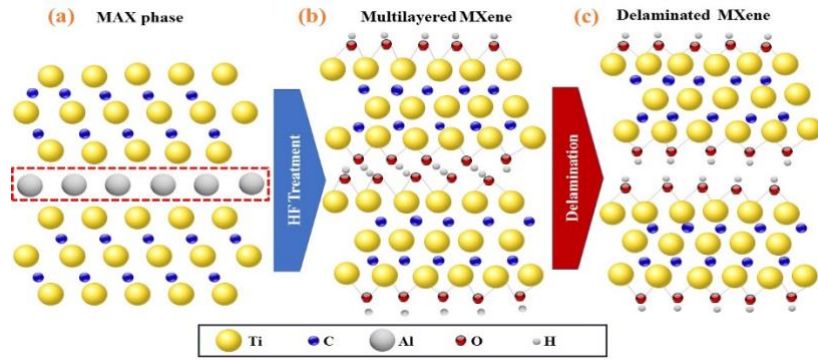


Figure 4. Process flow representation of the  $\text{Ti}_3\text{AlC}_2$  exfoliation process. (a) Assembly of  $\text{Ti}_3\text{AlC}_2$ ; (b) exchange process between the hydroxyl (OH) group and the aluminum atoms after the acid etching process; (c) delamination process through sonication of ML-MXene, which leads to detached nanosheets and results in hydrogen bond breakage [146].

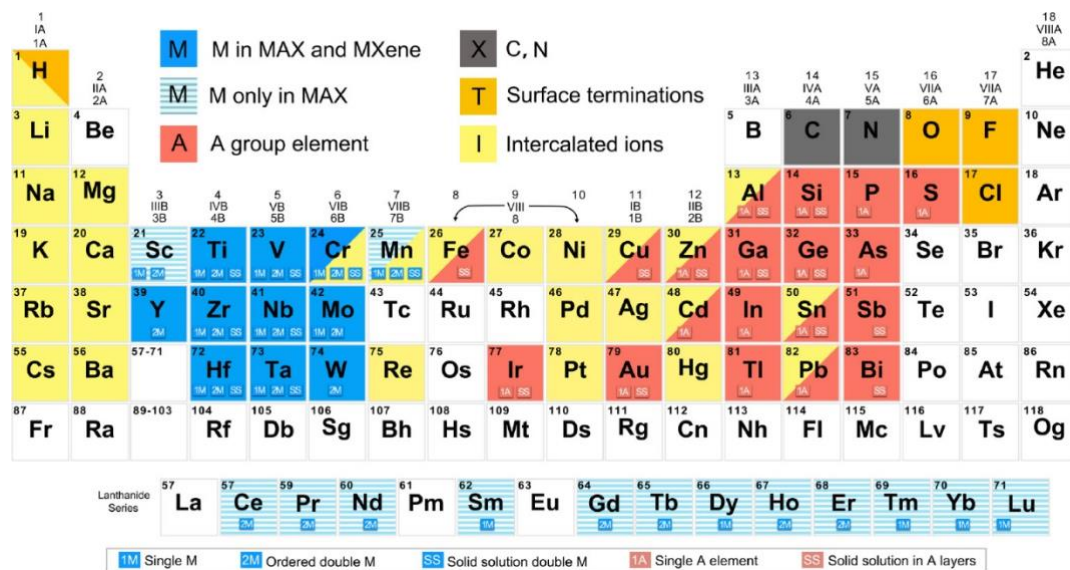


Figure 5. Principal components of the MAX phase and MXenes, including their intercalation ions. The elements in the blue boxes exhibit reports exclusively in the MAX phase and have not been produced in MXenes. The elements in the red boxes are the A element of the MAX phase and can be selectively etched to make MXenes. Yellow boxes represents cations that have been implanted in MXenes to date. Retrieved from [4]

### 1.6.1 MXenes' Unique Combination of Properties

The swiftly developing 2D transition metal carbides, i.e. MXenes, have shown good mechanical durability, good thermal and chemical stability, high surface area, favorable antifouling properties, high hydrophilicity (readily dissolved in water), metallic electronic conductivity, and film-making capability. Besides, MXene ( $\text{Ti}_3\text{C}_2\text{T}_x$ ) flakes can be loaded on polymers to fabricate multifunctional films with appealing mechanical and electrochemical properties, outstanding conductivities, controlled thicknesses, and brilliant flexibility [130].  $\text{Ti}_3\text{C}_2\text{T}_x$  is the most investigated MXene in water treatment and environmental sanitizing applications, including species elimination of ions, dyes, proteins, and heavy metals, among others [149].

### 1.6.2 MXene Membrane Applications

Due to the desirable properties of MXene, especially  $\text{Ti}_3\text{C}_2\text{T}_x$ , it has been widely utilized as a promising porous filler in membrane fabrication [150] for pollutant water treatment and water desalination [129, 142, 151, 152]. As we published recently [146], “MXene membranes are suitable and can be used for various applications, including heavy metal adsorption [129]. MXene membranes offer outstanding antibacterial properties against some types of bacteria, including *E. coli* and *B. subtilis*, and are thus suitable for applications related to wastewater treatment [153], antimicrobial coatings [154], capacitive deionization [155], and water purifying membranes [156].”

A MXene/PVA hybrid membrane with 40 wt.% MXene was prepared by Si et al. and the results exhibited a three-fold increase in tensile strength compared to the bare PVA membrane [157]. Zhi et al. synthesized a MXene/polyurethane (PU) nanocomposite membrane. The authors used only 0.5 wt.% MXene and determined a

noticeable upgrading in the tensile strength, hardness and yield stress of the composite membrane by ~ 20%, ~13% and ~ 70%, respectively [158]. Another study showed good pure water flux for MXene membranes ( $887 \text{ L m}^{-2} \text{ h}^{-1} \text{ bar}^{-1}$ ), with almost 100% membrane efficiency and excellent emulsified oil/water mixture and salt rejection and chemical resistance, including against hydrogen chloride (HCl), NaOH and NaCl [159]. The antimicrobial behaviors of MXene ( $\text{Ti}_3\text{C}_2\text{T}_x$ ) were also investigated by our group through the synthesis of a MXene membrane based on a hydrophilic PVDF polymeric substrate for water purification applications [154, 160, 161]. A PAN, polyethyleneimine (PEI) and MXene ( $\text{Ti}_3\text{C}_2\text{T}_x$ ) NF composite membrane offering good solvent resistance was prepared by Wu et al. [162].

Ding et al. grafted  $\text{Fe}(\text{OH})_3$ -NP, as a pore-forming material, into a MXene ( $\text{Ti}_3\text{C}_2\text{T}_x$ ) membrane to increase the water transport channels and enhance the permeation flux [142]. Another study predicted a new combination of  $\text{Ti}_3\text{C}_2\text{T}_x/\text{GO}$  membranes to attain good protein, dye and salt rejection [163, 164]. Liu et al. synthesized an ultrathin MXene ( $\text{Ti}_3\text{C}_2\text{T}_x$ ) and PAN membrane with a thickness around 60 nm, which exhibited a permeation flux of  $85.4 \text{ L m}^{-2} \text{ h}^{-1}$  and high levels of NaCl rejection (99.5%) [165].

A crosslinked MMM with 18% P84 copolyimide and 1% MXene was produced via the PI method. The results revealed good hydrophilic performance, a rejection of 100% gentian violet and good flux ( $268 \text{ L} \cdot \text{m}^{-2} \cdot \text{h}^{-1}$ ) at 0.1 MPa and room temperature [166]. A MXene/CS MMM was synthesized by Xu et al. for the pervaporation dehydration of solvents to purify organic solvents. The authors found that 3 wt.% MXene in a CS MMM offers the best membrane performance. They also confirmed that introducing MXene nanosheets into the CS membrane provides interlayer water channels that allow the transportation of water molecules across the membrane;



therefore, the flux of the CS membrane was enhanced, reaching  $\sim 1.4\text{--}1.5 \text{ kg}/(\text{m}^2 \text{ h})$  [167].

Recently, our group prepared 21%Ag@MXene (21% loading of Ag-NPs). The result showed an improvement in the membrane water flux ( $420 \text{ L m}^{-2} \text{ h}^{-1} \text{ bar}^{-1}$ ) (Fig.6(a)) and a 92.32% rejection rate of methyl green (MG) and a 79.93% rejection rate of rhodamine B (RhB) (Fig.6 (b)) as well as membrane fouling resistance. As Fig.7(a) depicts, our group studied *E. coli* cells on three different membranes, including MXene, The 21%Ag@MXene membrane revealed a bacterial (*E. coli*) inhibition of over 99%, which was the highest percentage in comparison with the other MXene membranes (Fig.7(b)) [5]

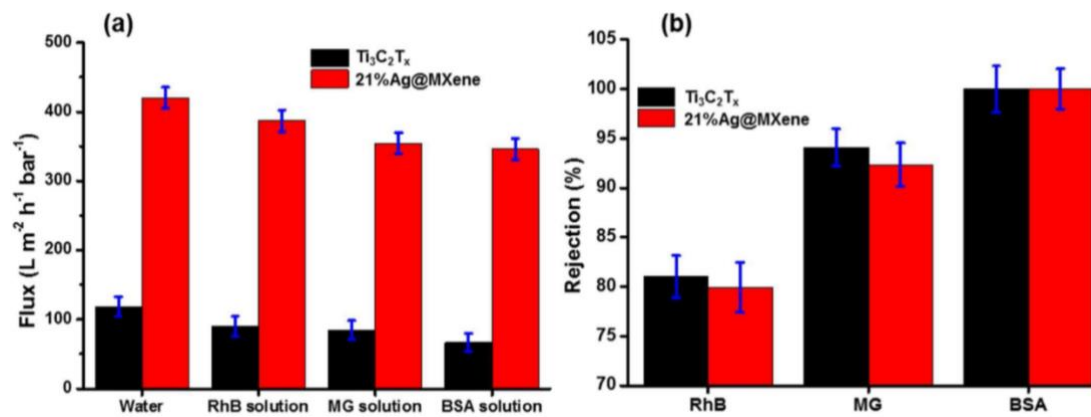


Figure 6. MXene ( $\text{Ti}_3\text{C}_2\text{T}_x$ ) and 21%Ag@MXene membrane performances, including filtration of RhB, MG and BSA species at ambient temperature. (a) Membrane water flux, and (b) membrane rejection rate. Retrieved from [5].

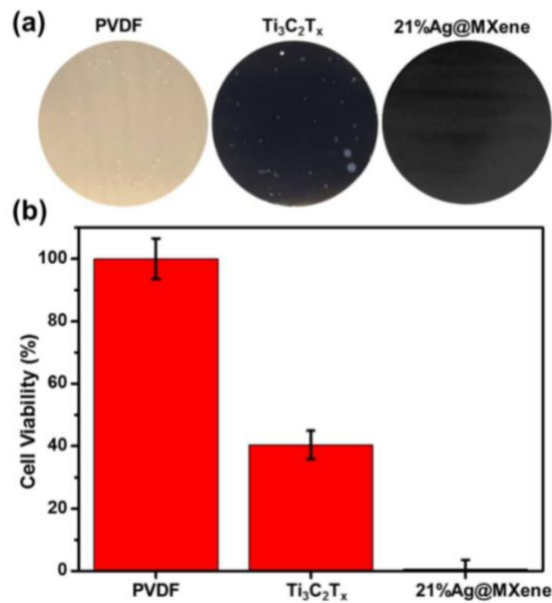


Figure 7. PVDF (control membrane), MXene (Ti<sub>3</sub>C<sub>2</sub>T<sub>x</sub>), and 21%Ag@MXene membrane antibacterial activities. (a) Photos of bacteria (*E. coli*) cells growing at 35°C. (b) Values for the cell viability of *E. coli*. Retrieved from [5].

More recently, our group fabricated crosslinked MXene in CA MMMs. As we recently published [6], “surface functional groups of DL-MXene, CA and CCAM-10% were investigated by FTIR (Fig. 8). The MXene functional groups (OH, -O-) make it well distributed in water; thus, active sites for formaldehyde (CH<sub>2</sub>O) crosslinking are offered for the easy fabrication of a durable MXene-based MMM [149]. As we expected, the MXene functional groups (-OH and -O-) and CA functional group (-OH) reacted with the CH<sub>2</sub>O material to create the -O-C-O- network. Our group studied the impact of chemical crosslinking of the MMM and MXene loading on membrane effectiveness concerning permeation flux and rejection”. Figure 9(a) shows the pure water flux for CAM-0%, CCAM-0%, CAM-10% and CCAM-10%, and the

results exhibit that the water flux of CCAM-X% has improved with higher MXene content. Introducing MXene into a CA matrix appreciably enhanced the permeation flux, which could be due to the creation of extra nanopores and MXene hydrophilicity. Generally, the water flux of CCAM-10% was enhanced compared to that of CCAM-0% (Fig.9(a)). Fig.9(b-d) illustrates the solute rejection of CAM-0%, CCAM-0%, CAM-10%, and CCAM-10% for various salts, dyes, and bovine serum albumin (BSA).

The rejection of  $\text{Na}_2\text{SO}_4$  for CCAM-2% at 60 °C and for 60 min was 3.28%, which was enhanced to a 58.65% rejection rate using CCAM-10% with the same crosslinking condition. The results indicate that the rejection rate of CCAM-X% enhanced with increasing MXene loading due to the formation of denser layers and chemical crosslinking. CCAM-10% showed the rejection of NaCl (28.14%),  $\text{MgCl}_2$  (40.35%),  $\text{MgSO}_4$  (56.08), RhB (92.34%), and MG (98.27%) and a 100% rejection of BSA. However, CAM-0% showed a trivial rejection performance for different salts, dyes, and BSA (65.25%). As we published recently [6], “the chemical crosslinking and introducing of MXene into the polymeric matrix considerably enhanced the rejection performance, which is attributed to the creation of small pore diameters and reduced macro voids” (Fig.9(c)&(d)). The separation performance of CCAM-10% compared to CAM-10% was clearly observed from the SEM morphologies [6].

The permeation flux is controlled by the density, pore size, and membrane hydrophilicity, whereas the rejection performance depends on the membrane pore size and surface charge”. According to the results, the chemical crosslinking of CCAM-10% causes a decrease in the membrane pore size as well as its density but continues to have good hydrophilicity because of the good dispersion of the MXene inside the CA matrix. Exceeding a 10 wt.% MXene load slightly raises the water flux and leads to a considerable decline in salt rejection, which can be explained by the MXene

agglomeration with extreme grafting. Therefore, introducing MXene until 10 wt.% enhances membrane hydrophilicity and reduces the macrovoids' pore diameter. As we recently published [6], “the pore diameter of fabricated CCAM-10% was computed according to the solute rejection data, and the average uniform pore diameter of CAM-10% and CCAM-10% were obtained as 7.47 nm and 1.89 nm, respectively.”

The surface charges of membranes were evaluated at pH=7. As shown from the results (see Fig.10), the CA and CCAM (0-10%) MMMs showed a negatively charged surface at pH=7, and it was found that with loading more MXene content, the zeta potential value increased. Also, it was noticed by our group that the highest zeta potential value (32.42 mV) corresponded to the CCAM-10% composite membrane, while the lower zeta potential value (24.84 mV) was related to pristine CA. The main factor that had a considerable effect on the CCAM-10% permeation flux and rejection rate values was the membrane thickness (Fig.11). As thickness increased, the permeation flux declined, and the rejection of Na<sub>2</sub>SO<sub>4</sub> increased. As we recently published [6], “our team examined the impact of varying CCAM-10% thickness (from 92 to 158 μm) on the permeation flux and rejection of Na<sub>2</sub>SO<sub>4</sub>. The results showed that the pure flux values were 293.94 and 178.31 L m<sup>-2</sup> bar<sup>-1</sup> h<sup>-1</sup>, respectively, and the rejection rates of Na<sub>2</sub>SO<sub>4</sub> were 58.65% and 65.28%, respectively. Accordingly, our group confirmed that the optimum thickness of CCAM-10% can achieve the best separation performance of 123 μm.”

In the same work, our team studied the effect of the chemical crosslinking time of CCA, CCAM-2%, CCAM-4%, CCAM-6%, CCAM-8% and CCAM-10% on the water flux and rejection of Na<sub>2</sub>SO<sub>4</sub>. The results revealed that the water flux declined for all the membranes as the crosslinking duration was between 30 and 120 mins (Fig.12), whereas the NA<sub>2</sub>SO<sub>4</sub> rejection rates exhibited a noticeable rise from 30 to 60

mins, followed by a steady rise in the rejection rate with time (Fig.13). According to these findings, our group considered that a 60-min crosslinking time was optimal for the further analysis of the membranes.

Examining the prolonged membrane durability is fundamental to establishing feasible demands with a monitored fouling rate. As we published recently [6], “Three cycles of filtration tests of CCAM-10% were applied by our team (Fig.14) with 0.1 g L<sup>-1</sup> of RhB solution at 1 bar, and each cycle was executed for 120 min. CCAM-10% was cleaned with DI water four times to eliminate any remaining RhB after each run. After applying three cycles with a total duration of 360 min for the RhB separation process, the water flux of CCAM-10% declined by a total of 4.30%. However, with a duration of 120 min in the first cycle, the flux declined by 3.37%. Furthermore, it was observed that the CCAM-10% in the first cycle of RhB filtration had 97.56% flux recovery, followed by 99.35% (for the second cycle) and 99.57% (for the third cycle) flux recoveries of RhB filtration. This outstanding achievement exhibited the superior stability and good flux recovery of the fabricated CCAM-10%. Our team studied the chemical stability of CCAM-10% after curing with a NaOCl aqueous solution at various intervals between 0 and 70 hours. Fig.15 exhibits the membrane weight loss percentages after applying the chemical curing, and CCAM-10% had the best chemical stabilization with just 1.7% in comparison to a 2.9% weight loss of pristine CA. The authors explained that this is probably according to the loading of MXene and the chemical crosslinking of the membrane. Also, they mentioned that all the treated membranes showed no significant weight loss after 45 h of treatment”.

As we recently published [6], “The biofouling resistance of the fabricated membranes was assessed by our group against different types of bacteria (*E. coli* and *B. subtilis* ) to evaluate the membrane biofouling resistance. Fig.16(a) shows a

photograph of *E. coli* and *B. subtilis* on the CCAM-0%, CCAM-2%, CCAM-6%, CCAM-8% and CCAM-10% membranes at 35 °C for 24 h. Cell viability was computed by considering the number of colonies and plotting this against CCAM-0% as a control. Prominently, bacterial growth was inhibited in the existence of MXene compared to CCAM-0% and the growth prohibition was enhanced by loading more MXene content into the CA MMMs. The cell viability of *E. coli* and *B. subtilis* in terms of the growth values on all fabricated membranes (CCAM-0-10%) is plotted in Fig.16 (b), which demonstrates that the membranes' cell viability values diminished with rising MXene content. Above 98% and 96% bacterial growth prohibition for *E. coli* and *B. subtilis*, respectively, was revealed by CCAM-10% in comparison with pristine CCA. Thus, it was confirmed that MXene ( $\text{Ti}_3\text{C}_2\text{T}_x$ ) offers robust bacterial resistance versus all tested types of bacteria and the bacterial anti-biofouling activity was dependent on the MXene content.”

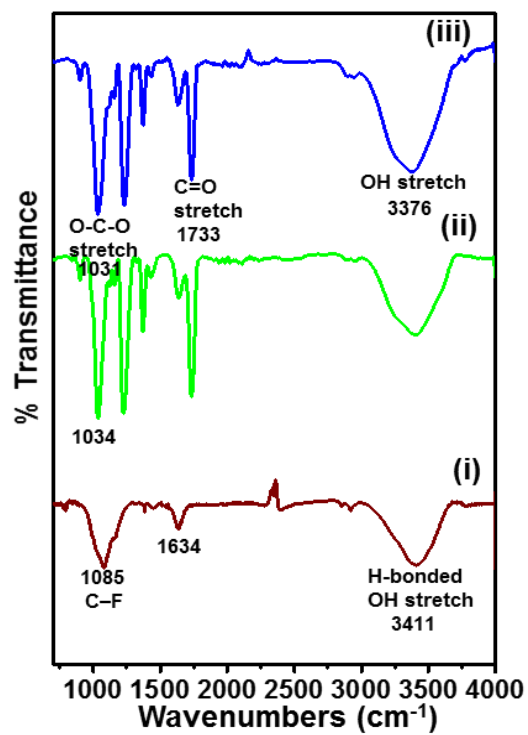


Figure 8. FT-IR spectra fo: (i) DL-MXene, (ii) CA and (iii) CCAM-10%; retrieved from [6]

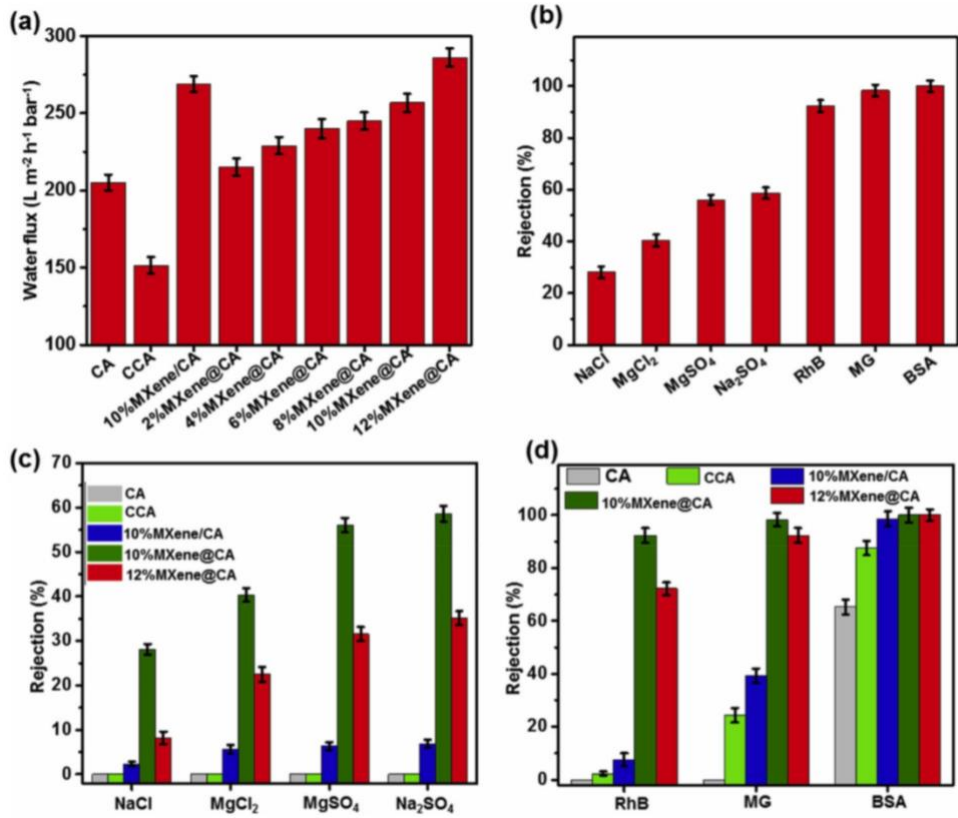


Figure 9. (a) Pure water flux of non-crosslinked and crosslinked membranes; (b) rejection performance rate of the fabricated CCAM-10%; (c) rejection performance comparison among CAM-0%, CCAM-0% , CAM-10%, and CCAM-10% for various salts, different dyes and proteins; (d) rejection performance comparison among CAM-0%, CCAM-0%, CAM-10%, and CCAM-10% for various dyes and proteins; retrieved from [6].



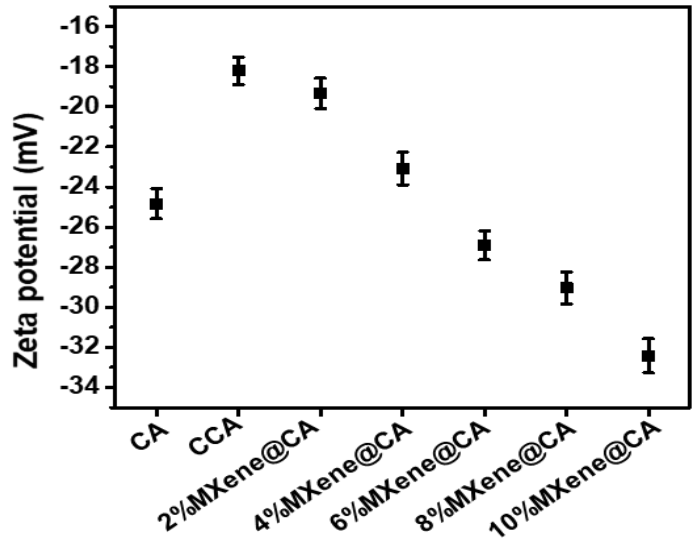


Figure 10. Zeta potential values of CAM, CCAM, CCAM-10% at pH 7; retrieved from [6].

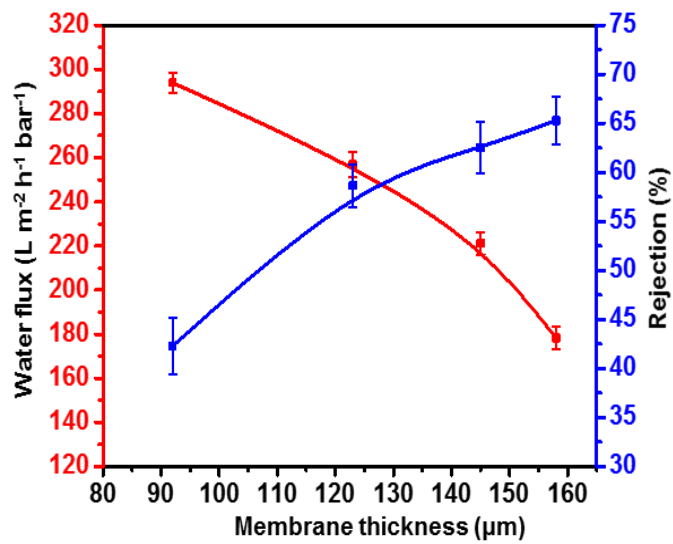


Figure 11. The effect of membrane thickness on the water flux and Na<sub>2</sub>SO<sub>4</sub> rejection (CCAM-10%). Aqueous solution of Na<sub>2</sub>SO<sub>4</sub> (2000 ppm) were used as feed; retrieved from [6].

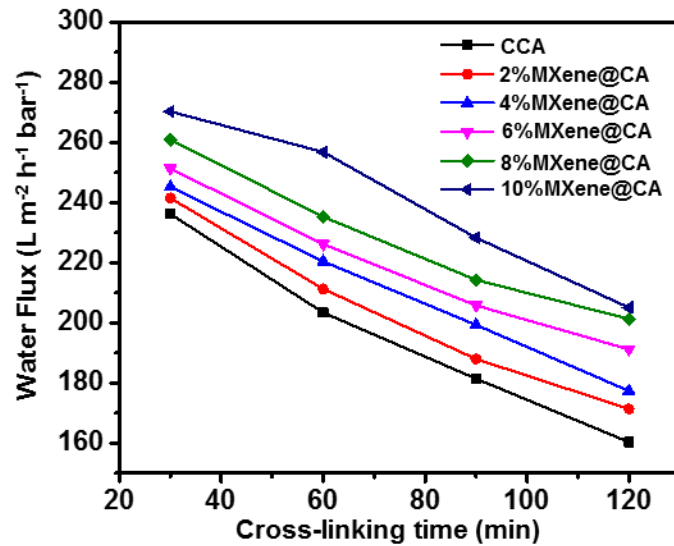


Figure 12. Impact of crosslinking duration on the pure water flux of CCAM, CCAM-2%, CCAM-4%, CCAM-6%, CCAM-8% and CCAM-10% composite membranes; retrieved from [6].

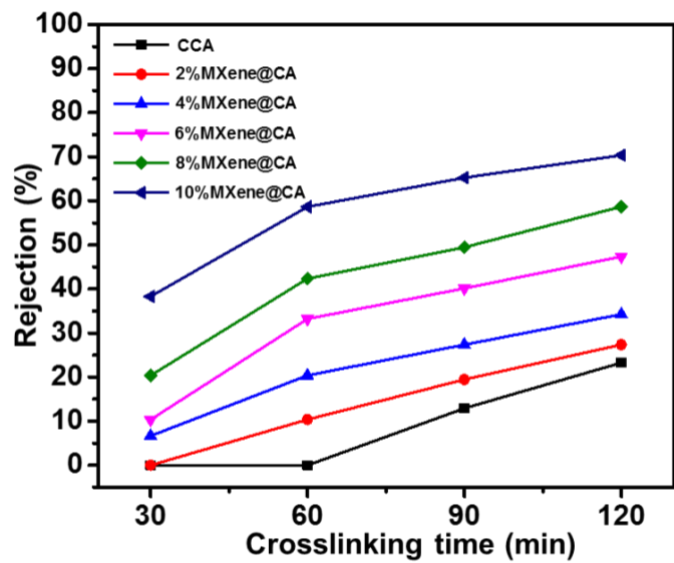


Figure 13. Crosslinking time impacts on the rejection performance of different MXene@CA hybrid membranes crosslinked for 30, 60, 90, and 120 min. Aqueous solution of Na<sub>2</sub>SO<sub>4</sub> (2000 ppm) was used as feed; retrieved from [6].

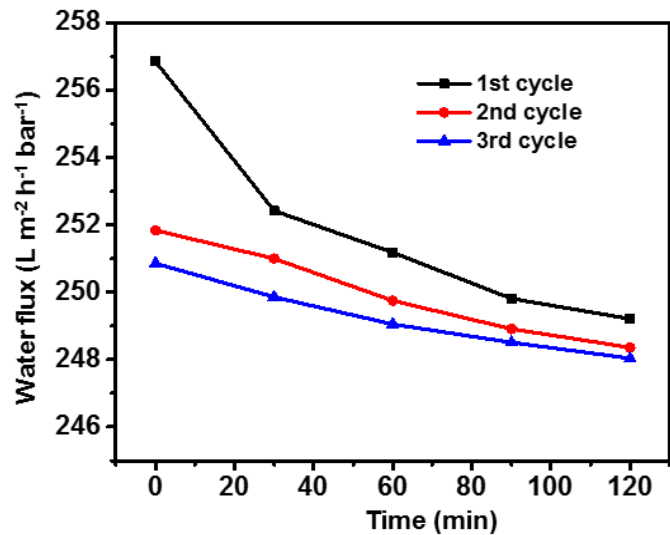


Figure 14. Durability and flux recovery test of the 10%MXene@CA membrane during three cycles filtration of RhB (0.1g/L) solution at pressure of 1 bar; retrieved from [6].

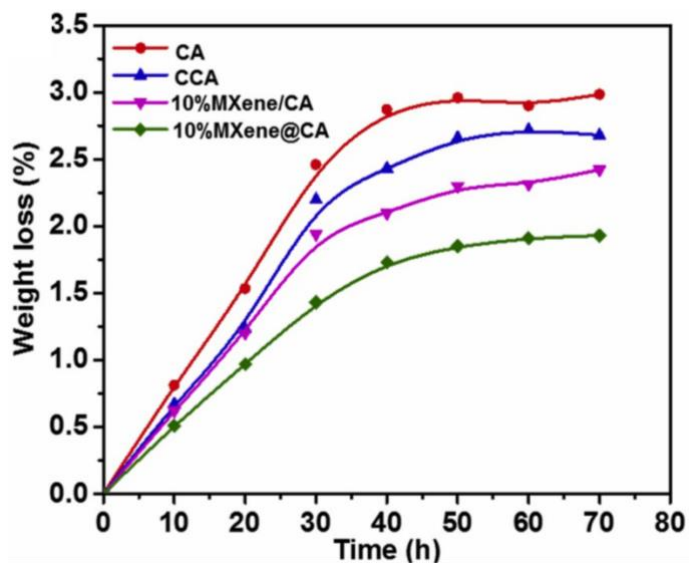


Figure 15. The oxidative stability of the fabricated mixed matrix membranes after curing in NaOCl (0.1%) aqueous solution at temperature of 70<sup>0</sup>C with various intervals (0–70 h); retrieved from [6].

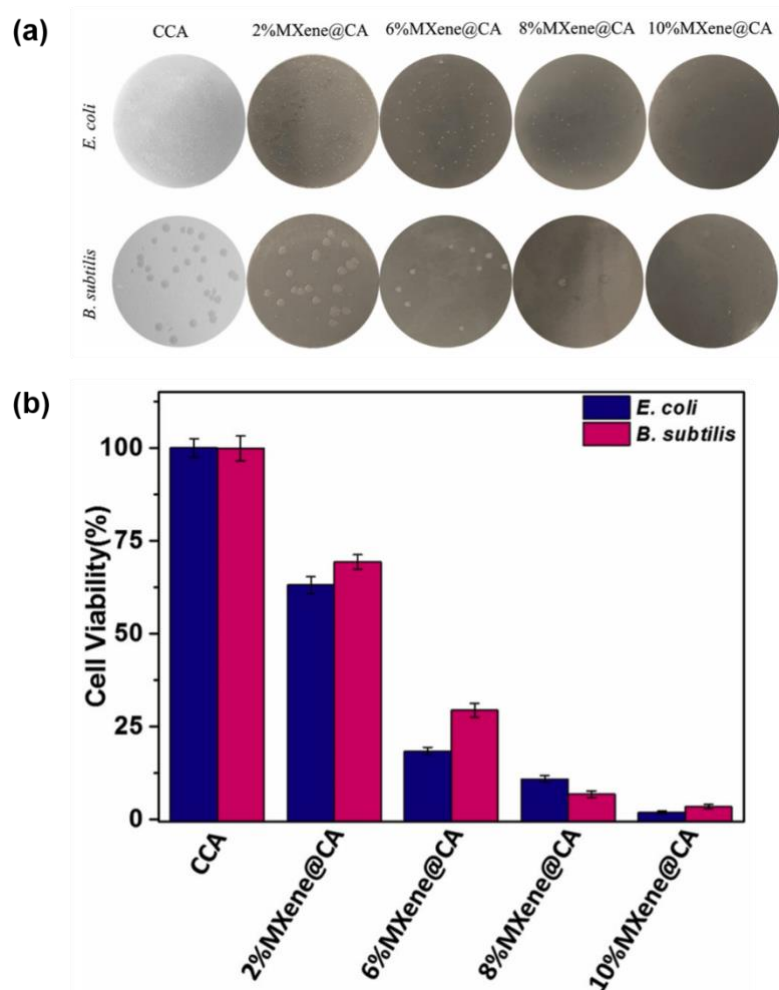


Figure 16. Antibacterial activity of prepared membranes (CCAM-0-10%): (a) Pictures of bacterial (*E. coli* and *B. subtilis*) growth on various CCAM-X% membranes incubated for 24 h at temperature of 35°C. (b) Bacterial cell viability amounts of *E. coli* and *B. subtilis* on various prepared membranes after 24 h.

## 1.7 Membranes' Chemical Crosslinking

MXene membranes are characterized by their interlayer spacing among packed sheets, which contribute significantly to explaining the efficiency of separation, flow rate and selectivity of lamellar MXene membranes. Like other 2D nanomaterials, MXene membranes can endure swelling of the membrane in an aqueous environment, which leads to a drop in the ion rejection rate and selectivity. To overcome the current issue, the channel size needs to be adjusted by manipulating the d-spacing among the MXene sheets through intercalating and crosslinking treatment to prevent the swelling or failure of 2D MXene layers [168]. Crosslinking treatment [169], comprising two types of crosslinking (chemical and thermal), is a promising technique that is used to enhance the thermal as well as chemical stabilities of polymeric membranes. Currently, numerous research works concentrate on chemical crosslinking modification, during which, in the presence of a catalyst, the polymer reacts chemically with crosslinking agents to create a crosslinked structure [170-174]. PVA crosslinked membranes were synthesized by Rhim [175] and Heydari [176] using two distinct crosslinking agents, namely sulfosuccinic acid and fumaric acid, respectively. The chemically crosslinked CS membranes made by Beppu [177] and Shenvi [178] used the crosslinking agents of glutaraldehyde and sodium tripolyphosphate, respectively. Generally, the technique of chemical crosslinking is applied to aid hydrophilicity and improve the separation effectiveness of polymeric membranes [169].

## 1.8 MXene Composite Membranes and Their Fabrication Techniques

NC membrane fabrication methods are mainly based on the PI technique. Numerous research works have used this technique to fabricate membranes, as shown in Table 4. Nanofiller materials are distributed into the polymer matrix solution before the PI method, and the two fabrication methods are flat sheet or hollow fiber configuration [11]. Throughout the PI process, a polymer is blended with a solvent to form a mixture, which is cast on either a proper supporting layer or a glass plate prior to cold coagulation bath immersions, which contain a non-solvent liquid, such as deionized (DI) water. Precipitation occurs, as solvents and non-solvents exchange. A basic condition for this process to work is that the polymer should be soluble in a solvent blend. Finally, the membrane structure is controlled by the combination of phase separation and mass transfer control [179].

Han et al. loaded MXene on a PES UF mixed matrix composite membrane with an MWCO of 10,000 using the PI method [129].

Table 4. MMM filler types, polymer types, fabrication methods used, and the filler advantages; adapted from Ref [11]

Filler type		Polymer type		Fabrication Method	Key advantage of filler	References
Inorganic material	Metal Oxide	TiO <sub>2</sub>	PAI; PVDF; PSU; PAN; PPESK; PVB; PES; CA; PVDF/SPES; PU	Blending +PI	Hydrophilicity	[64, 123, 180-210]
		SiO <sub>2</sub>	PES; PSU; Nafion	PI; Casting and drying	Hydrophilicity	[211-219]
		Al <sub>2</sub> O <sub>3</sub>	PVDF; PES	Blending +PI	Hydrophilicity	[181, 220-223]
		Fe <sub>3</sub> O <sub>4</sub>	PVA; PES; PVC	Blending +PI	Hydrophilicity, magnetic property, core for shell coating	[224-228]
		ZrO <sub>2</sub>	PES	Blending +PI	Hydrophilicity	[181, 223]
		Hydr ous MnO <sub>2</sub>	PES	Blending +PI	Hydrophilicity, Heavy metal adsorption	[229, 230]
		ZnO	PSU	Blending +PI	Hydrophilicity	[231]
	Metal	Ag	CA; PI; PSU; PES; PVDF; PAN; PLA; PU	Blending +PI; electrospinning	Anti-microbial functionality	[23, 212, 232-244]
		Cu	PSU; PLA; PES	Blending +PI; electrospinning	Anti-microbial functionality	[212, 236, 240, 245]
		Zeolite	PU; Ultem; PAN; PVDF PSU;	Solvent evaporation; Blending +PI	Molecular sieving, Hydrophilicity, crosslink property	[23, 230, 246-250]
	CNTs	PVDF; BPPO; PEI; PA; PVA; PES; PAN	Blending +PI; Crosslinking	Electrical conductivity, potential water channel, mechanical properties, hydrophilicity after modification	[204, 251-267]	

Filler type	Polymer type	Fabrication Method	Key advantage of filler	References	
Organic Material	GO	PSU; PES	Blending +PI	Hydrophilicity, negative charge, high surface area support	[122, 219, 268-270]
	PANI	PSU; PAN-CO-PMA PES	Blending/ In site blending +PI	Hydrophilicity	[271-276]
	Poly pyrrole	PSU	Blending +PI	Hydrophilicity	[277]
	Polyhedral oligomeric silsesquioxane	CA	Blending +PI	Special structure, anti-compaction	[278]
Hybrid Material	TiO <sub>2</sub> /MWNTs; Au/xGnPs; Fe/Mn; SiO <sub>2</sub> /GO	PES; PSU	Blending +PI	Synergistic effect	[204, 219, 270, 279]



## 1.9 A Gap in The Literature

After a thorough investigation of the existing literature, numerous studies were found to have fabricated MXene membranes for different applications, including water treatment. As we published recently [6], “owning to MXene’s rich and stable surface chemistry, it has excellent metallic conductivity [149]. Besides, MXene ( $\text{Ti}_3\text{C}_2\text{T}_x$ ) is hydrophilic, meaning the presence of  $\text{H}_2\text{O}$  molecules in-between the MXene layers promotes superfast water flux. Also, MXene resists cations with hydration radii greater than the interlayer spacing and shows great selectivity concerning various kinds of charged metal and dye cations of different sizes. MXene has fouling resistance ability, mechanical flexibility, chemical and thermal durability due to the MXene lamellar assembly, the intercalation of ions ability, numerous surface features, adjustable metallic and electronic conductivity, and admirable film-making abilities. Hence, MXene membranes show superior performance in comparison with other 2D materials in the rejection of greater charge cations, which makes them promising membrane materials [5] [280].”

However, most MXene membranes were fabricated using VAF on a polymeric substrate/support. For example, our group used an anti-microbial MXene to fabricate a water treatment membrane supported on PVDF[153], and an NF membrane based on PAN/PEI-MXene ( $\text{Ti}_3\text{C}_2\text{T}_x$ ) to purify alcohol-based mixtures was prepared by Wu et al. [281]. Ding et al. used  $\text{Fe}(\text{OH})_3$  NPs (positively charged) as the pore-making material to increase water transport channels and thus improve the water flux of a MXene membrane [164]. Wei et al. prepared MXene/GO membranes and achieved outstanding salt and dye rejection [164]. A MXene/polyethersulfone (PES) UF membrane was investigated by Han et al., which showed effective Congo red rejection [129]. Liu et al. fabricated an ultrathin  $\text{Ti}_3\text{C}_2\text{T}_x$  membrane with a thickness of ~60 nm

onto a PAN substrate, which revealed excellent NaCl rejection of 99.5% at 65°C and good permeating flux ( $85.4 \text{ L m}^{-2} \text{ h}^{-1}$ ) [151]. Our group recently prepared a 21%Ag@MXene membrane (21% incorporation of Ag-NPs) with good separation performance and fouling resistance [5]. A P84 copolyimide on a MXene composite membrane demonstrated a rejection of gentian violet (100%) and permeation flux ( $268 \text{ L m}^{-2} \text{ h}^{-1}$ ) at a pressure of 0.1 MPa [166]. Xu et al. fabricated MXene on a chitosan hybrid membrane and used it for solvent pervaporation dehydration [167].

Most MXene membranes reported above have exhibited the supreme antibacterial properties and excellent rejection performance of the top MXene layer, but the MXene remained mechanically unstable in the support layer. This caused an easy leaching of the MXene layer, leading to an overall drop in membrane separation performance and thus fouling issues [168]. Consequently, research has focused on synthesizing mixed matrix MXene composite membranes with various polymeric matrices (e.g. PES, PVA, PVDF) to overcome the constraints of neat MXenes, such as aggregation and durability [149]. As mentioned in previous studies, fillers may offer good hydrophilicity, better antifouling resistance, and high selectivity while polymers may provide attractive mechanical strength and cost-effective processability. For that reason, MMMs attract great attention as they merge the advantages of both dispersed fillers, such as carbon molecular sieves, zeolite, activated carbon, CNTs, and 2D materials, and a polymer matrix.

Herein, a chemically crosslinked MXene at CA nanocomposite MMM for water treatment is prepared using the PI method. MXene dispersion into a CA polymeric matrix is projected to develop the membrane anti-fouling properties and rejection rate while maintaining a good membrane permeation flux. The performance of the fabricated membrane was assessed using dead-end (DE) and crossflow (CF) filtration processes with regards to the flux and rejection of various salts, dyes, and proteins.

## CHAPTER 2: MATERIALS AND METHODOLOGY

### 2.1 Materials

MAX phase ( $\text{Ti}_3\text{AlC}_2$ ) was bought from Y-Carbon, Ltd. PEG400, Hydrochloric acid (HCl), acetone, acetic acid ( $\geq 34.5$  wt%), and sulfuric acid ( $\text{H}_2\text{SO}_4$ ) (98.8%), were purchased from Merck. CA (average Mn  $\sim 30,000$ ), lithium fluoride (LiF) (99.0% (F)), formaldehyde ( $\text{CH}_2\text{O}$ ) ( $\geq 34.5$  wt. %), bovine serum albumin (BSA), sodium chloride (NaCl), sodium sulfate ( $\text{Na}_2\text{SO}_4$ ), magnesium chloride ( $\text{MgCl}_2$ ), and MG were bought from Sigma-Aldrich. A commercial Whatman CA membrane (Whatman CA with a pore size of  $0.2 \mu\text{m}$ ) was obtained from GE Healthcare Life Science and a PVDF membrane with a diameter of 47 mm was obtained from EMD Millipore.

### 2.2 Equipment

- Qsonica Q500 Sonicator ultrasonic processor, Branson® CPXH Ultrasonic Baths 1800
- Orion™ Versa Star Pro™ pH Benchtop Meter
- VWR® Professional Hot Plate Stirrers
- Sorvall Legend XT/XTR centrifuge
- Benchtop freeze drier
- VWR® Vortex Mixer
- JASCO V-760
- METTLER TOLEDO Balance
- Drummond Portable Pipet Aid XP
- Millipore vacuum/pressure pump
- Thermo Scientific Heratherm™ General Protocol Ovens
- ARCTIKO Dixell freezer LCF models
- Thomas® Thermometer Kangaroo Traceable
- Sterlitech - Model HP4750 - Stirred Cell
- Vacuum desiccator
- Elcometer 3580 Casting Knife Film Applicator.
- Lab coat Master casting system (PHILOS, Gyeonggi-do, Korea))

## 2.3 Methods

### 2.3.1 Preparation of Delaminated MXene

As we published recently [6], “the acid (LiF/HCL) etching of precursor MAX ( $\text{Ti}_3\text{AlC}_2$ ) to eliminate the aluminum layer was performed to produce multi-layered MXene (ML-MXene) sheets, followed by ultrasonication to form delaminated MXene (DL-MXene) layers, as mentioned earlier, with some minor adjustment [143]. More precisely, during the acid (LiF/HCL) etching, 80 mg of LiF was inserted into an HCl solution (10 ml) (1:1 ratio by volume for HCl and water). After that, 50 mg of MAX was gently added to the mixture and magnetically stirred for 24 hours at 35°C. After completing the etching process, the etched ML-MXene was centrifuged at 3000 rpm for 5 min to separate it from excess reagents. The residues were washed with DI water and the supernatants were decanted. The centrifugation and dispersion procedures were applied four times to attain a neutral supernatant (pH of 6-7). After that, the solution was kept in the freezer for 1 hr at - 85 °C, prior to freeze-drying to collect MXene powder after 3 to 4 days. Then, the collected dried multilayered MXene ( $\text{Ti}_3\text{C}_2\text{T}_x$ ) powder was added to degassed water (underflow of nitrogen gas for 60 min) and sonicated using a probe sonicator. The produced solution was placed in centrifugation for 15 min at 5000 rpm to allow the ML-MXene to settle. Then, the supernatant was poured out and kept in a freezer prior to freeze-drying (Fig.15) to collect the DL-MXene nanosheets powder. The vacuum-assisted filtration (VAF) process was also used to collect the DL-MXene powder. The supernatant after probe sonication was filtered using a hydrophilic PVDF membrane with a 0.2 micrometer diameter from Millipore via VAF (as shown in Fig.15) and the DL-MXene powder was collected after drying it in an oven at 30 °C (Fig.17)”.

### *2.3.2 Preparation of The Chemically Crosslinked MXene At CA Mixed Matrix Nanoporous Membrane*

The PI method was used to prepare the MXene at CA nanoporous membranes, after which the membranes underwent CH<sub>2</sub>O crosslinking. As we published recently [6], “Normally, 0-12 wt.% of DL-MXene relative to CA was mixed with acetic acid (10 mL) and acetone solution (10 mL) (1:1 ratio). 0.5g of PEG-400 was gently poured into the dispersed solution and kept in bath sonication for 1 h to ensure that the MXene had dissolved into the solution and a homogenous mixture was achieved. Eventually, 1.5 g of CA powder was gently mixed with the above solution under a stirrer (24 h at 25°C). After that, the above solution had transformed into a viscous and homogenous base that was ready to be cast. However, to ensure there were no trapped bubbles inside the solution, it was kept inside a vacuum desiccator attached to the pump for one day, as shown in Fig.17.

After that, the viscous solution was poured onto a glass plate and by using a Casting Knife Film Applicator (Elcometer 3580 ) and a Labcoat Master casting system (PHILOS, Gyeonggi-do, Korea), a thin film with a thickness of 280 μm was formed on the clean glass plate. The thin-film membranes were kept drying for half an hour under room temperature and submerged in a cold DI water (~15 °C) coagulation bath for 2 h (Fig.18). Then the membranes were splashed with DI water to remove possible solvent residuals on the membrane surface. (Fig.18). CH<sub>2</sub>O crosslinking was completed by exposing the membrane to a solution containing acidic formaldehyde (HCHO (2.5% w/v) and H<sub>2</sub>SO<sub>4</sub> (~98 % w/v )) at 60°C for 1h [6, 282, 283] (Fig.18).

Basically, the crosslinking solution consisted of 12 g of Na<sub>2</sub>SO<sub>4</sub>, 4.328 g of CH<sub>2</sub>O and 10 g of H<sub>2</sub>SO<sub>4</sub> added to 37.6 ml of DI water, and the magnetic bead was inserted into the solution to stir it at 800 rpm for ~10 mins until the solution became homogeneous at ambient temperature.”

The prepared crosslinked membranes were kept in a glass beaker filled with DI water, as shown in Fig.19. The prepared crosslinked membranes were neat CA crosslinked membranes (CCAM) and MXene crosslinked CA membranes (CCAM-X%) whereby X% refers to the weight ratio of MXene to CA in the prepared membrane. After immersion in DI water for 24h following chemical crosslinking, the prepared membranes were dried using a glass plate inside an oven at 30 °C for 24 h prior to physicochemical characterization (Fig.19). A schematic representation of the PI of the MXene content into the CA polymeric matrix is provided in Fig.20.

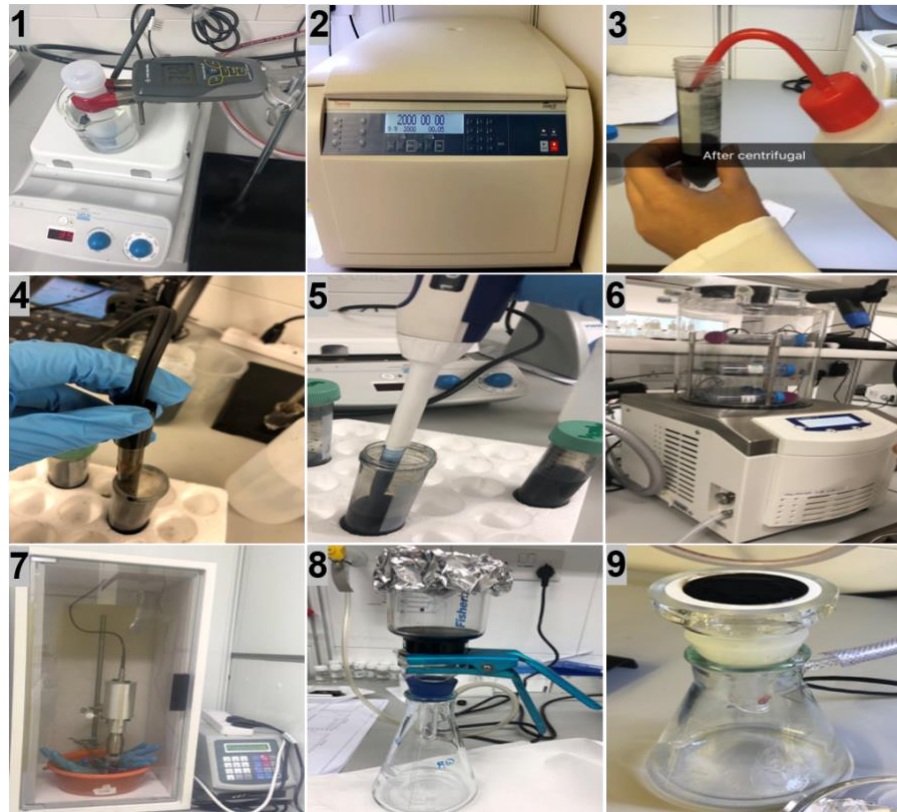


Figure 17. DL-MXene preparation procedures: 1) Acid (LiF/HCL) etching of aluminium layer from MAX ( $Ti_3AlC_2$ ) using a Teflon bottle for 24hr. 2) Centrifugation. 3) Washing with DI water. 4) Measuring the pH value using a voltmeter. 5) Neutral supernatant with pH  $\sim 6$  is collected in an empty bottle. 6) The frozen bottle is kept in a freeze-drier. 7) Ultrasonication process of the ML-MXene to produce DL-MXene. 8) VAF of DL-MXene solution in PVDF filter paper. 8) the PVDF filter paper with a MXene layer.



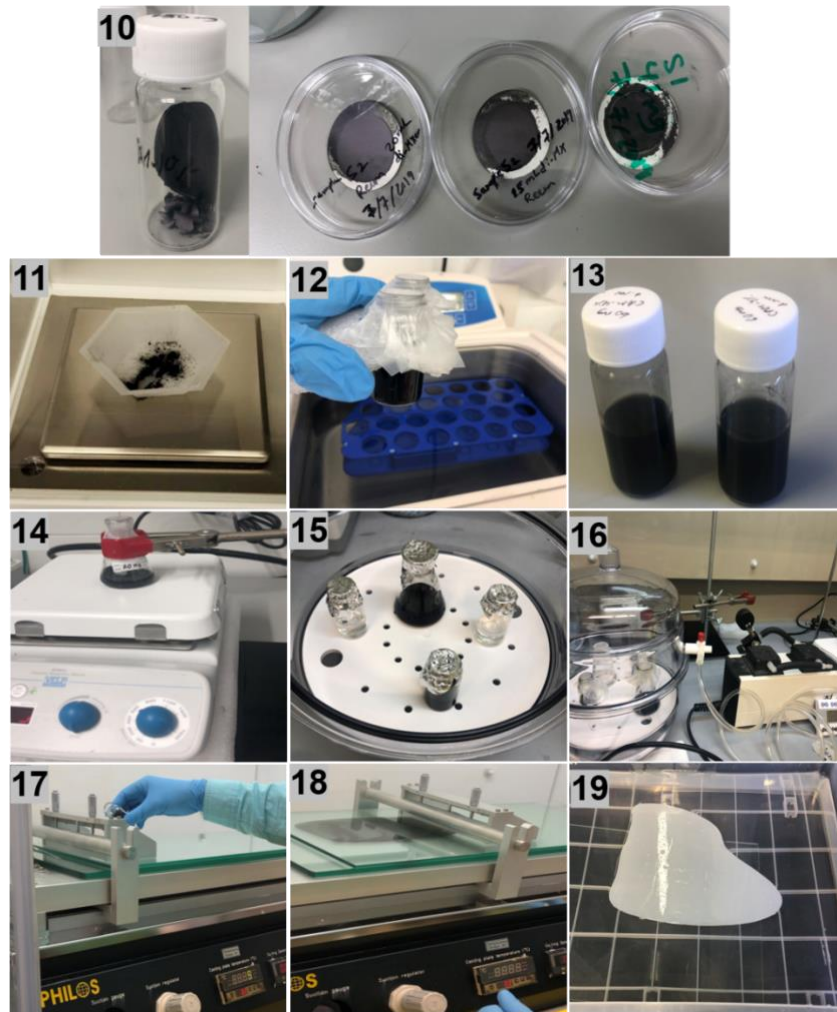


Figure 18. Preparation of the MXene at CA solution and membrane casting procedure: 10) Dried DL-MXene sheet is collected from the oven. 11) The sheet is crushed into a powder and the weight of the DL-MXene is measured. 12) Bath sonication to dissolve the MXene content into the solution and obtain a homogenous mixture. 13) Homogenous membrane solution. 14) The membrane in solution is kept for stirring for 24 hours. 15) The mixture is covered with foil and a small hole is made on the top of the glass to allow for degassing. 16) Degassing the mixture using a vacuum desiccator attached to a pump. 17) The viscous membrane solution is poured onto a glass plate. 18) By using a Casting Knife Film Applicator (Elcometer 3580 ) and a Labcoat Master casting system (PHILOS, Gyeonggi-do, Korea), a thin film is formed on a clean glass plate with a thickness of 280  $\mu\text{m}$ . 19) The thin-film membranes are kept drying for half an hour at room temperature.

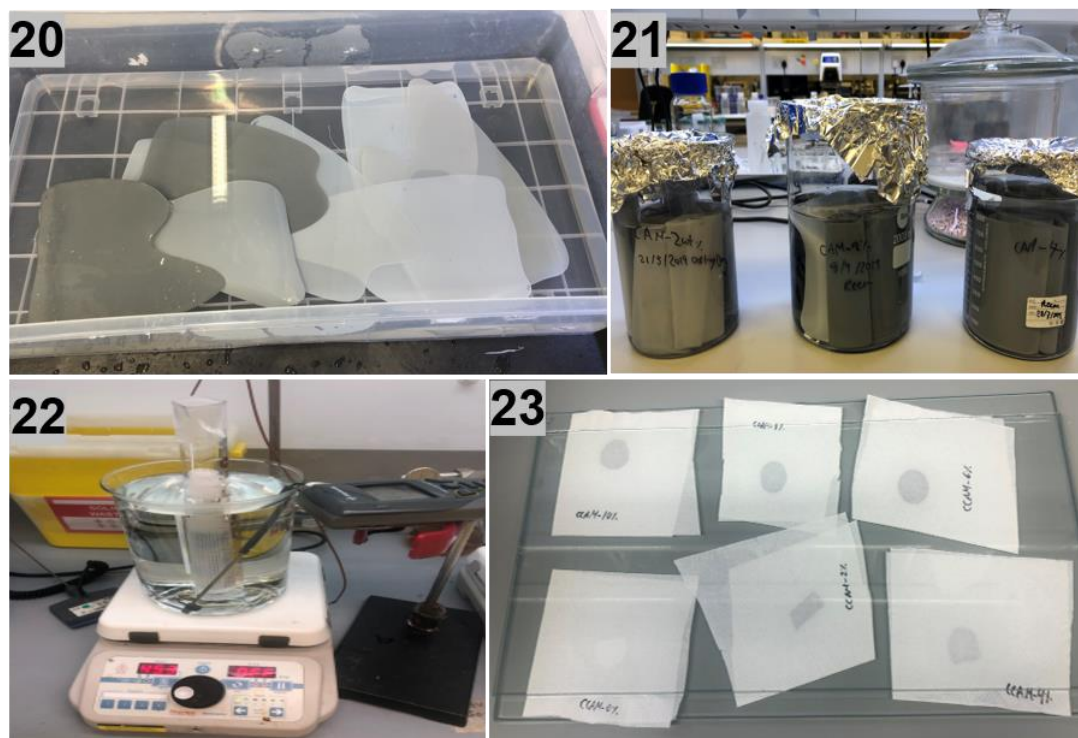


Figure 19. 20) The casted thin film membranes are submerged in a cold DI water ( $\sim 15$  °C) coagulation bath for 2 h. 21) The membranes are splashed with DI water several times and kept in glass containers. 22)  $\text{CH}_2\text{O}$  crosslinking 23) The prepared membranes are dried using a glass plate inside an oven at  $30$  °C for 24 h prior to physicochemical characterization.

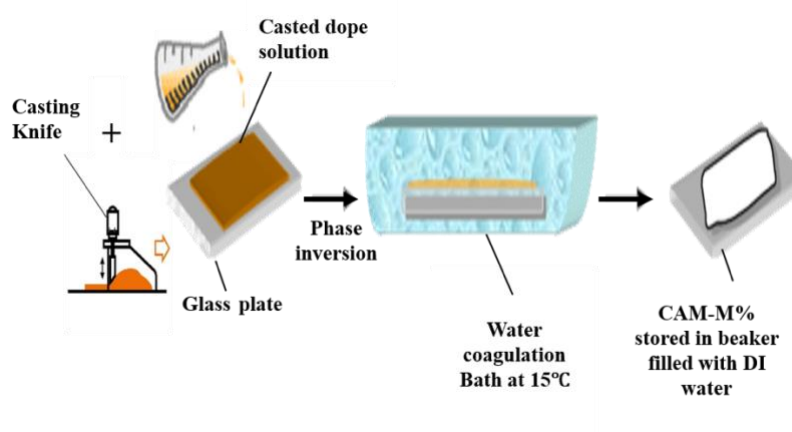


Figure 20. Schematic representation of the phase inversion of MXene at cellulose acetate membrane.

## 2.4 Material and Membrane Characterization

The prepared membranes were dried using a glass plate inside an oven at 30 °C for 24 h prior to physicochemical characterization.

### 2.4.1 *Fourier-Transform Infrared (FTIR)*

The Fourier-Transform Infrared (FTIR) spectra were acquired through the attenuated total reflectance (ATR) method and a Nicolet™ iS50 FTIR Spectrometer in the span of 3800–600  $\text{cm}^{-1}$  (Fig.21). FTIR is an analytical system utilized to recognize organic and, in some cases, inorganic materials. This instrument is used to measure the absorption of infrared radiation exposed by the sample material against the wavelength. The molecular structure and composition are detected based on the Infrared absorption bands. The light wavelength absorbed by a specific molecule from a specimen depends on the energy difference between the excited and stagnant vibrational states. The molecular structure of the sample is characterized by the wavelengths absorbed by the sample. A detector calculates the intensity of the reflected light according to its wavelength. The analyzed signal from the detector is an interferogram, which should be evaluated by the attached computer using FT to produce a single-beam infrared band. A plot of intensity versus wavenumber is normally revealed from the FTIR spectra and wavelength is the reciprocal of the wavenumber.



Figure 21. Nicolet™ iS50 FTIR Spectrometer

#### 2.4.2 *Scanning Electron Microscopy*

The membranes' morphologies were examined using scanning electron microscopy (SEM). Samples of prepared membranes were coated by gold sputter before using FEI Quanta 650 FEG SEM (Fig.22). The membranes were analyzed as a cross-section and surface and 5 kV was used to image the samples. The cross-section was prepared by immersion in the LN2 method. All samples were coated with 5 nm thin gold layer and carbon tape was used to fix all the samples. SEM was used to examine the membrane's area of interest and generate images at nanometer resolution and high magnification. Unlike normal optical microscopies, SEM offers a thorough depth of field. In SEM, a minor electron beam is focused across a sample area of interest and generates a signal that is reported and transformed into an image, which is produced pixel by pixel. The SEM characterization tool provides valuable data regarding the surface and cross-section morphology, sample composition, and sample surface topology.

The Quanta 650 instrument from FEI is a flexible and advanced solution for

numerous research applications. It includes three scanning modes, namely low vacuum, high vacuum, and ESEM TM, which have a wider range than any other SEM system. These tools are engineered to offer full data, including microanalysis and imaging, on all the tested samples, with or without preparation according to the nature of the specimen. This method enables the characterization of various types of samples from metals, polished parts, and fractures to non-conductive soft materials [281]. SEM instruments accommodate two thermo-guns, a microscope column, a tungsten bulb, and a specimen chamber consisting of three attached detectors, as shown in Fig.22 and Fig.23. Detectors are secondary electron detectors (topographical data), backscatter detectors (compositional data), and X-ray detectors (thickness atomic composition).

The secondary electron detector is mostly utilized to detect sample surface assembly as it converts the electrons reflected by the sample surface into signals that can be presented as a picture on the monitor. A backscatter detector works similar to the secondary electron detector in that it detects the electrons that are being reflected by the specimen and reveals them in images. However, a backscatter detector provides a grayscale shown in images that is a direct outcome of detecting elements that are inside the area of interest. Elements with a greater atomic number to absorb a lot of electrons compared to an element with a lower atomic number.

### *2.4.3 Energy-Dispersive X-ray Spectroscopy*

The X-ray detector is a robust kind of detector that is applied to execute energy-dispersive X-ray spectroscopy (EDS). The EDS system is an analytical method utilized to identify the elemental composition of an area of interest in a specimen that was practically identified and detected via secondary electron and backscatter detectors, whereby 15 kV is used for the EDS acquisition of the prepared samples (Fig.23). This works by exposing the specimen to a focused beam of electrons that generate the X-ray spectrum and provide a chemical analysis to find out the elemental compositions. Besides, EDS accommodates two analysis modes: qualitative analysis and quantitative analysis. The qualitative analysis includes the detection of the X-ray lines in the spectrum, while the quantitative analysis measures the line intensities to identify the concentration of each element in the sample area of interest.

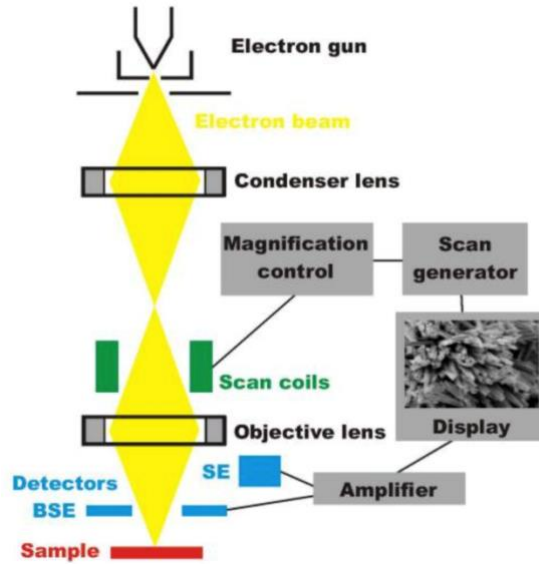


Figure 22. Schematic representation of SEM; adapted from Ref [282].

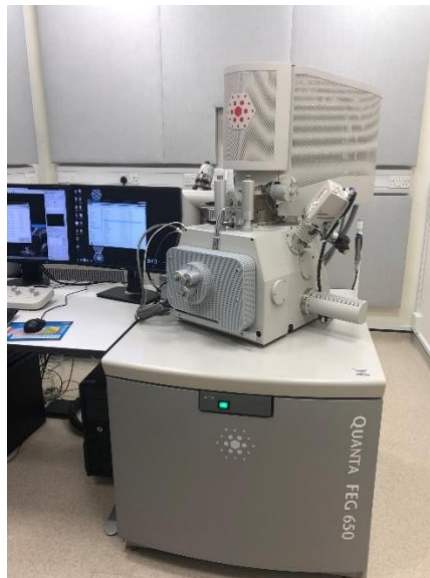


Figure 23. FEI Quanta 650 FEG SEM instrument with a Bruker Flat Quad 5060F energy dispersive X-ray detector (EDS).

#### 2.4.4 X-ray Diffractometry

X-ray diffractometry (XRD) was conducted using powder X-ray diffractometer (Bruker AXS, Germany) (Fig.24) was used with a copper X-ray tube (Cu/K), a radiation ( $\lambda$ ) of 1.5406 Å with a voltage of 40 kV at a current of 15.0 mA, a scanning speed of  $1^\circ \text{ min}^{-1}$  and a step scan of  $0.02^\circ$  per step. The crystalline phases for various types of materials can be identified using the XRD method. Basically, XRD is used for quantitative analysis and it is one of the essential non-destructive devices used to recognize a lot of materials from fluids to crystals and powders. The three-dimensional atomic structure of crystalline solid matters can be obtained by using XRD. The crystal structure of a material is an essential factor as it defines the material's functions and properties. XRD is widely used in many field applications, including research, production, and engineering. The common relationship among the wavelengths of the incident X-rays, angle of incidence, and spacing between the crystal lattice planes of the atoms are identified as Bragg's law.

This relationship correlates electromagnetic radiation wavelengths with the lattice spacing and diffraction angle (Fig.25) [283] and is referred to as Bragg's law. The reflected X-rays from the adjacent crystal planes undergo constructive interference (Fig.24); in this case, the path distinction among them is an integer multiple (n) of the wavelength of the X-rays (Bragg's law) (Fig.25), where n is the "order" of a reflection wavelength of the X-ray, d is the interplanar spacing of the crystal between adjacent crystal planes,  $\lambda$  is the wavelength of the incident X-rays, and theta ( $\theta$ ) is the angle between the scattering plane and incident X-ray beams [284].





Figure 24. Bruker D8 Advance: Powder X-ray Diffractometer (XRD)

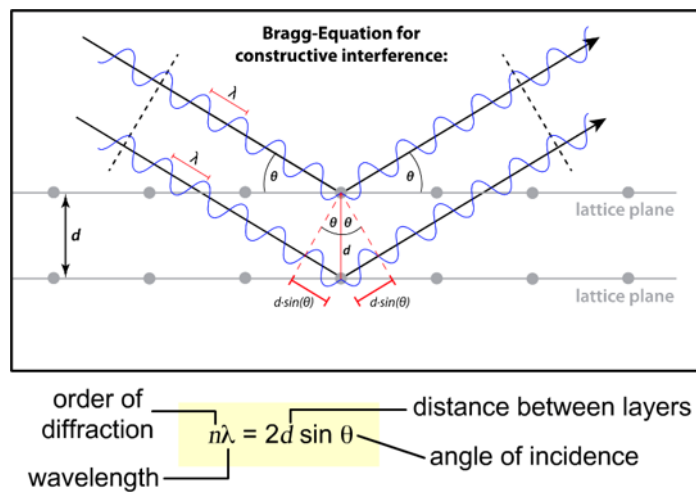


Figure 25. Diffraction schismatic in solid crystals as stated by Bragg's law for constructive interference; adapted from Ref [285].

#### 2.4.5 Zeta Potential Analysis

The zeta potential ( $\xi$ ) was determined using a SurPASS Electro kinetic Analyzer (Anton Paar KG, Austria). SurPASS is used for solid surface charge analysis. The zeta potential parameter is an indicator of surface functionality, and it provides data on how the solid surface will interact with ions in liquids.

SurPASS (Fig.26) depends on the measurements of streaming current and streaming potential to determine the zeta potential. The measuring cell accommodating the solid specimen is circulated by a dilute electrolyte, thus generating a pressure difference. In the electrochemical double layer, a relative movement of charges takes place and begins the streaming potential. Electrodes are placed at both sides of the specimen, which detect the streaming potential or the streaming current. The pH value, electrolyte conductivity, and temperature are determined concurrently. SurPASS is used in many fields, including membrane and fillers, synthetic and natural fibers and textiles, polymer and composites, and mineral powders [286].



Figure 26. SurPASS Electro Kinetic Analyzer (Anton Paar KG, Austria).

#### *2.4.6 Brunauer-Emmett-Teller (BET) Accelerated Surface Area and Porosimeter*

##### *Analysis ASAP 2420*

Two important physical properties that can affect the quality and strength of solid materials are the surface area and porosity. Thus, the physical properties of materials with identical physical dimensions can reveal totally different actions if their physical surface areas are distinct. The measurement of the material's physical surface area is a basic analysis which is used in most industries, including the manufacture of catalysts, batteries, artificial bones, and metal powders for additive fabrication besides other numerous applications. The BET accelerated surface area and porosimeter analysis using the ASAP 2420 instrument (Fig.27) offers the accurate and specific surface area assessment of samples through nitrogen adsorption, calculated based on relative pressure. The material surface area is identified by calculating the quantity of adsorbed nitrogen gas according to a monomolecular layer on the material surface. To identify the total specific surface area, the approach involves both exterior area and pore area assessment. BET is utilized to identify a wide range of materials, including solid microporous, disperse and mesoporous materials.

BET is utilized to define a variety of dispersed and solid microporous to mesoporous materials. BJH utilizes adsorption-desorption approaches to characterize specific pore volumes and the pore area of the material. The pore size distribution can be calculated using the BJH method and it is independent of the exterior area due to sample particle size [287].



Figure 27. Micromeritics ASAP® 2420 Accelerated Surface Area and Porosimetry System.

#### *2.4.7 Water Contact Angle Analysis*

The water contact angles for the fabricated mixed matrix MXene at CA membranes were evaluated using a KRUSS Drop Shape Analyzer DSA25 (Fig.28) attached to an image analysis system and with a mounted video camera. By measuring the contact angles of polymeric membranes, hydrophobic and hydrophilic features can be verified.

Membrane performance, including membrane water flux, membrane rejection rate and membrane fouling properties, is affected by membrane hydrophilicity.

The KRUSS Drop Shape Analyzer DSA25 instrument is easy to handle and reliable for contact angle assessment with a wide range of methods from a

straightforward wetting test to the precise appraisal analysis of surface energy (SFE). This instrument offers flexible options for analyzing wetting and adhesion on solid surfaces [288, 289].



Figure 28. KRUSS Drop Shape Analyzer DSA25 equipped with a camera and photo analysis system.

#### 2.4.8 Atomic Force Microscope (AFM)

The surface topologies of the fabricated membrane were described with regards to surface roughness/morphology using an Asylum Research MFP-3D Origin+ Atomic Force Microscope (AFM) (Fig.29). Atomic force microscopy is considered as the most adaptable and effective microscopy technology for examining specimens at the nanoscale. In addition, AFM can reveal images with three-dimensional topography and can perform the various surface measurements required by engineers and scientists. AFM is able to produce images with a very fine (angstrom) scale resolution height data, with simple sample preparation [290].

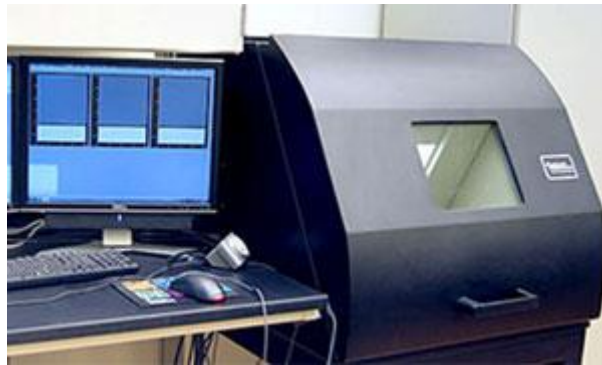


Figure 29. Asylum Research MFP-3D Origin+ Atomic Force Microscope

#### 2.4.9 *Thermogravimetric Analysis*

Thermogravimetric analysis (TGA) using a thermogravimetric analyzer (TGA 4000 – Perkin Elmer; Fig.30) is an essential thermal analysis approach that helps in detecting the change of mass based on time or temperature. This important evaluation is commonly used in the research and development of numerous materials to characterize the composition and thermal stability of these materials.

Lately, TGA has primarily been utilized by polymer processing manufacturers in quality control and assurance in terms of raw materials and innovation as well as the failure analysis of products. TGA offers complementary and supplementary characterization information to differential scanning calorimetry (DSC). TGA can offer in-depth data on materials to aid the researcher in characterizing and understanding their nature. International standards define the basic principles of TGA for polymers, such as ISO 11358, and TGA technique for the compositional analysis of rubber (ASTM D6370). TGA can offer vital measurement data, including mass changes, multicomponent composition materials, decomposition, oxidation or reduction behavior, filler content, product lifetime, temperature stability, moisture content and thermos-kinetic analysis [291].



Figure 30. Thermogravimetric analyzer (TGA 4000 – Perkin Elmer)

#### *2.4.10 Differential Scanning Calorimetry*

Differential scanning calorimetry (DSC) using a differential scanning calorimeter (DSC 8500 - Perkin Elmer) (Fig.31) is an effective applied thermal analysis approach. DSC is used to examine any energetic impact on a solid or liquid that may be revealed through thermal treatment. DSC permits heat to pass into and through the specimen, which is tested together with the reference, and the heat is analyzed in terms of temperature. The tested sample at first undergoes an endothermic reaction (heating), then is kept at a fixed temperature. After that, the sample is cooled down and undergoes an exothermic reaction. After those two cycles, the DSC instrument shows the amount of heat released and absorbed by the sample material.

DSC provides very substantial data for upgrading polymers, such as thermophysical properties (specific heat), advanced material analysis, thermo-kinetics, and process and product data. The process and product information include thermomechanical history failure analysis and product characterization and



identification, including the melting and crystallization temperatures, glass transition temperature, and enthalpy of crystallinity [292].



Figure 31. Differential scanning calorimetry: (DSC 8500 - Perkin Elmer)

## 2.5 Dead-end and Crossflow Filtration

Filtration technologies used in manufacturing processes can be categorized under two aspects, namely conventional DE filtration (Fig.32) and CF filtration (Fig.33).

The DE filtration process is one in which the transport of the feed is perpendicular to the surface of the membrane and the feed is pushed across the membrane under pressure. This is unlike CF as all the feed solution is transported across as the permeate and there is no rejected solution. The benefits of DE filtration are high product recovery and easy operation. However, the internal pores in cartridge filters

usually become blocked and are then discarded because they cannot be backwashed or clean. On the other hand, in CF processes, the feed is transported tangentially under pressure across the surface of the membrane. Large suspended foulants stay on the retentate side, but foulants smaller than the pores of the membrane go through

In addition, CF is a unique process because the concentrated feed flows across the surface of the membrane with minor foulant accumulation, while maintaining a steady low flow resistance. In addition, membranes in the CF method are an unconsumable part. CF is mostly used in wastewater filtration applications. The turbulence produced across the surface of the membrane during CF offers optimal permeation flux performance and extends filter functionality. The differences between the two filtration processes are presented in the schematic below (Fig.34)

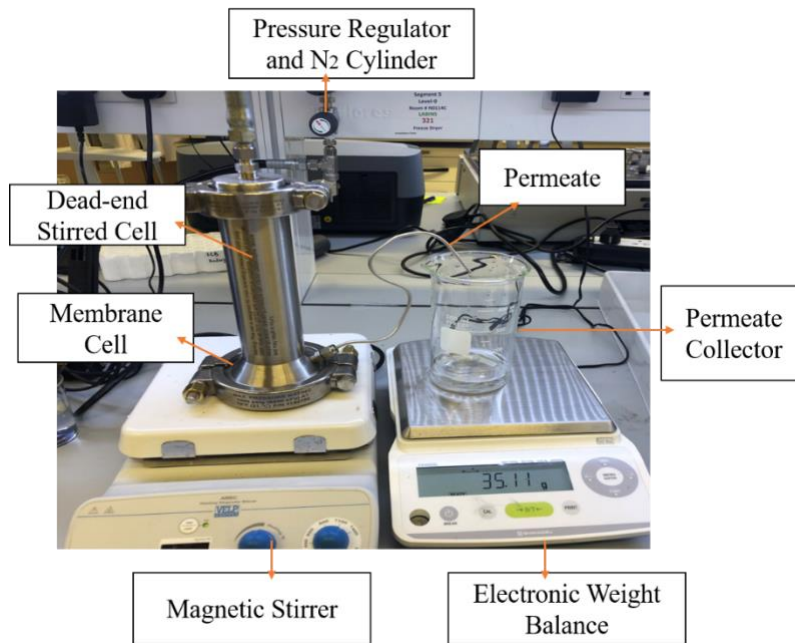


Figure 32. Dead-end filtration process setup.

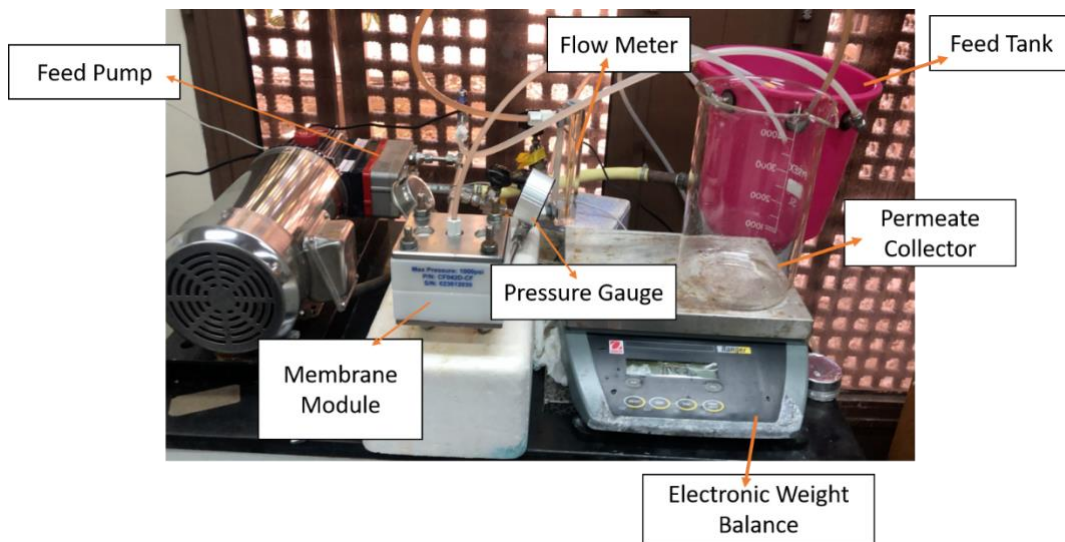


Figure 33. Cross flow filtration process setup.

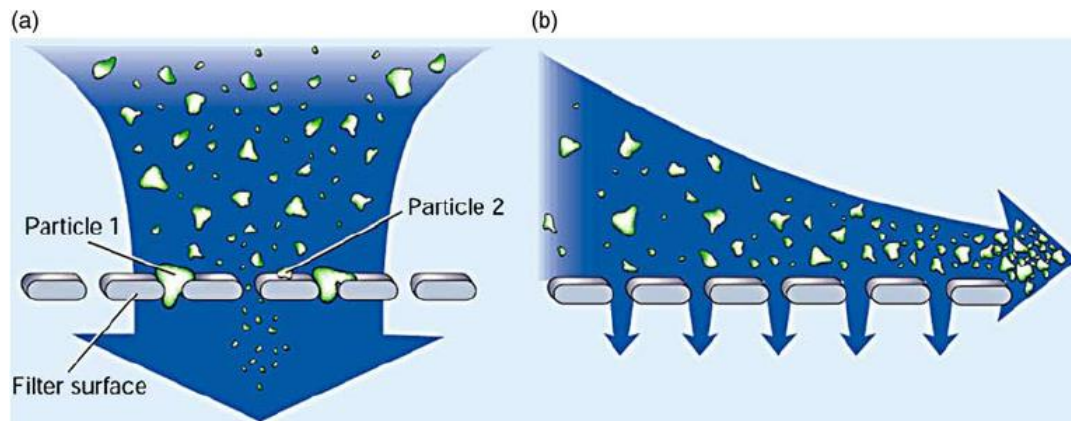


Figure 34. Schematic representation of (a) the dead-end filtration principle and (b) the CF principle; taken from Ref [291].

### 2.5.1 Water Uptake and Membrane Porosity Studies

Water uptake (WU) represents the water content in a fabricated membrane. In this study, it was computed by determining the membrane weight under two different conditions, namely the dry (under vacuum) condition and the wet condition, which were equilibrated in DI water for a period of 24 hours. More accurately, square pieces of the membrane samples were dipped in distilled water for 24 hours, and the weight of the wet samples was recorded from the balance after removing the superficial water. Then, the membrane samples were dried at 60 °C under a vacuum and the weight was constantly documented until a fixed weight was shown for the same sample; thus, the dry membrane weight was confirmed and recorded.

The following equation (eq.1) was utilized to identify the percentage of WU of the membrane.

$$\text{Water uptake (\%)} = \frac{W_{wet} - W_{dry}}{W_{dry}} \times 100 \quad (1)$$

where  $W_{dry}$  and  $W_{wet}$  denote the membrane weight prior and after water absorption, respectively. To evaluating the membrane porosity, recognized area and weight, the dry membrane samples were submerged in DI for a period of 24 hours. After using filter paper to remove superficial water, the wet membrane was evaluated.

Membrane porosity was measured using the equation (eq.2) below.

$$\text{Porosity (\%)} = \left( \frac{W_{wet} - W_{dry}}{Ad\rho} \right) \quad (2)$$

where  $W_{wet}$  and  $W_{dry}$  denote the wet and dry weight conditions of the membranes, respectively.  $A$  indicates area,  $d$  denotes thickness, and  $\rho$  is the density of water (1 ppm or 1 mg/L).

### 2.5.2 Membrane Flux, Rejection Rate, Pore Radius Measurements, and

#### MWCO

The separation effectiveness of the fabricated membranes was assessed first, using a DE filtration setup (Fig.32) (HP4750 Stirred cell, STERLITECH, WA, USA) with an effective filtration area equal to 9.60 cm<sup>2</sup>, and second, using CF (Fig.33) with an effective filtration area equal to 42 cm<sup>2</sup>.

The water flux ( $J_w$ ) of the fabricated membrane was assessed by estimating the water permeation flow as a function of a volume or mass of permeate solution per area per time per applied pressure ( $Lm^{-2}h^{-1}bar^{-1}$ ), applying the following equation (eq.3):

$$J_w = V/AtP \quad (3)$$

where  $V$  denotes the quantity (volume/mass) of permeation,  $A$  indicates the effective surface area ( $m^2$ ),  $P$  is the applied pressure in bar, and  $t$  denotes the time in hours of the prepared membranes.

A feed solution stream comprising 2000 mg L<sup>-1</sup> salts (NaCl, MgCl<sub>2</sub>, and Na<sub>2</sub>SO<sub>4</sub>), 100 mg L<sup>-1</sup> MG, and 150 mg L<sup>-1</sup> BSA was utilized to calculate the membrane rejection rate.

The rejection (R) equation (eq.4) for solutes was calculated as follows:

$$R (\%) = \frac{C_f - C_p}{C_f} \times 100 \quad (4)$$

where  $C_f$  and  $C_p$  denote the concentration of the feed and permeate solutes in mg/L, respectively. The effective pore diameter ( $a$ ) of the prepared hybrid NF membranes was measured via the Ferry equation (eq. 5), as shown below [293]:

$$R = 100[1 - (1 - r/a)^2]^2 \quad (5)$$

$R$  indicates the solute rejection rate (%) and  $r$  refers to the diameter of the solute. The MWCO of the fabricated membrane is the molar mass of the solutes which are 90% rejected by the membrane. Plotting the rejection (%) of the solute against their corresponding molar mass in Dalton allows the MWCO to be calculated [32].

### 2.5.3 Antifouling Performance Evaluation

The membrane was tested with pure water at 1 bar for 30 min, then the flux was recorded as  $J_{w0}$  ( $L m^{-2} h^{-1}$ ). After that, the pure water was replaced with BSA solution consisting of 500 ppm and with a pH=7 at 1 bar; the flux was recorded after 1 hour ( $J_p$  ( $L m^{-2} h^{-1}$ )) and the rejection was analyzed and measured using UV. The membrane was washed with pure water for 30 minutes with no pressure and with the same CF

velocity. Next, the membrane was operated at 1 bar with pure water for a period of 30 mins and then the flux was recorded ( $J_{w1} (L m^{-2} h^{-1})$ ), indicating the end of one cycle. This was done to evaluate the antifouling property of CCAM-10%.

The flux recovery ratio (FRR) was characterized as follows (eq. 6):

$$FRR = \left( \frac{J_{w1}}{J_{w0}} \right) \times 100\% \quad (6)$$

To accurately determine the fouling processes, resistance ratio measurements were applied to characterize the fouling resistance potential of the mixed matrix CCAM-10%. Resistance during the filtration process may indicate membrane fouling.

The total fouling ratio was computed by applying the following equation (eq.7):

$$R_t(\%) = \left( 1 - \frac{J_p}{J_{w0}} \right) \times 100\% \quad (7)$$

Where  $R_t$  denotes the total flux reduction, which is produced by the overall fouling and is known as the sum of the reversible fouling ratios; this describes the fouling resulting in concentration polarization. The irreversible fouling ( $R_{ir}$ ) signifies fouling caused by BSA molecule adsorption to the surface of the membrane;  $R_r$  is the reversible fouling ratio. The below equations (eq.8 and eq.9) are used to calculate the reversible and irreversible fouling ratios, respectively [294].

$$R_r(\%) = \left( \frac{J_{w1} - J_p}{J_{w0}} \right) \times 100\% \quad (8)$$

$$R_{ir}(\%) = \left( 1 - \frac{J_{w1}}{J_{w0}} \right) \times 100\% = R_t - R_r \quad (9)$$

## CHAPTER 3: RESULTS AND DISCUSSION

### 3.1 Structural Characterization and Surface Morphology of Chemically Cross-linked MXene At CA Mixed Matrix Nanoporous Membranes

MXene was synthesized using the acid (LiF/HCL) etching of the precursor MAX ( $Ti_3AlC_2$ ) to eliminate the aluminum layer, followed by ultrasonication to produce ML-MXene and DL-MXene, respectively. As we published recently [295] [129], “both ML-MXene and DL-MXene were described using SEM and XRD analysis. Fig.35 (a) reveals the SEM surface morphology of ML-MXene, which can be described as a dense and compact MXene sheet with an accordion-like morphology. The XRD spectra verified the elimination of the Al atoms from the MAX ( $Ti_3AlC_2$ ) precursor (Fig.3(b)&(d)). There are two major representative peaks in the MAX phase ( $Ti_3AlC_2$ ) at  $2\theta \sim 9.6^\circ$  and  $39^\circ$ , which correspond to the (002) peak and the Al atom, respectively [129].

The XRD pattern of the ML-MXene (Fig.35(b)) showed a broadening and negative shift of the characteristic MXene peak (002) towards a lower angle ( $2\theta = \sim 8.3^\circ$ ). This was due to the elimination of the Al layer, which is replaced by the MXene terminating group (OH, F, and/or O), as well as the structural enlargement as a result of the MAX etching process, which leads to a higher c-lattice parameter [147, 296]. Besides, Fig.21(b) shows that the most intense peaks of the MAX phase decreased, thereby confirming the successful etching of the MAX phase. The delamination of ML-MXene by ultrasonication changes the dense ML-MXene into separated single-layered sheets (wrinkled flakes), showing the effective delamination of MXene, as demonstrated in SEM (Fig.35 (c)) [297] [298]. Besides, the (002) peak shifts more towards a smaller angle ( $2\theta = \sim 7.40^\circ$ ) as a consequence of the increasing c-lattice parameter [299], while the characteristic MAX phase peaks at  $39^\circ$  and  $9.6^\circ$  virtually



vanished, which is typical of  $Ti_3C_2T_x$ , as verified from the XRD patterns (Fig.35 (d)) [1, 296].

Figure 36 describes the XRD, whereby the broad characteristic peaks of pristine CA were detected ( $2\theta = \sim 16^\circ, 30^\circ, \text{ and } 41^\circ$ ), signifying a non-crystalline configuration and an amorphous nature [300]. As revealed in Fig.36, the characteristic peak of CA is still observed in the CCAM-10%, while the (002) DL-MXene diffraction peak moves by  $\sim 2^\circ$  to a smaller angle ( $2\theta = \sim 5.6^\circ$ ) (Fig.36) [129]. The interlayer spacing inside the stacked DL-MXene in the bare MXene and CCAM-10% was computed as 3.66 Å and 6.64 Å, respectively. Therefore, MXene exhibited a high interaction with CA after introducing the 2D MXene sheets (2%-10%) into the CA mixed matrix. This confirms the good dispersion of MXene into the CA polymer matrix (Fig.36) and proves that the CA chains intercalated reasonably with the MXene sheets. Moreover, CCAM-X% is characterized by broad peaks (002) at  $2\theta = \sim 10^\circ, \sim 18^\circ \text{ and } \sim 23.5^\circ$  (Fig.23) [300].

The (002) diffraction peak moved toward a smaller angle in CCAM-10% as a result of the greater dispersion of MXene sheets along with the CA polymeric matrices [61]. This signifies that the MXene sheets had a stable nature among the CA polymeric mixed matrix with  $CH_2O$  crosslinking.

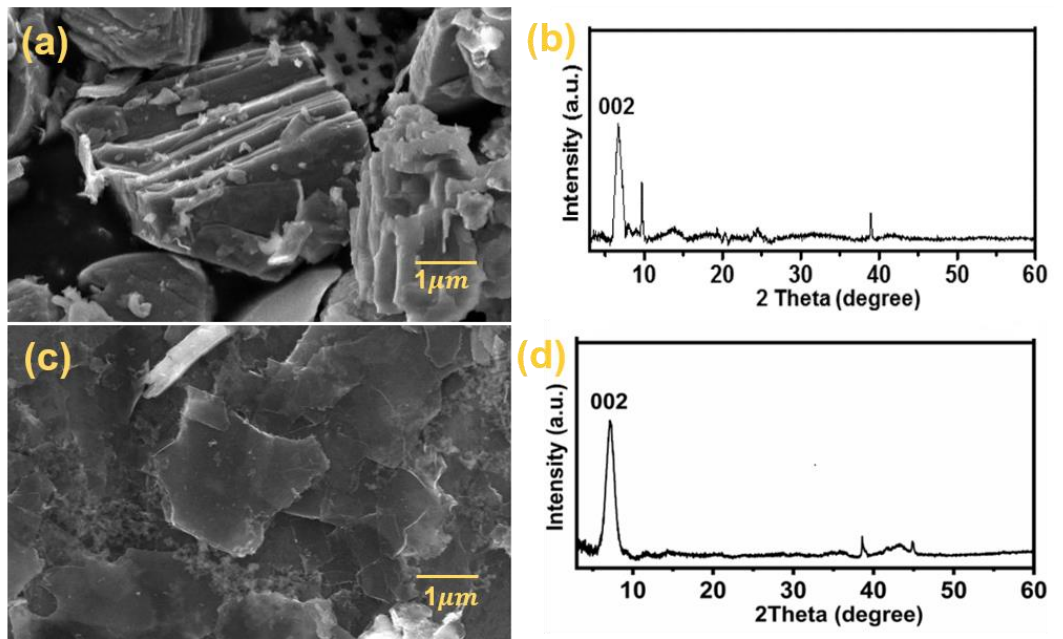


Figure 35. (a) SEM image of the ML-MXene surface morphology; (b) XRD ML-MXene spectrum; (c) SEM image of the DL-MXene surface morphology; and (d) XRD DL-MXene spectrum

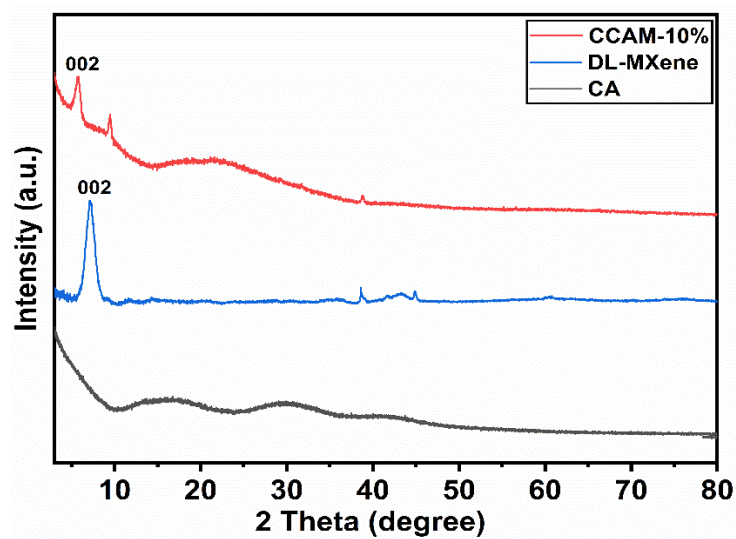
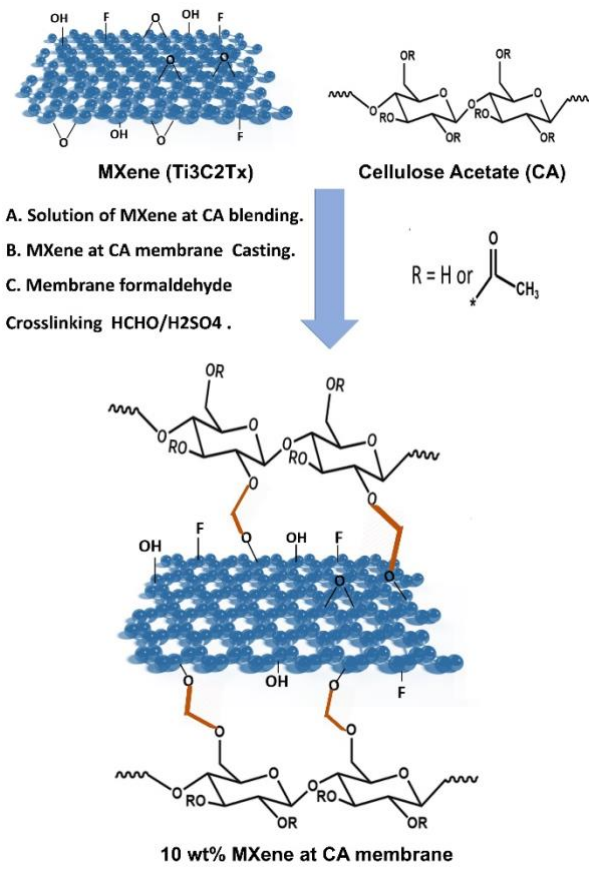


Figure 36. XRD model of CA, DL-Ti<sub>3</sub>C<sub>2</sub>T<sub>x</sub> and CCAM-10%

$\text{Ti}_3\text{C}_2\text{T}_x$  (MXene) is characterized by surface functional groups (OH and -O-) that allow it to disperse extremely well in water and also provide a reactive site to allow  $\text{CH}_2\text{O}$  crosslinking. This facilitates the preparation of MXene/CA MMMs [301]. As we published recently [146], “a chemically crosslinked CA at  $\text{Ti}_3\text{C}_2\text{T}_x$  (MXene) membrane was fabricated by casting a composite membrane comprising 0-10 wt.% DI-MXene with CA and then cross-linking it with  $\text{CH}_2\text{O}$ ”. The detailed membrane fabrication steps are described in scheme 1. As we published previously [147], “The MXene (-OH and -O-) and CA (-OH) surface terminal groups are expected to react with  $\text{CH}_2\text{O}$  to create -O-C-O- bonding [32, 147, 302]. Moreover, a self-crosslinking is expected among the CA particles. However, here we have a low content (between 0% and 10%) of MXene in the membrane phase, and the MXene is homogeneously dispersed in the CA matrix. Thus, there is no realistic way to create self-crosslinking among the MXene particles. FTIR spectra were performed to trace the functional groups of the fabricated DL- $\text{Ti}_3\text{C}_2\text{T}_x$  (MXene) and CCAM-10% (Fig.8 & Fig37). The absorption peaks of DL-MXene were found at  $\sim 1085$ ,  $\sim 1634$  and  $\sim 3411$  (broad band)  $\text{cm}^{-1}$  and were assigned to the C-F group, absorbed external water, and stretching vibration of the strongly hydrogen-bonded OH group in the MXene, respectively [279].

The CCAM-10% FTIR spectrum reveals a wide absorption group at  $\sim 3376$   $\text{cm}^{-1}$ , which is assigned to the stretching vibration of strong hydrogen-bonded OH groups related to the MXene and CA groups. Meanwhile, the absorption peak at  $\sim 1733$   $\text{cm}^{-1}$  is the typical peak of CA, which corresponds to the carbon-oxygen double bond (C=O) related to the ester group stretching vibrations [144]. The two absorption peaks at  $\sim 1373$  and  $\sim 1229$   $\text{cm}^{-1}$  were assigned to the CA symmetric C-H and C-O stretching vibration groups, respectively”.



Scheme 1. Anticipated reaction path for the fabrication of crosslinked 10 wt.% MXene at CA nanoporous MMM

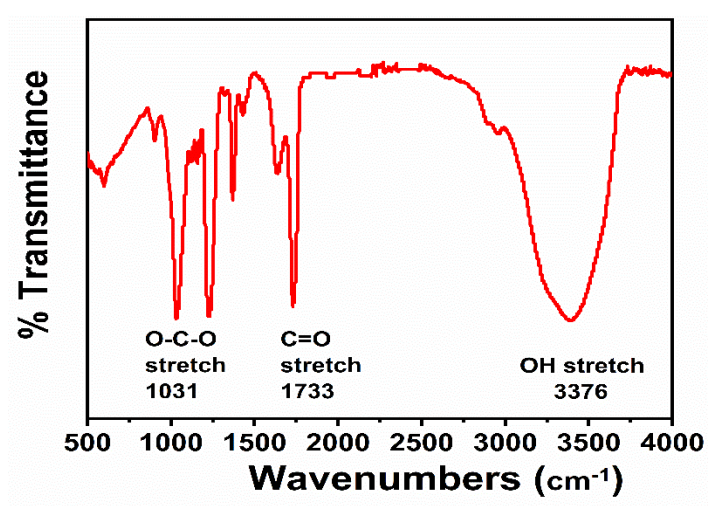


Figure 37. FT-IR spectra for the CCAM-10% membrane.

SEM was used to study the two kinds of fabricated membranes, including the crosslinked CA membrane (CCAM-0%) and the crosslinked MXene at CA membrane (CCAM-x%), whereby X% denotes the wt.% of MXene to CA in the membrane. MXene loadings of 0%, 2%, 4%, 6%, 8%, 10% and 12%, here expressed as CCAM-0%, CCAM-2%, CCAM-4%, CCAM-6%, CCAM-8%, CCAM-10% and CCAM-12%, respectively, were fabricated and evaluated using SEM and XRD analyses. The SEM morphologies, including the surface and cross-sections are explained in Fig.38. CCAM-0% revealed a dense structure with observed nanopores (Fig.38(a)&(e)). The surface SEM morphologies of CCAM (0-10%) indicate a homogeneous surface with no major surface defects (Fig.38(a-d)).

As predicted, the “MXene (–OH and –O– surface-terminal groups) and CA (–OH group) can form a homogeneous structure that permits a good dispersion of MXene in the CA polymeric matrix, leading to a smooth membrane surface morphology [129]. The homogenous dispersion and compatibility of the MXene 2D sheets in the CA polymer mixed matrix were proved by SEM (cross-section) images. All prepared membranes showed a comparable finger-like pore morphology due to the PI method used in their manufacture [303, 304]. Loading more MXene content into CCAM did not have a major effect on the finger-like pore configuration of CCAM-0% until CCAM-8% (Fig.38(e-g)). However, the surface and cross-section morphology of CCAM-10% differed in that it had a denser structure with disordered channel arrangements, probably attributable to the condensation on the MXene sheets in the channels and chemical cross-linking among MXene and CA [32, 305]. Introducing MXene into CCAM is anticipated to improve membrane hydrophilicity and enhance membrane fouling resistance[129].

All the CCAM-X% variants were studied by XRD to illustrate the effect of the

distribution of the 2D MXene sheets into the CCA polymer matrix (Fig.39). CCAM-0% is characterized by (002) diffraction peaks at  $2\theta = \sim 23^\circ$  and  $30^\circ$  [303]. The DL-MXene (002) diffraction peak is spotted at  $2\theta = \sim 6.9^\circ$ . MXene showed great interaction with CA because loading MXene into the CA matrix leads to a shift of the (002) MXene diffraction peak by  $2^\circ$  to a smaller angle [301]. This shows that membrane material crystallinity is influenced by the amorphous nature related to the polymeric material and the MXene crystalline nature that causes this shift. Likewise, the (002) diffraction peak movement in the direction of smaller angles after introducing MXene content into the CA matrix is due to a greater dispersion of the MXene sheets along the CA matrices [300]. Furthermore, the formation of a  $\text{Ti}_3\text{C}_2\text{T}_x$  (MXene)/CA hybrid membrane is also proved as the CA chains intercalated among the MXene sheets are held [152]. EDS mapping analysis (cross-section) verified the good dispersion of the MXene into the CA membrane matrix (Fig.40(a-c)), as shown by the good distribution of titanium molecules in various MXene contents (CCAM-X%). The good dispersion of the MXene content into the composite CA membrane helps to maintain favorable hydrophilicity, thereby generating a superior permeation flux and developing membrane fouling resistant properties throughout the separation process [152] [306].”

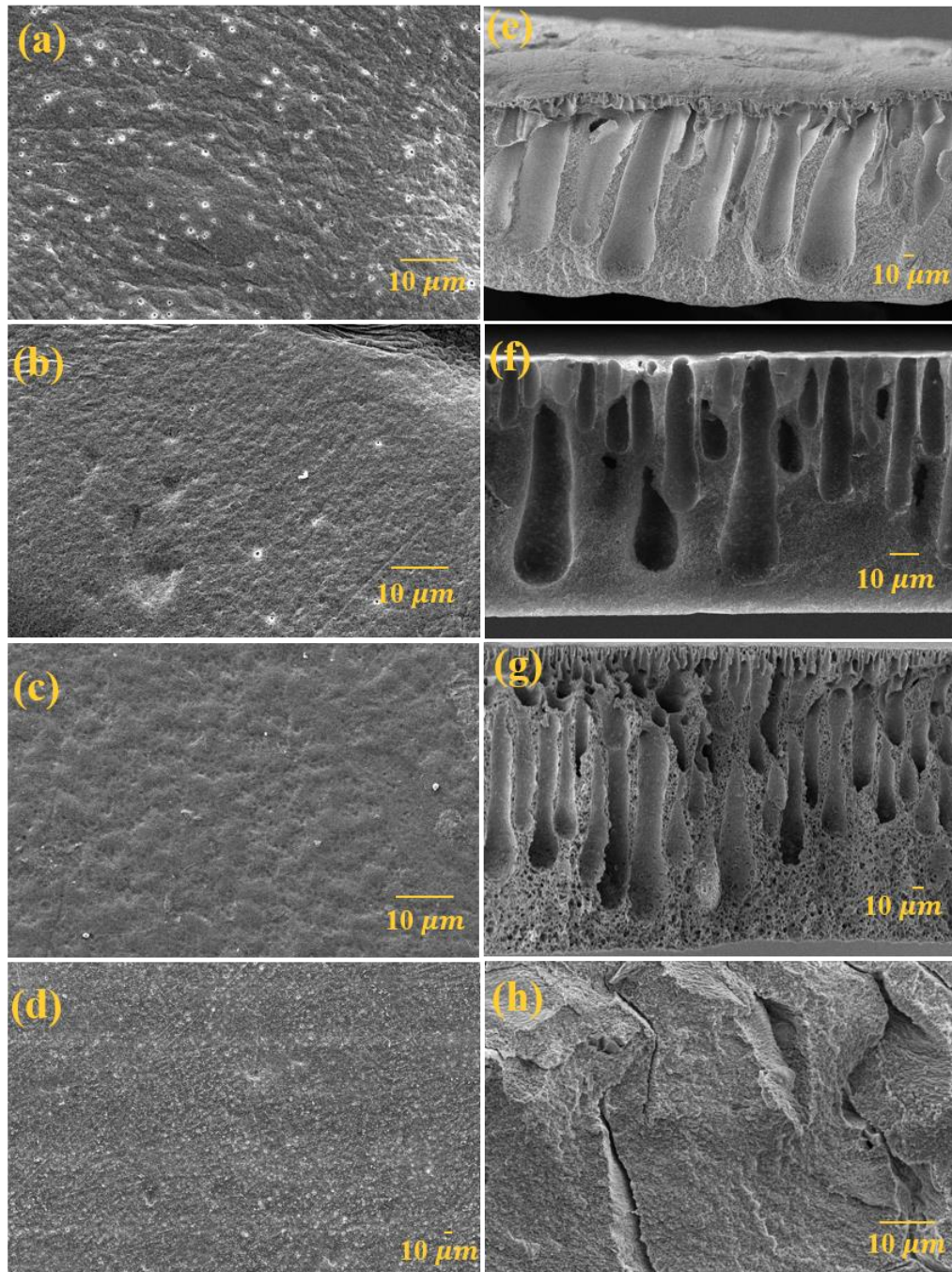


Figure 38. SEM pictures of the prepared membranes: (a) Surface CCAM-0% showing a dense structure; (b) surface CCAM-2%; (c) surface CCAM-8%; (d) surface CCAM-10% presenting a reduction in pore size after introducing MXene into the CA matrix; (e) cross-section of CCAM-0% displaying a dense structure; (f) cross-section of CCAM-2%; (g) cross-section of CCAM-8%; and (h) CCAM-10% cross-section showing a dense structure.

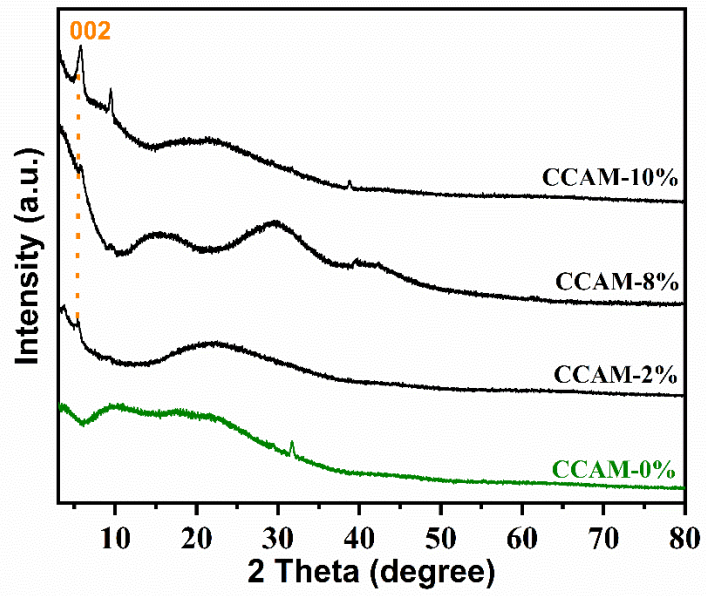


Figure 39. XRD of crosslinked cellulose acetate MXene membranes



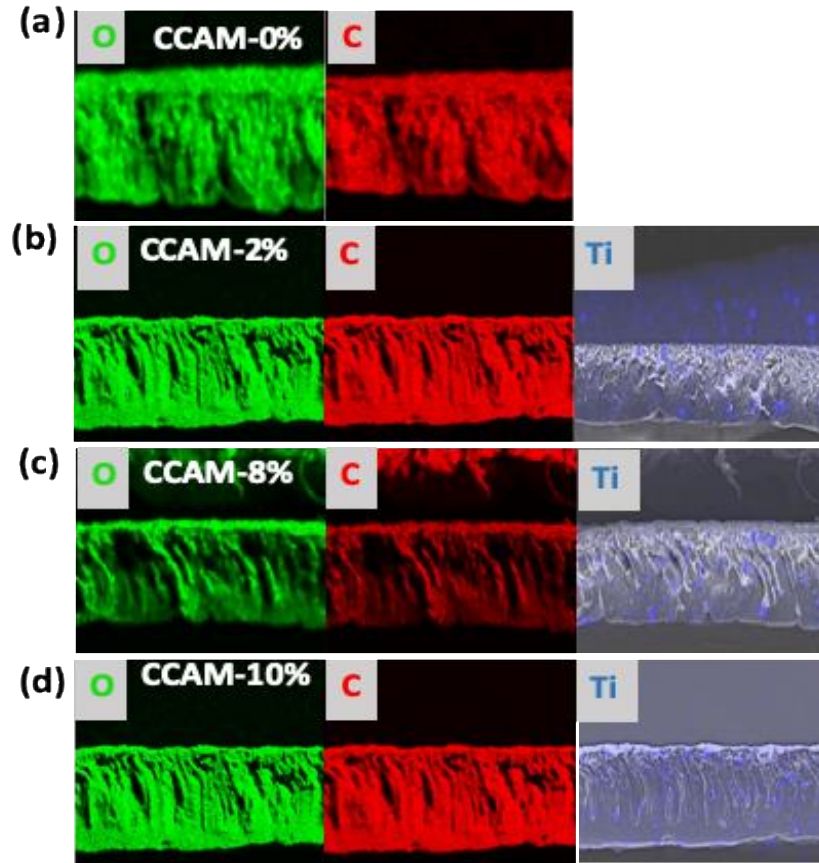


Figure 40. EDS cross-section mapping analysis images for (a) CCAM-0%, (b) CCAM-2%, (c) CCAM-8%, and (d) CCAM-10% .

### 3.2 Contact Angle Measurements and Surface Topology of MXene At CA MMMs

Contact angle measurements are fundamental physical properties for a membrane that can indicate its hydrophilicity and fouling tendency. The favored membrane hydrophilicity is characterized by a lower water contact angle, which leads to having better water flux and superior fouling resistance [129, 307].

Water contact angles of  $71.3^\circ$ ,  $63.3^\circ$ ,  $61.5^\circ$ ,  $56.8^\circ$ ,  $50.8^\circ$  and  $48.6^\circ$  for CCAM-0%, CCAM-2%, CCAM-4%, CCAM-6%, CCAM-8% and CCAM-10%, respectively, are tabulated in Fig.41. The water contact angle reduced from  $71.3^\circ$  for CCAM-0% to

48.6° for CCAM-10% with the introduction of MXene into the CA membrane matrix, which is attributed to the good hydrophilic characteristic of MXene [308].

The contact angle results (Fig.41) showed the enhancement of the membrane surface hydrophilicity with increasing MXene grafting in the CA matrix. CCAM-10% has the highest hydrophilicity and is considered as the optimal membrane composition. Atomic force microscopy (AFM) was utilized to inspect the surface roughness of the crosslinked mixed matrix composite membranes. The AFM images (Fig.42) of the membranes illustrate the lightest area, which indicates the maximum point of the membrane surface, while the dark area represents the lower topography or valleys of the membrane pores [129]. It should be noted that the membrane surface roughness changed due to the loading with MXene. The surface roughness of CCAM-0% (pristine membrane) is virtually free of any significant features [309].

However, there are small bumps distributed across the surface of CCAM-10%, which indicates that MXene has good compatibility with the CA mixed matrix [163, 310]. The most common surface roughness parameters obtained from the AFM analysis are average roughness (Ra) and root square roughness (Rq) [311]. The surface roughness parameters of CCAM-0% and CCAM-10% are tabulated in Table.5. As revealed from Fig.42(b) and Table 5, CCAM-10% (Ra=47.4 and Rq=60.2(nm)) had a rougher surface than CCAM-0% (Ra= 22.5and Rq= 28.4 (nm)) due to the hydrophilic nature of MXene, which may have caused faster solvent and non-solvent exchange throughout the PI [312]. This indicates the excellent adherence of MXene 2D-sheets to the membrane surface. Consequently, surface roughness can influence the membrane's water contact angle as the degree of roughness increases the hysteresis of wetting, thus a contact angle on a smoother surface is less than on

rough surfaces. However, in this study, as shown in Fig.41, the contact angles declined with the increase in membranes surface roughness. Moreover, surface roughness can impact the flux of the membrane, whereby a rougher surface offers a more open area for membrane transport and thus the permeation flux is enhanced with increased surface roughness [117].

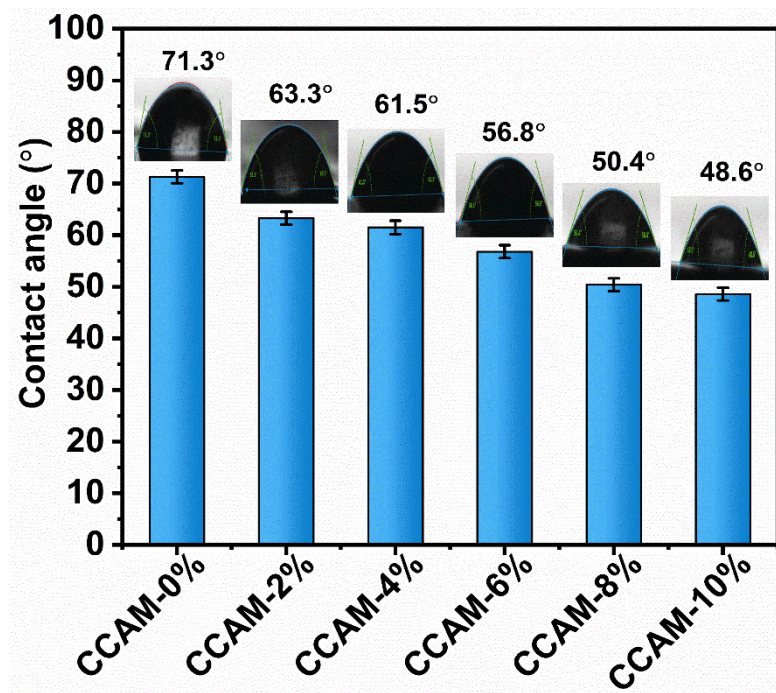


Figure 41. Water contact angle of cross-linked CCAM-X% with MXene contents (X) from 0% to 10%.

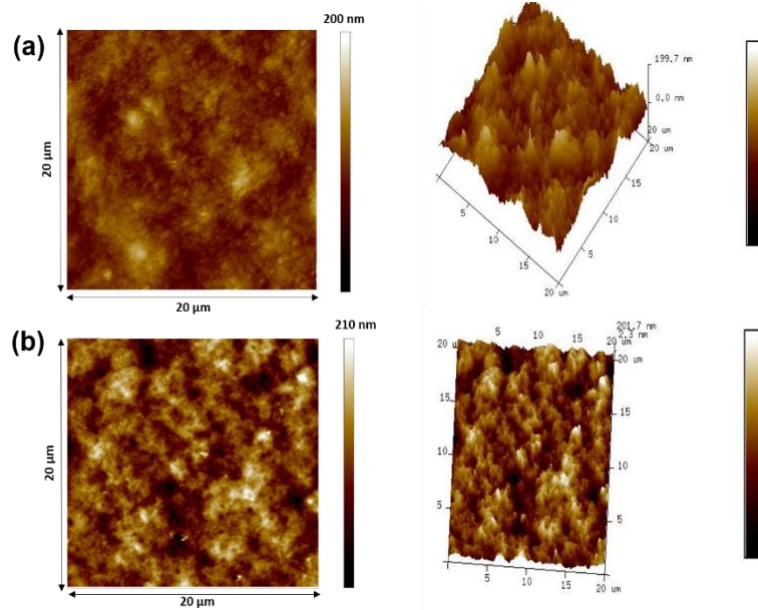


Figure 42. Atomic force microscopy (AFM) 2D and 3D images for (a) CCAM-0% and (b) CCAM-10%.

Table 5. Surface roughness parameters of CCAM-0% and CCAM-10%.

Membranes	CCAM-0%	CCAM-10%
Average roughness (Ra (nm))	22.5	47.4
Root square roughness (Rq (nm))	28.4	60.2

### 3.3 Membrane Thermal Stability

The thermal properties of the CAM-0%, CCAM-0%, CAM-10%, and CCAM-10% membranes were studied by TGA and the findings are shown in Fig.43. These demonstrate that the CA polymeric matrix began to decompose at  $T = \sim 270^{\circ}\text{C}$ . It was observed that all the membranes underwent three weight loss steps. The absorbed and water evaporation release in the membrane matrix (at temperatures up to  $\sim 150^{\circ}\text{C}$ ) is recognized as the first step. The second step can be assigned to the removal of stable oxygen functionalities and the decomposition of the polymer backbone (from  $T = 250^{\circ}\text{C}$  to  $375^{\circ}\text{C}$ ). The third step occurs at temperatures above  $375^{\circ}\text{C}$  and corresponds to the dissolution of the remaining carbon atoms from CA and MXene. The thermal stability of non-crosslinked membranes was significantly improved by the incorporation of MXene as the decomposition temperature rises to  $\sim 290^{\circ}\text{C}$ . Likewise, the thermal stability of CCAM-10% was further enhanced due to the chemical crosslinking of the membranes as the decomposition temperature changed to  $\sim 310^{\circ}\text{C}$  [313].

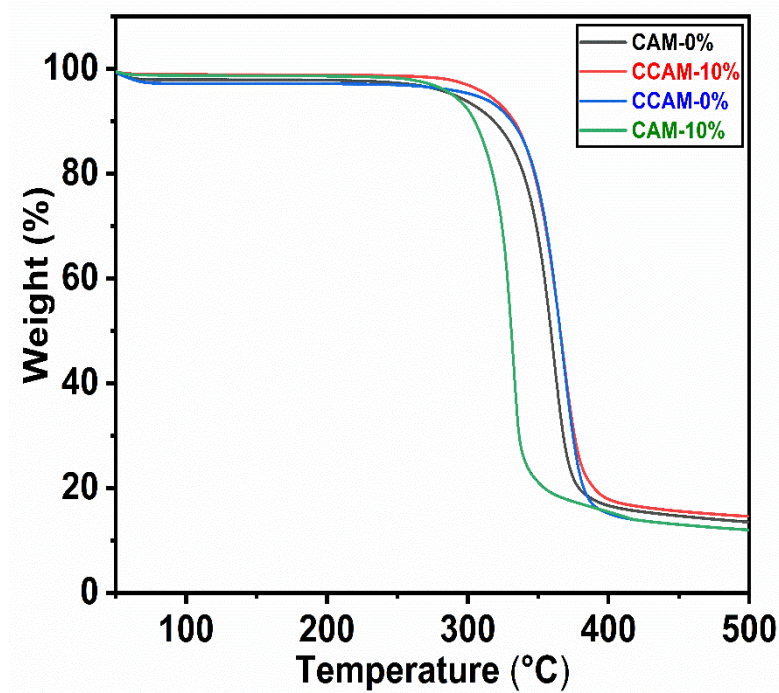


Figure 43. TGA of CAM-0%, CCAM-0%, CAM-10% and CCAM-10%.

### 3.4 Membrane Water Uptake, Porosity, MWCO, and BET Analysis

The WU and porosity values calculated for the CA MMMs with 0-10 wt.% crosslinked MXene are revealed in Fig.44 (a) and Fig.44(b), respectively. The void volumes and hydrogen bonds inside the MMM form an ionic band that has a direct relationship with WU and porosity of the membrane [129]. Fig.44(a&b) shows that there is an increasing trend between the MXene content and WU and porosity for all crosslinked CA at MXene MMMs. The porosity of CCAM-0% equals 58.2% and it increases with MXene loading to 60.11%, 63.4%, 64.12%, 67.23% and 72.3 for CCAM-2%, CCAM-4%, CCAM-6%, CCAM-8% and CCAM-10%, respectively.

In comparing CCAM-10% with CCAM-0%, the results show a ratio of 1.46 WU for CCAM-10% (125.3%) to the CCAM-0% (85.8%) and porosity ratio of 1.24 for CCAM-10% (72.35%) to the CCAM-0% (58.2%).Table 6 summarizes the BET

specific surface area, average pore diameter, and pore volume values for CCAM-0% and CCAM-10% measured by nitrogen adsorption. The specific surface area of CCAM-0% was 44.27 m<sup>2</sup>/g and it increases significantly for CCAM-10%, reaching 124.3 m<sup>2</sup>/g. This means that incorporation of MXene into the CA polymer matrix improves the membrane surface, thus enhancing the membrane adsorption sites. Therefore, it offers an ideal way to attract the target effluents and consequently enhance the adsorption rate. A comparable increasing profile is observed in the case of the pore volume, although there is a dramatic decrease in the mean pore size from 12.83 nm for CCAM-0% to 1.91 nm for CCAM-10%, whereby the porosity of the membrane increases by a ratio of 1.24 Fig.44 (b). By using (eq.5), the optimum CCAM-10% mean pore diameter is computed and found to be ~1.73 nm.

The MWCO of the fabricated membrane is known as the molar mass of the solutes that represent 90% of the membrane rejections and based on the membrane rejection (%), the values of solutes are plotted against their corresponding molar mass (Dalton) [129]. The MWCO of the optimal CCAM-10% can be determined from Fig.45 to be around 435 Dalton at a rejection of 90%.

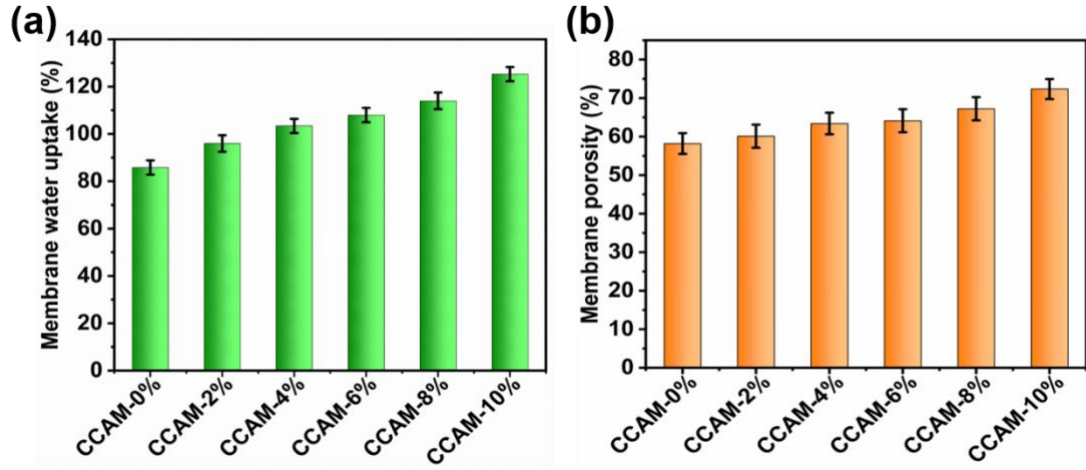


Figure 44. (a) Water uptake and (b) porosity of CCAM at different MXene contents (0-10 wt.%).

Table 6. BET surface area, mean pore diameter, and pore volume of CCAM-0%, and CCAM-10%.

Membrane	Specific surface area (m <sup>2</sup> /g)	Mean pore diameter (nm)	Adsorption micro-porous volume (cm <sup>3</sup> /g)
CCAM-0%	44.27	12.83	0.284
CCAM-10%	124.3	1.910	0.781



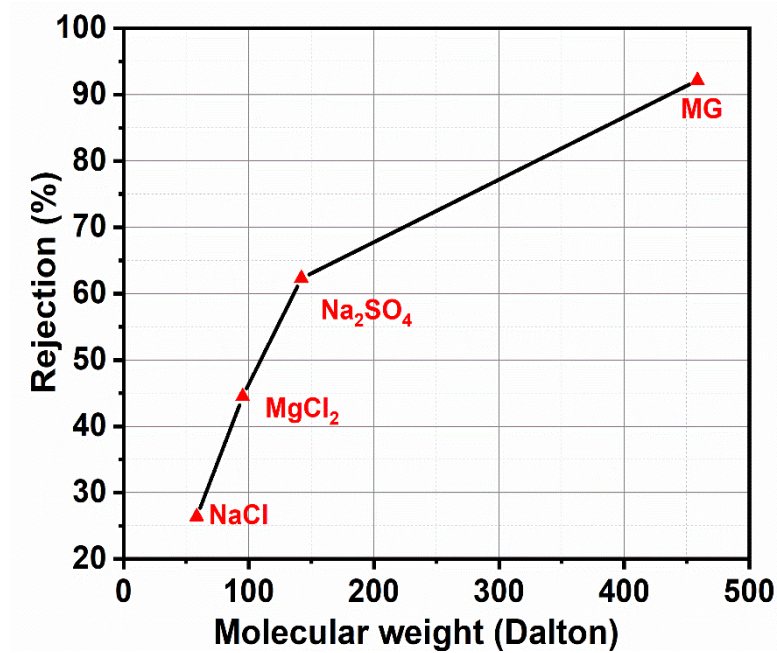


Figure 45. Molecular weight cut-off (MWCO) trend of CCAM-10%

### 3.5 Membrane Separation Performance

The permeation flux and rejection performance of the prepared CCAM (0-10%) was tested using the CF and DE techniques. It is important to start the experiments using lab-scale DE, which is easy to use and gives a good indication of the membrane performance with lower energy consumption compared to other filtration technique. Furthermore, it offers good quality products and is better than other conventional technique, ensuring a 100% elimination of total suspended solids (TSS). It also has a minor footprint compared to other filters, such as media or CF membrane filtration, produces potable water in a single step and provides a complete blockade against microbiological organisms [314, 315]. However, the DE mode is usually employed in

MF for sterilization and clarification with a quite clean feed solution. However, in the majority of applications, the buildup of rejected species is very harsh, meaning DE filtration becomes unfeasible and a CF operation must be employed. In the CF mode, the flow is tangential, which helps to remove the accumulated rejected particles or molecules at the surface of the membrane. This reduces the cake layers and thus maintains a good permeate flux. Also, CF offers the value of an improved membrane lifetime by preventing irreversible fouling [316].

In this work, the DE filtration mode was used first to evaluate the membrane water flux and rejection performance. Subsequently, the CF filtration mode was adopted to test the membrane separation and antifouling performance in terms of a better fouling resistance that can withstand a severe environment.

The separation effectiveness of the prepared membranes was estimated using a DE filtration setup (Fig.32) (HP4750 Stirred cell, STERLITECH, WA, USA ) with an effective filtration area of 9.60 cm<sup>2</sup> and using CF filtration (Fig.33) with an effective filtration area of 42 cm<sup>2</sup>. The water flux ( $J_w$ ) of the membranes was calculated using (eq.3), and the feed solution stream comprising 2000 mg L<sup>-1</sup> salts (NaCl, MgCl<sub>2</sub>, and Na<sub>2</sub>SO<sub>4</sub>), 100 mg L<sup>-1</sup> MG, and 150 mg L<sup>-1</sup> BSA was utilized to calculate the rejection performance of the fabricated membranes using (eq.4) for a 1 h in each experiment. According to the work done by our group, CCAM-10% with a thickness of 123 μm and 60 min CH<sub>2</sub>O crosslinking are the best conditions for achieving excellent separation performance (Fig.10-13) [317].

The impact of MXene loading and CH<sub>2</sub>O crosslinking on the separation efficiency was calculated with respect to the permeation flux and rejection rates

(Fig.46(a)). A commercial CA membrane (CMCA) (Omni pore™ with a pore size of 0.2 micrometers) was tested using DE filtration and was found to have the highest water flux of  $315.99 \text{ L m}^{-2} \text{ bar}^{-1} \text{ h}^{-1}$ ; however, it is very close to the water flux found for CCAM-12% ( $272.96 \text{ L m}^{-2} \text{ bar}^{-1} \text{ h}^{-1}$ ) and CCAM-10% ( $253.57 \text{ L m}^{-2} \text{ bar}^{-1} \text{ h}^{-1}$ ) and all were tested by DE filtration. Noticeably, the water flux of membranes which were tested by DE filtration (Fig.46(a)) improved gradually with the introduction of MXene from CCAM-0% ( $138.44 \text{ L m}^{-2} \text{ bar}^{-1} \text{ h}^{-1}$ ) to CCAM-12% ( $272.96 \text{ L m}^{-2} \text{ bar}^{-1} \text{ h}^{-1}$ ) due to the hydrophilic nature of MXene and the formation of extra nanopores [129].

The water flux of the membranes (CCAM (0-10%)) that were tested by CF filtration (Fig.46(a)) showed the highest water flux for CCAM-10% ( $522.25 \text{ L m}^{-2} \text{ bar}^{-1} \text{ h}^{-1}$ ). As expected, the water flux resulting from CF filtration was more than that resulting from DE filtration for all the prepared membranes; for example, for CCAM-8% the water fluxes were  $245.24 \text{ L m}^{-2} \text{ bar}^{-1} \text{ h}^{-1}$  and  $500 \text{ L m}^{-2} \text{ bar}^{-1} \text{ h}^{-1}$  when tested by DE and CF filtration, respectively (Fig.46(a)). This is because the membrane surface in the DE filtration configuration undergoes a higher amount of stress [2, 129]. The water flux changes according to the membrane hydrophilicity, pore size and density, whereas the effluent rejection is controlled by the pore size and surface charge of the membrane. This is clear from the results of the water flux in both the DE and CF modes (Fig.46(a)). In the DE mode, CCAM-0% ( $138.44 \text{ L m}^{-2} \text{ bar}^{-1} \text{ h}^{-1}$ ) was enhanced to CCAM-2% ( $208.84 \text{ L m}^{-2} \text{ bar}^{-1} \text{ h}^{-1}$ ) and in the CF mode, CCAM-0% ( $348.512 \text{ L m}^{-2} \text{ bar}^{-1} \text{ h}^{-1}$ ) was improved to CCAM-2% ( $422.329 \text{ L m}^{-2} \text{ bar}^{-1} \text{ h}^{-1}$ ) after introducing 2 wt.% of MXene, which helps to enhance membrane hydrophilicity, as was also exhibited from the contact angle results (Fig.41) for CCAM-0% ( $71.3^\circ$ ) and CCAM-2% ( $63.3^\circ$ ). The crosslinking of the CA membrane with 10 wt.% MXene decreases the

membrane pore size and density while preserving favorable hydrophilicity owing to a good distribution of 2D-MXene sheets inside the CA polymeric matrices [3].

Fig.46 (b) shows the different salt, MG and BSA rejection performances of CMCA, CCAM-0%, CCAM-8%, CCAM-10% and CCAM-12% using DE filtration. As reported recently in our published paper [129], “the rejection behavior of the fabricated membrane is a physical filtration phenomenon.”

All the prepared membranes were crosslinked under the same conditions (for 60 min at 60 °C), and the results confirmed that CCAM-10% has the best rejection performance among the other prepared and commercial membranes, with a 97.97% rejection of BSA, and rejection rates of 26.40%, 44.5%, 62.3% and 92.13% for NaCl, MgCl<sub>2</sub>, Na<sub>2</sub>SO<sub>4</sub> and MG, respectively (Fig.46(b)). Although the commercial membrane shows the best flux performance (315.99 L m<sup>-2</sup> bar<sup>-1</sup> h<sup>-1</sup>), its rejection rate is insignificant for salts and MG, and even BSA exhibited only 18.23% rejection. The rejection rate increased with the incorporation of 10 wt.% MXene; for example, the Na<sub>2</sub>SO<sub>4</sub> showed a 7% rejection using CCAM-0%, 50.1% rejection using CCAM-8% and 62.3% rejection using CCAM-10% (Fig.31(b)). The significant improvement in the rejection rate along with increasing MXene content is due to the CH<sub>2</sub>O crosslinking as well as the creation of denser layers.

A prepared membrane beyond 10 wt.% MXene, such as CCAM-12%, which was tested by DE filtration (Fig.46(b)), results in a higher permeation flux, from CCAM-10% (253.57 L m<sup>-2</sup> bar<sup>-1</sup> h<sup>-1</sup>) to CCAM-12% (272.96 L m<sup>-2</sup> bar<sup>-1</sup> h<sup>-1</sup>). At the same time, it exhibited a decline in salt, dye and protein rejection; for example, the rejection of Na<sub>2</sub>SO<sub>4</sub> was 62.3% for CCAM-10% decreasing to 46.012% for CCAM-12%, the rejection of MG and BSA for CCAM-10% was 92.13% and 97.97%, respectively, decreasing to 76.5% for BSA rejection and 84.31% for MG rejection for

CCAM-12%. This is attributable to MXene agglomerations after 10 wt.% grafting. According to the previous results, the loading of MXene up to 10 wt.% content reduces the pore diameter of the macrovoids and enhances membrane hydrophilicity [129]. By using (eq.5), the pore diameter of the synthesized CCAM-10% was calculated according to the solute rejection results. The mean pore diameter of the optimal membrane CCAM-10% was found to be 1.73 nm.

After studying the performance of different membranes in terms of the rejection rate using DE filtration, the CCAM-0%, CCAM-8%, and CCAM-10% membranes were tested again using CF filtration to reject MG ( $100 \text{ mg L}^{-1}$ ) and BSA ( $150 \text{ mg L}^{-1}$ ) for 1 h at 1 bar (Fig.46(c)). The results showed an increasing rejections trend with increasing MXene content; for example, for the BSA rejection, CCAM-0% exhibited 82.75%, CCAM-8% was 97.23%, and CCAM-10% showed 99.5%. The increase in the rejection rate is due to the CF configuration mode, which is characterized by a tangential flow, which creates a shearing impact on the CCAM-X% surface and thus prevents cake accumulation on the membrane surface. This is in contrast to the DE mode, which is exposed to a high resistance to filtrate flow due to the rejection solutes [129]. As expected, the DE filtration test showed a similar increasing trend due to the introduction of MXene, which leads to the formation of a denser layer, smaller pore diameter and decreases macrovoids [2]. CCAM-10% is the optimum membrane as it exhibited 96.6% and 99.49% rejection for MG and BSA, respectively, as tested by CF (Fig.46(c)). Furthermore, a highly competitive separation performance was revealed by CCAM-10% in comparison with what was previously reported in the literature regarding GO, CNT, zeolite, CA, and MXene membranes (Table 2 & Table 3). In comparing the rejection of MG and BSA using DE and CF filtration, a better rejection rate was shown using CF filtration for all tested membranes.

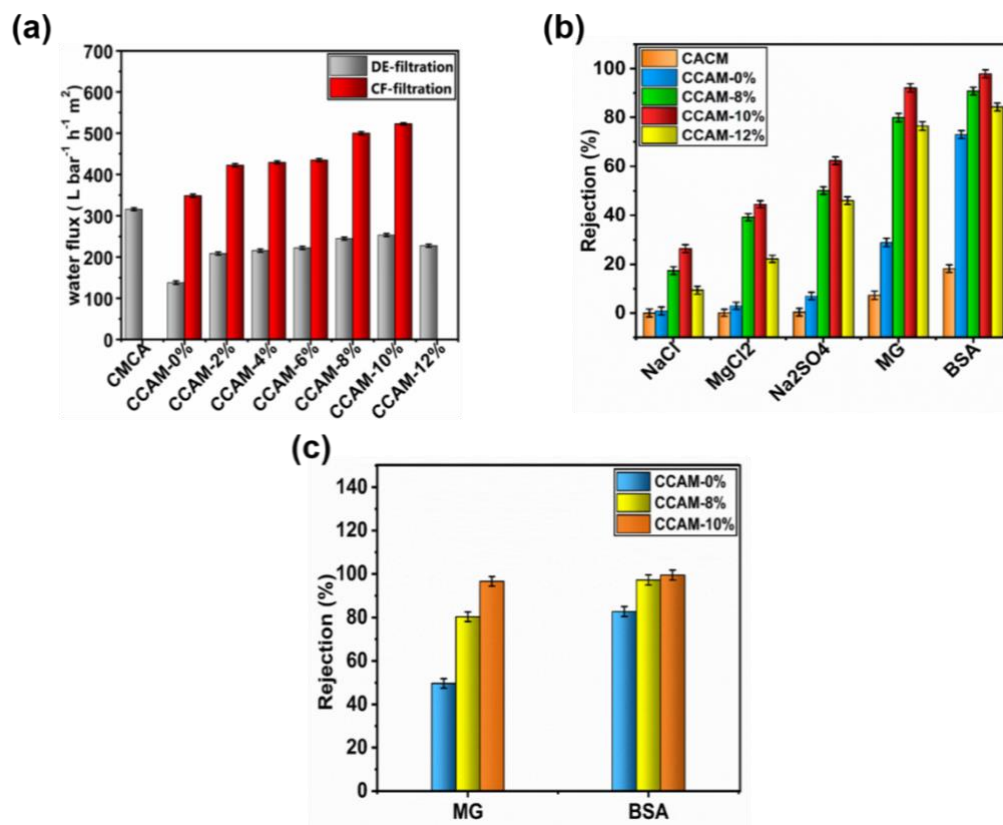


Figure 46. (a) Permeation flux of CMCA and CCAMs with various MXene contents (0-12%) using DE and CF filtration; (b) rejection of various salts, MG and BSA by CACM, CCAM-0%, CCAM-8%, CCAM-10% and CCAM-12% using DE filtration; (c) rejection of MG and BSA by CCAM-0%, CCAM-8%, CCAM-10% using CF filtration.

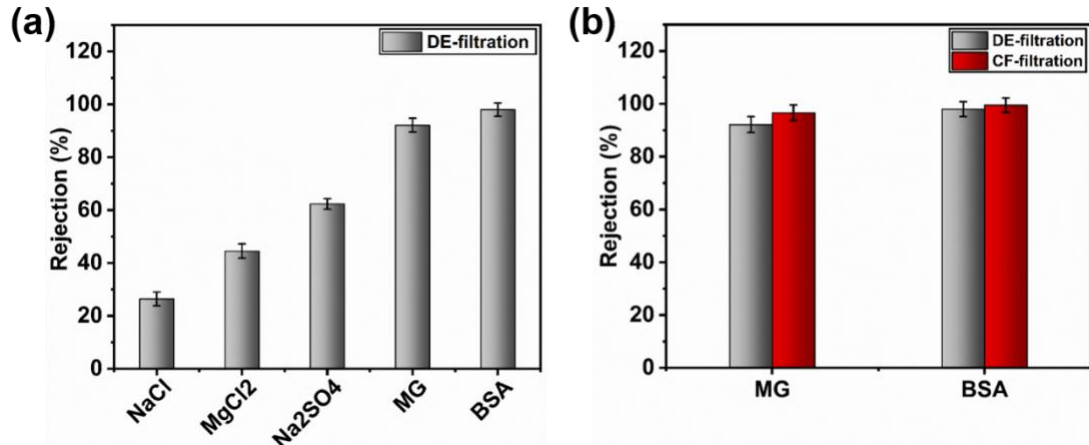


Figure 47. (a) Rejection of different salts, MG and BSA by CCAM-10% using DE filtration; (b) comparison between DE and CF filtration using CCAM-10% for the rejection of MG and BSA.

### 3.6 Impact of Operating Conditions on The Separation Performance

To optimize the membrane performance, it is essential to examine the impact of the process parameters, including the operating pressure and feed concentration, on the water flux and rejection rate [318].

The impact of operating pressure (0.5-2 bar and 1-2 bar) was tested by DE and CF filtrations for 1 h, respectively, on the permeation flux and rejection rate of CCAM-0% and CCAM-10% (Fig.48(a-c)). Also, the effects of the concentration of Na<sub>2</sub>SO<sub>4</sub> (1000-4000 ppm) on the separation rate of CCAM-0% and CCAM-10% were tested using DE filtration and CF filtration for 1h (Fig.48 (d)).

As expected, the plotted results (Fig.48(a)) exhibited an increasing trend of water flux with an increasing operating pressure of CCAM-0% from 135.204 L m<sup>-2</sup> h<sup>-1</sup> at 0.5 bar to 143.11 L m<sup>-2</sup> h<sup>-1</sup> at 2 bar, and for CCAM-10% from 244.05 L m<sup>-2</sup> h<sup>-1</sup> at 0.5 bar to 323.3 L m<sup>-2</sup> h<sup>-1</sup> at 2 bar, which were tested by DE filtration. The rejection rate of Na<sub>2</sub>SO<sub>4</sub> declined with an increase in the operating pressure of CCAM-0% from

9.32% at 0.5 bar to 2.67% at 2 bar and for CCAM-10% from 65.51% at 0.5 bar to 54.88% at 2 bar (Fig.48(b)), which was tested by DE filtration. In addition, the rejection rate of MG and BSA for both filtration modes DE and CF decreased for CCAM-10% with increasing operating pressure (Fig.48(c)). CCAM-10% showed 92.13% and 97.97% at 1 bar for MG and BSA, respectively, but at 2 bar CCAM-10% exhibited 83.32% and 4.98% for MG and BSA, respectively, and was tested by DE filtration. CCAM-10% was also tested by CF filtration at 1 bar and exhibited 96.6% and 99.49% rejection for MG and BSA, respectively, while at 2 bar it showed 86.72% and 96.59% rejection of MG and BSA, respectively (Fig.48(c)).

In comparing the DE and CF modes at 2 bar operating pressure, CCAM-10% exhibited a better rejection rate using the CF mode with 86.7% and 96.6% rejection of MG and BSA, respectively (Fig.48(c)). As the feed concentration rate of  $\text{Na}_2\text{SO}_4$  increased from 1000ppm to 4000 ppm, the rejection performance reduced for both CCAM-0% (from 11.29% to ~1.3%) and CCAM-10% (from 64.9% to ~ 51.5%) (Fig.48(d)); this was tested using DE filtration. As we recently published [318] [129], this is “mainly because of the improvement of the electrostatic shield impacts caused by the increase in the feed solute concentration.”



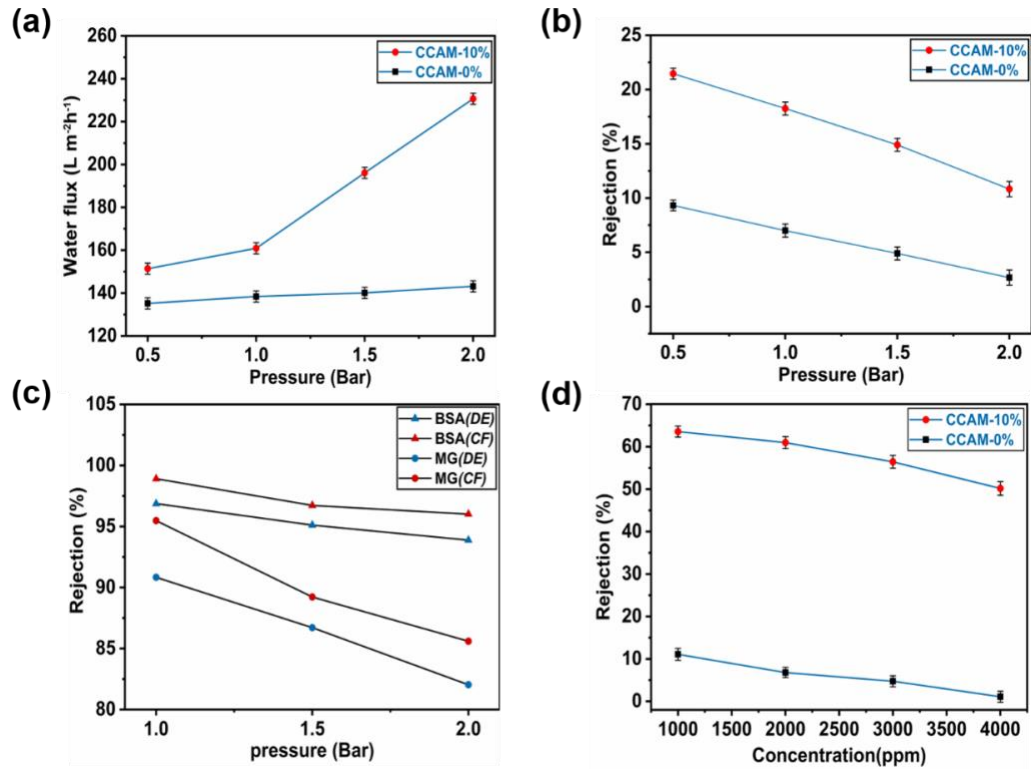


Figure 48. (a) Effects of operating pressure (0.5-2 bar) on water flux using DE filtration; (b) operating pressure impacts on the rejection of  $Na_2SO_4$  (2000 ppm) using DE filtration; (C) operating pressure impacts on the rejection of MG and BSA using a pressure range (1-2 bar) using DE (blue symbol) and CF (red symbol) filtration; (d) effect of  $Na_2SO_4$  concentration (1000-4000 ppm) on the rejection performance of CCAM-0% and CCAM-10% tested by DE filtration.

### 3.7 Membrane Antifouling Performance Evaluation

In this study, the CF process was applied to analyze the antifouling effectiveness. A typical protein (BSA) was selected to assess the antifouling ability of the crosslinked mixed matrix CA at MXene membranes. The membrane was tested with pure water at 1 bar for 30 min, then the flux was recorded as  $J_{w0}$  ( $L m^{-2} h^{-1}$ ). After that, the pure water was replaced with a BSA solution consisting of 500 ppm and pH=7 at 1 bar; the flux was recorded after 1 h as  $J_p$  ( $L m^{-2} h^{-1}$ ), and the rejection was analyzed and measured using UV. The membrane was washed with DI water for 30 minutes at no pressure and the same CF velocity. Next, the membrane was operated at 1 bar with DI water for 30 minutes, and then the flux was recorded  $J_{w1}$  ( $L m^{-2} h^{-1}$ ), indicating the end of one cycle. The best parameters for estimating the membrane antifouling properties are the FRR using (eq.6), total fouling resistance ratio ( $R_t$ ) using (eq.7), the reversible fouling resistance ratio ( $R_r$ ) using (eq.8) and the irreversible fouling resistance ratio ( $R_{ir}$ ) using (eq.9).

The FRR% of the prepared CCAM-0%, CCAM-8%, and CCAM-10% are presented in Fig.34(a). A higher percentage of FRR signifies a better antifouling property of the membrane. Increasing the MXene loading improves the FRR% and thus indicates better fouling resistance performance, from CCAM-0% (48.4%) to the highest FRR% for CCAM-10% (67.3%) (Fig.49(a)). The fouling resistance performance of the membrane is most likely affected by the membrane hydrophilicity, and the increasing trend of FRR% (Fig.49(a)) is matched with the decrease in the membranes' contact angle values with increasing MXene content (Fig.49). The existence of the hydrophilic MXene 2D sheets induces a water molecule layer formation on the surface of the membrane, which possibly holds a suspension of the adsorbed protein and other effluents to the surface of the membrane [129, 319]. Based on the results, the

incorporation of MXene nanosheets into the CA MMM is effective for achieving good antifouling performance.

Moreover, other important parameters related to membrane fouling are the reversible ( $R_r$ ) and irreversible ( $R_{ir}$ ) fouling resistance ratios, exhibited in Fig.49(b). These results confirm that CCAM-10% demonstrated significant fouling resistance in comparison to CCAM-0% and CCAM-8%. Foulant trapping and buildup in the membrane pores and surface caves are the cause of irreversible fouling. These are removed from the membrane surface via the wash process.

The irreversible ratio of CCAM-0% was decreased from 51.7% to 40.5% (CCAM-8%) and then further decreased to 32.7% (CCAM-10%). The enhancement could be assigned to the more hydrophilic and negative surface charge of the CCAM-10%, which plays a fundamental role in resisting the foulants and preventing them from being continuously adsorbed to the membrane surface. This indicates that the reversible fouling ratio was the major trend in the overall fouling of the CCAM-10% (38.7%) (Fig.49(b)) and thus, foulants trapped inside the membrane pores and the surface can be easily eliminated by simple hydraulic washing using DI water. The CCAM-10% is ascribed solely to the fact that the incorporation of 10 wt.% MXene into the CA MMM improved the membrane surface properties, including hydrophilicity and charge, which caused a reduction in membrane fouling [319, 320].

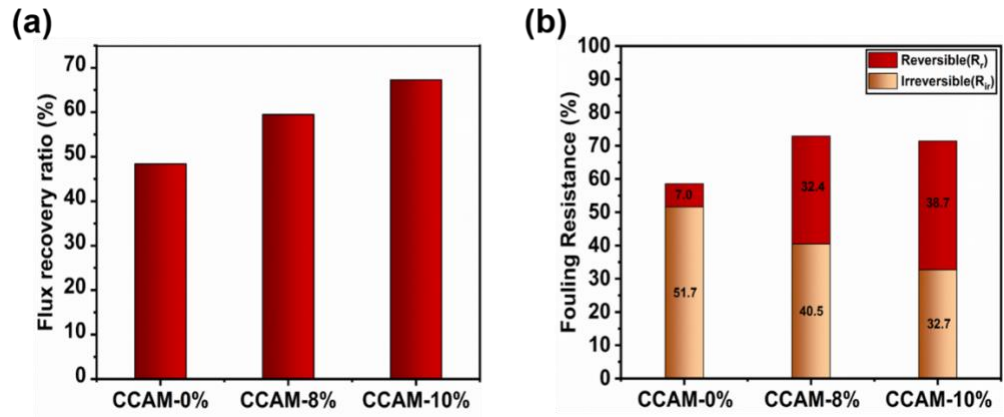


Figure 49. (a) Water recovery ratio of CCAM-0%, CCAM-8%, and CCAM-10% after fouling using 500 ppm BSA protein solution using CF filtration; (b) fouling resistance ratios of CCAM-0%, CCAM-8%, and CCAM-10% using CF filtration.

## CHAPTER 4: CONCLUSIONS AND RECOMMENDATIONS

The obtained results show that MXene at CA composite membranes (CCAM 0-10%) can be effectively fabricated using the PI method prior to CH<sub>2</sub>O crosslinking. The fabricated membranes, particularly CCAM-10%, exhibited outstanding hydrophilicity and good surface roughness, offering admirable permeation flux, good thermal stability, high WU, excellent anti-fouling resistance properties, and a high surface area. The contact angle results confirmed the improvements of the membrane surface hydrophilicity with increasing MXene loading in the CA polymer matrix. CCAM-10% exhibited the highest hydrophilicity (with a contact angle of 48.06°) and was considered as the optimal membrane composition. CCAM-10% showed a rougher surface compared to CCAM-0%, with Ra=47.4 nm and Rq=60.2 nm; the rougher surface provided the benefit of opening more area for membrane transport, and hence, improved the permeation flux with increased surface roughness. The thermal stability of the membranes was significantly enhanced by introducing MXene into the CA polymeric matrix, whereby the decomposition temperature reached 290°C, and the thermal stability was further enhanced by the CH<sub>2</sub>O crosslinking of the membranes as the decomposition temperature of CCAM-10% reached ~310°C. CCAM-10% showed a 1.46-fold WU (125.3%) and a 1.24 porosity ratio (72.35%). Increased membrane porosity leads to a higher permeation flux [320]. The size of the pores and porosity also determine the permeability and rejection rate of the membrane surface [118].

The average pore diameter and MWCO of the CCAM-10% MMMs were calculated and found to be  $\sim 1.73$  nm and 435 Dalton, respectively. Chemical crosslinking at  $60^{\circ}\text{C}$  for 60 min leads to decreased membrane pore size and density and the maintenance of good hydrophilicity because of the good distribution of 2D-MXene sheets along the CA polymeric matrix membrane. The CCAM-10% membrane exhibited good salt rejection and highly efficient rejections of 96.6% and 99.49% for MG and BSA, respectively. CCAM-10% exhibited the highest permeation flux of  $522.25 \text{ L m}^{-2} \text{ bar}^{-1} \text{ h}^{-1}$  due to the CF tangential flow, which created a shearing effect on the surface of the membrane and thus prevented cake accumulation on the membrane surface [6]; this is in contrast to the DE filtration configuration, which undergoes higher stress [2].

CCAM-10% revealed the best rejection rate among the other prepared and commercial membranes when tested using DE filtration, with 97.97%, 26.40%, 44.5%, 62.3% and 92.13% rejection rates for BSA, NaCl,  $\text{MgCl}_2$ ,  $\text{Na}_2\text{SO}_4$  and MG, respectively. Although the commercial membrane showed the highest water flux performance ( $315.99 \text{ L m}^{-2} \text{ bar}^{-1} \text{ h}^{-1}$ ), its rejection rate was insignificant for salts, MG, and even BSA, which was only 18.23%. CCAM-12% was tested using DE filtration, and the results confirmed that loading MXene beyond 10 wt.% leads to improved water flux to  $272.96 \text{ L m}^{-2} \text{ bar}^{-1} \text{ h}^{-1}$ , although it reduces the rejection rate of  $\text{Na}_2\text{SO}_4$  to 46.012%. The water flux of CCAM-10% improved significantly from  $244.05 \text{ L m}^{-2} \text{ h}^{-1}$  at 0.5 bar to  $323.3 \text{ L m}^{-2} \text{ h}^{-1}$  at 2 bar, and the  $\text{Na}_2\text{SO}_4$  rejection rate reduced with increasing membrane operating pressure, although it still showed a better rejection rate compared to CCAM-0%. Hence, CCAM-10% is considered as the optimum membrane as it showed a 96.6% and 99.49% rejection of MG and BSA, respectively, as tested by CF filtration.

As the feed solution concentration of Na<sub>2</sub>SO<sub>4</sub> increased (1000-4000 ppm), the CCAM-10% membrane's rejection rate declined (from 64.9% to ~51.5%), although it showed a superior rejection rate compared with the neat membrane due to the development of the electrostatic shield impacts attributable to higher feed solute concentrations [3]. The CCAM-10% water flux and rejection separation performance demonstrated their appropriateness for various water treatment applications. CCAM-10% had the highest FRR% and R<sub>r</sub> values of 67.3% and 38.7%, respectively, and the lowest R<sub>ir</sub> value of 32.7%. A higher FRR% indicates a better membrane fouling resistance ability and the improvements could be based on the good hydrophilic nature and negative CCAM-10% surface charge, which play an important role in preventing foulants from continuously adsorbing to the membrane surface. Also, a lower R<sub>ir</sub> indicates better antifouling properties as R<sub>ir</sub> refers to the fouling resulting from the deposition of BSA particles on the membrane surface.

The results in terms of the fouling resistance, excellent physicochemical properties, and separation performance of the MXene at the CA composite membrane could pave the way for efficient and highly profitable UF/NF membranes based on MXene MMMs. In the future, as discussed in the previous section, silver nanoparticles (Ag-NPs) could be combined into polymer membranes to improve the biofouling and chlorine resistance, permeability, and mechanical strength [129].

Hence, a self-reduction of silver nitrite on the MXene sheets surface solution could be prepared and then fabricated with 10 wt.% MXene and CA polymer with the same conditions used to prepare CCAM-10%, i.e. using the PI method and then CH<sub>2</sub>O crosslinking [1]. This might enhance the membrane's mechanical strength as well as its antibiofouling properties and offer good permeation flux and rejection rate performance. Also, another fabrication method could be applying a self-reduction silver

nitrite to the surface after preparing the CCAM-10% membrane to prepare different membranes of Ag@CCAM-10% with various silver loadings (0-25%). The fabrication of MMMs on a porous support/substrate to address better membrane mechanical stability is another option that would allow the testing of the membrane separation performance in a high-pressure range. Also, MMM research could develop certain commercial applications and cost analyses to strengthen the technology for water applications [129]. One of the main engineering challenges, regardless of the good application of MXene membranes, is the synthesis of a defect-free membrane with the proper thickness; hence, efforts in terms of the synthesis method should be made to enhance the economic feasibility of CCAM-10%. Furthermore, the manufacture of CCAM-10% needs to be scaled up and the issues of its stability, lifespan, degradation and recyclability should be addressed in order for it to be used in water treatment industries and thereby provide a service for the community to compensate for the shortage in clean water production [321, 322].



## REFERENCES

- [1] R. P. Pandey, K. Rasool, V. E. Madhavan, B. Aïssa, Y. Gogotsi, and K. A. Mahmoud, "Ultrahigh-flux and fouling-resistant membranes based on layered silver/MXene (Ti<sub>3</sub>C<sub>2</sub>T<sub>x</sub>) nanosheets," *Journal of Materials Chemistry A*, 10.1039/C7TA10888E vol. 6, no. 8, pp. 3522-3533, 2018.
- [2] J. N. M. BE, "DEAD-END AND CROSSFLOW MICROFILTRATION OF YEAST AND BENTONITE SUSPENSIONS:  
EXPERIMENTAL AND MODELLING STUDIES INCORPORATING THE USE OF ARTIFICIAL NEURAL NETWORKS," PHD, At Dublin City University, School of Biotechnology *Journal of Membrane Science* 2008.
- [3] T. w. membranes. *Dead End Filtration Vs Cross Flow Filtration*. Available: <https://www.thewaymembranes.com/post/dead-end-filtration-vs-cross-flow-filtration>
- [4] *Human Development Report 2016 Human Development for Everyone*. Washington DC, USA: United Nations Development Programme, 2016.
- [5] M. Bodzek, K. Konieczny, and A. Kwiecińska, "Application of membrane processes in drinking water treatment—state of art," *Desalination and Water Treatment - DESALIN WATER TREAT*, vol. 35, pp. 164-184, 11/01 2011.
- [6] J. Yin, "Fabrication and modification of nanocomposite membranes for enhanced water purification," Doctor of Philosophy, University of Missouri-Columbia 2014.
- [7] "Pressure-Driven Membrane Filtration Processes," ed, 2018.
- [8] F. A. a. F. SA, "The role of membrane technology in sustainable decentralized wastewater systems," *water Science & Technology* 2005.

- [9] D. M. e. a. Warsinger, "A Review of Polymeric Membranes and Processes for Potable Water Reuse," *Science Direct*, 2018.
- [10] S. R.-V. C. n. Xinglin Lu, ‡Devin L. Shaffer,‡Jun Ma,\*,†and Menachem Elimelech, "In Situ Surface Chemical Modification of Thin-Film Composite Forward Osmosis Membranes for Enhanced Organic Fouling Resistance," *Environmental Science & Technology*, 2013.
- [11] S. J. Bradley P. Ladewig<sup>1\*</sup>, Yuening Li<sup>2</sup>, "A review of reverse osmosis membrane fouling and control strategies," *SciELO Network*, 2011.
- [12] I. Fang Li<sup>I</sup>, I. Chunhua Deng<sup>I</sup>, \*, C. Du<sup>IV</sup>, I. Bo Yang<sup>I</sup>, and I. Qing Tian<sup>I</sup>, "Fouling mechanism and cleanability of ultrafiltration membranes modified with polydopamine-graft-PEG," *scielo south africa*, July 2015.
- [13] T. Nguyen, F. A. Roddick, and L. Fan, "Biofouling of water treatment membranes: a review of the underlying causes, monitoring techniques and control measures," (in eng), *Membranes*, vol. 2, no. 4, pp. 804-840, 2012.
- [14] R. Komlenic, "Rethinking the causes of membrane biofouling," *Filtration & Separation*, vol. 47, pp. 26-28, 09/01 2010.
- [15] K. Shameli *et al.*, "Silver/poly (lactic acid) nanocomposites: preparation, characterization, and antibacterial activity," (in eng), *International journal of nanomedicine*, vol. 5, pp. 573-579, 2010.
- [16] Y. Lin and Z. Yang, "Preparation, Characterization and Antibacterial Property of Cerium Substituted Hydroxyapatite Nanoparticles," *Journal of Rare Earths - J RARE EARTH*, vol. 25, pp. 452-456, 08/01 2007.
- [17] J. Lu, X. Wang, and C. Xiao, "Preparation and characterization of Konjac glucomannan/poly (diallyldimethylammonium chloride) antibacterial blend films," *Carbohydrate Polymers*, vol. 73, pp. 427-437, 08/01 2008.

- [18] C. Liao, P. Yu, J. Zhao, L. Wang, and Y. Luo, "Preparation and characterization of NaY/PVDF hybrid ultrafiltration membranes containing silver ions as antibacterial materials," *Desalination*, vol. 272, no. 1, pp. 59-65, 2011/05/03/ 2011.
- [19] Y. Chen, Y. Zhang, J. Liu, H. Zhang, and K. Wang, "Preparation and antibacterial property of polyethersulfone ultrafiltration hybrid membrane containing halloysite nanotubes loaded with copper ions," *Chemical Engineering Journal*, vol. 210, pp. 298-308, 2012/11/01/ 2012.
- [20] K. P. Lee, T. C. Arnot, and D. Mattia, "A review of reverse osmosis membrane materials for desalination—Development to date and future potential," *Journal of Membrane Science*, vol. 370, no. 1, pp. 1-22, 2011/03/15/ 2011.
- [21] "What is Nano NF Water Purifier, Advantages and Disadvantages of NF Nano Water purifiers," ed.
- [22] M. Safarpour, V. Vatanpour, and A. Khataee, "Preparation and characterization of graphene oxide/TiO<sub>2</sub> blended PES nanofiltration membrane with improved antifouling and separation performance," *Desalination*, vol. 393, pp. 65-78, 2016/09/01/ 2016.
- [23] M. Peydayesh, T. Mohammadi, and O. Bakhtiari, "Water desalination via novel positively charged hybrid nanofiltration membranes filled with hyperbranched polyethyleneimine modified MWCNT," *J. Ind. Eng. Chem.*, vol. 69, pp. 127-140, 2019/01/25/ 2019.
- [24] Y. Zhao, Z. Zhang, L. Dai, and S. Zhang, "Preparation of a highly permeable nanofiltration membrane using a novel acyl chloride monomer with -PO(Cl)<sub>2</sub> group," *Desalination*, vol. 431, pp. 56-65, 2018/04/01/ 2018.

- [25] M. Guo, S. Wang, K. Gu, X. Song, Y. Zhou, and C. Gao, "Gradient cross-linked structure: Towards superior PVA nanofiltration membrane performance," *J. Membr. Sci.*, vol. 569, pp. 83-90, 2019/01/01/ 2019.
- [26] Y.-F. Mi, F.-Y. Zhao, Y.-S. Guo, X.-D. Weng, C.-C. Ye, and Q.-F. An, "Constructing zwitterionic surface of nanofiltration membrane for high flux and antifouling performance," *J. Membr. Sci.*, vol. 541, pp. 29-38, 2017/11/01/ 2017.
- [27] S. Sarkar, A. K. SenGupta, and P. Prakash, "The Donnan Membrane Principle: Opportunities for Sustainable Engineered Processes and Materials," *Environ. Sci. Technol.*, vol. 44, no. 4, pp. 1161-1166, 2010/02/15 2010.
- [28] L. Chen *et al.*, "Graphene oxide based membrane intercalated by nanoparticles for high performance nanofiltration application," *Chem. Eng. J.*, vol. 347, pp. 12-18, 2018/09/01/ 2018.
- [29] G. Liu, W. Jin, and N. Xu, "Graphene-based membranes," *Chem. Soc. Rev.*, 10.1039/C4CS00423J vol. 44, no. 15, pp. 5016-5030, 2015.
- [30] N. Wang, S. Ji, G. Zhang, J. Li, and L. Wang, "Self-assembly of graphene oxide and polyelectrolyte complex nanohybrid membranes for nanofiltration and pervaporation," *Chem. Eng. J.*, vol. 213, pp. 318-329, 2012/12/01/ 2012.
- [31] L. Chen *et al.*, "A large-area free-standing graphene oxide multilayer membrane with high stability for nanofiltration applications," *Chem. Eng. J.*, vol. 345, pp. 536-544, 2018/08/01/ 2018.
- [32] A. K. Singh, S. Prakash, V. Kulshrestha, and V. K. Shahi, "Cross-linked Hybrid Nanofiltration Membrane with Antibiofouling Properties and Self-Assembled Layered Morphology," *ACS Appl. Mater. Interfaces*, vol. 4, no. 3, pp. 1683-1692, 2012/03/28 2012.

- [33] B. P. Tripathi, N. C. Dubey, and M. Stamm, "Polyethylene glycol cross-linked sulfonated polyethersulfone based filtration membranes with improved antifouling tendency," *Journal of Membrane Science*, vol. 453, pp. 263-274, 2014/03/01/ 2014.
- [34] M. Paul and S. D. Jons, "Chemistry and fabrication of polymeric nanofiltration membranes: A review," *Polymer*, vol. 103, pp. 417-456, 2016/10/26/ 2016.
- [35] H. Abadikhah, E. Naderi Kalali, S. Khodi, X. Xu, and S. Agathopoulos, "Multifunctional Thin-Film Nanofiltration Membrane Incorporated with Reduced Graphene Oxide@TiO<sub>2</sub>@Ag Nanocomposites for High Desalination Performance, Dye Retention, and Antibacterial Properties," *ACS Applied Materials & Interfaces*, vol. 11, no. 26, pp. 23535-23545, 2019/07/03 2019.
- [36] Z. Wang *et al.*, "Nanoparticle-templated nanofiltration membranes for ultrahigh performance desalination," *Nature Communications*, vol. 9, no. 1, p. 2004, 2018/05/21 2018.
- [37] P. E. R. A. J. Paul Guyer, *An Introduction to Water Desalination*. Guyer Partners, 2018.
- [38] H. Abadikhah *et al.*, "High flux thin film nanocomposite membrane incorporated with functionalized TiO<sub>2</sub>@reduced graphene oxide nanohybrids for organic solvent nanofiltration," *Chemical Engineering Science*, vol. 204, pp. 99-109, 2019/08/31/ 2019.
- [39] E. Bagheripour, A. R. Moghadassi, S. M. Hosseini, B. Van der Bruggen, and F. Parvzian, "Novel composite graphene oxide/chitosan nanoplates incorporated into PES based nanofiltration membrane: Chromium removal and antifouling enhancement," *Journal of Industrial and Engineering Chemistry*, vol. 62, pp. 311-320, 2018/06/25/ 2018.

- [40] A. Anand, B. Unnikrishnan, J.-Y. Mao, H.-J. Lin, and C.-C. Huang, "Graphene-based nanofiltration membranes for improving salt rejection, water flux and antifouling—A review," *Desalination*, vol. 429, pp. 119-133, 2018/03/01/ 2018.
- [41] J. Zheng, M. Li, K. Yu, J. Hu, X. Zhang, and L. Wang, "Sulfonated multiwall carbon nanotubes assisted thin-film nanocomposite membrane with enhanced water flux and anti-fouling property," *Journal of Membrane Science*, vol. 524, pp. 344-353, 2017/02/15/ 2017.
- [42] F. Santos, C. Borges, and F. da Fonseca, "Polymeric Materials for Membrane Contactor Devices Applied to Water Treatment by Ozonation," *Materials Research*, vol. 18, pp. 1015-1022, 10/01 2015.
- [43] K. Scott, "INTRODUCTION TO MEMBRANE SEPARATIONS," in *Handbook of Industrial Membranes*, K. Scott, Ed. Amsterdam: Elsevier Science, 1995, pp. 3-185.
- [44] C. Ren, "Interaction of Ions with Two-Dimensional Transition Metal Carbide (MXene) Films," Ph.D. Thesis, 2017.
- [45] S. Kar, R. C. Bindal, and P. K. Tewari, "Carbon nanotube membranes for desalination and water purification: Challenges and opportunities," *Nano Today*, vol. 7, no. 5, pp. 385-389, 2012/10/01/ 2012.
- [46] M. E. Suk and N. R. Aluru, "Water Transport through Ultrathin Graphene," *The Journal of Physical Chemistry Letters*, vol. 1, no. 10, pp. 1590-1594, 2010/05/20 2010.
- [47] C. Casado-Coterillo, "Mixed Matrix Membranes," *membranes* 5 November 2019 2019.

- [48] J. Lee *et al.*, "Graphene oxide nanoplatelets composite membrane with hydrophilic and antifouling properties for wastewater treatment," *Journal of Membrane Science*, vol. 448, pp. 223-230, 12/01 2013.
- [49] P. Sun *et al.*, "Selective Trans-Membrane Transport of Alkali and Alkaline Earth Cations through Graphene Oxide Membranes Based on Cation- $\pi$  Interactions," *ACS Nano*, vol. 8, no. 1, pp. 850-859, 2014/01/28 2014.
- [50] H. Huang, Y. Ying, and X. Peng, "Graphene oxide nanosheet: an emerging star material for novel separation membranes," *Journal of Materials Chemistry A*, 10.1039/C4TA02359E vol. 2, no. 34, pp. 13772-13782, 2014.
- [51] D. Cohen-Tanugi and J. C. Grossman, "Nanoporous graphene as a reverse osmosis membrane: Recent insights from theory and simulation," *Desalination*, vol. 366, pp. 59-70, 2015/06/15/ 2015.
- [52] E. Drioli, C. A. Quist-Jensen, and L. Giorno, "Molecular Weight Cutoff," in *Encyclopedia of Membranes*, E. Drioli and L. Giorno, Eds. Berlin, Heidelberg: Springer Berlin Heidelberg, 2016, pp. 1326-1327.
- [53] A. Antony and G. Leslie, "22 - Degradation of polymeric membranes in water and wastewater treatment," in *Advanced Membrane Science and Technology for Sustainable Energy and Environmental Applications*, A. Basile and S. P. Nunes, Eds.: Woodhead Publishing, 2011, pp. 718-745.
- [54] S. Kadel, G. Pellerin, J. Thibodeau, V. Perreault, C. Lainé, and L. Bazinet, "How Molecular Weight Cut-Offs and Physicochemical Properties of Polyether Sulfone Membranes Affect Peptide Migration and Selectivity during Electrodialysis with Filtration Membranes," *Membranes*, vol. 9, no. 11, 2019.
- [55] S. Shenvi, A. Ismail, and A. Isloor, "Enhanced Permeation Performance of Cellulose Acetate Ultrafiltration Membranes by Incorporation of Sulfonated

- Poly(1,4-phenylene ether ether sulfone) and Poly(styrene- co -maleic anhydride)," *Industrial & Engineering Chemistry Research*, vol. 53, pp. 13820-13827, 09/03 2014.
- [56] K. Müller *et al.*, "Review on the Processing and Properties of Polymer Nanocomposites and Nanocoatings and Their Applications in the Packaging, Automotive and Solar Energy Fields," (in eng), *Nanomaterials (Basel, Switzerland)*, vol. 7, no. 4, p. 74, 2017.
- [57] L. Yan, Y. S. Li, and C. B. Xiang, "Preparation of poly(vinylidene fluoride)(pvdf) ultrafiltration membrane modified by nano-sized alumina (Al<sub>2</sub>O<sub>3</sub>) and its antifouling research," *Polymer*, vol. 46, no. 18, pp. 7701-7706, 2005/08/23/ 2005.
- [58] A. Bottino, G. Capannelli, and A. Comite, "Preparation and characterization of novel porous PVDF-ZrO<sub>2</sub> composite membranes," *Desalination*, vol. 146, no. 1, pp. 35-40, 2002/09/10/ 2002.
- [59] T.-H. Bae and T.-M. Tak, "Effect of TiO<sub>2</sub> nanoparticles on fouling mitigation of ultrafiltration membranes for activated sludge filtration," *Journal of Membrane Science*, vol. 249, no. 1, pp. 1-8, 2005/03/01/ 2005.
- [60] D.-J. Lin, C.-L. Chang, F.-M. Huang, and L.-P. Cheng, "Effect of salt additive on the formation of microporous poly(vinylidene fluoride) membranes by phase inversion from LiClO<sub>4</sub>/Water/DMF/PVDF system," *Polymer*, vol. 44, no. 2, pp. 413-422, 2003/01/01/ 2003.
- [61] M. Khayet, J. P. G. Villaluenga, J. L. Valentin, M. A. López-Manchado, J. I. Mengual, and B. Seoane, "Filled poly(2,6-dimethyl-1,4-phenylene oxide) dense membranes by silica and silane modified silica nanoparticles: characterization



- and application in pervaporation," *Polymer*, vol. 46, no. 23, pp. 9881-9891, 2005/11/14/ 2005.
- [62] X. Zhang, A. J. Du, P. Lee, D. D. Sun, and J. O. Leckie, "TiO<sub>2</sub> nanowire membrane for concurrent filtration and photocatalytic oxidation of humic acid in water," *Journal of Membrane Science*, vol. 313, no. 1, pp. 44-51, 2008/04/10/ 2008.
- [63] M. R. Esfahani *et al.*, "Nanocomposite membranes for water separation and purification: Fabrication, modification, and applications," *Separation and Purification Technology*, vol. 213, pp. 465-499, 2019/04/15/ 2019.
- [64] S.-T. Kang, A. Subramani, E. M. V. Hoek, M. A. Deshusses, and M. R. Matsumoto, "Direct observation of biofouling in cross-flow microfiltration: mechanisms of deposition and release," *Journal of Membrane Science*, vol. 244, no. 1, pp. 151-165, 2004/11/15/ 2004.
- [65] M. Al-Ahmad, F. A. Abdul Aleem, A. Mutiri, and A. Ubaisy, "Biofouling in RO membrane systems Part 1: Fundamentals and control," *Desalination*, vol. 132, no. 1, pp. 173-179, 2000/12/20/ 2000.
- [66] H.-C. Flemming and J. Wingender, "The Biofilm Matrix," *Nature reviews. Microbiology*, vol. 8, pp. 623-33, 09/01 2010.
- [67] W. Hijnen, D. Biraud, E. Cornelissen, and D. van der Kooij, "Threshold Concentration of Easily Assimilable Organic Carbon in Feedwater for Biofouling of Spiral-Wound Membranes," *Environmental science & technology*, vol. 43, pp. 4890-5, 08/01 2009.
- [68] Y. Wen, J. Yuan, X. Ma, S. Wang, and Y. Liu, "Polymeric nanocomposite membranes for water treatment: a review," *Environmental Chemistry Letters*, vol. 17, 05/28 2019.

- [69] C. Gómez-Suárez *et al.*, "Influence of extracellular polymeric substances on deposition and redeposition of *Pseudomonas aeruginosa* to surfaces," vol. 148, no. 4, pp. 1161-1169, 2002.
- [70] V. Chen and P. Ma, "Nano-fibrous poly(L-lactid) scaffolds with interconnected spherical macropores," *Biomaterials*, vol. 25, pp. 2065-73, 06/01 2004.
- [71] P. Nguyen-Tri, T. A. Nguyen, P. Carriere, and C. Ngo Xuan, "Nanocomposite Coatings: Preparation, Characterization, Properties, and Applications," *International Journal of Corrosion*, vol. 2018, p. 4749501, 2018/02/13 2018.
- [72] J. Chen, B. Liu, X. Gao, and D. Xu, "A review of the interfacial characteristics of polymer nanocomposites containing carbon nanotubes," *RSC Advances*, 10.1039/C8RA04205E vol. 8, no. 49, pp. 28048-28085, 2018.
- [73] M. S. Reid, J. Erlandsson, and L. Wågberg, "Interfacial Polymerization of Cellulose Nanocrystal Polyamide Janus Nanocomposites with Controlled Architectures," *ACS Macro Letters*, vol. 8, no. 10, pp. 1334-1340, 2019/10/15 2019.
- [74] M. Adamczak, G. Kamińska, and J. Bohdziewicz, "Preparation of Polymer Membranes by In Situ Interfacial Polymerization," *International Journal of Polymer Science*, vol. 2019, p. 6217924, 2019/03/14 2019.
- [75] G.-P. Sheng, H.-Q. Yu, and X.-Y. Li, "Extracellular polymeric substances (EPS) of microbial aggregates in biological wastewater treatment systems: A review," *Biotechnology Advances*, vol. 28, no. 6, pp. 882-894, 2010/11/01/ 2010.
- [76] Z. Cui *et al.*, "Electrospinning and crosslinking of polyvinyl alcohol/chitosan composite nanofiber for transdermal drug delivery," *Advances in Polymer Technology*, vol. 37, no. 6, pp. 1917-1928, 2018/10/01 2018.

- [77] K. Bilge, A. Ürkmez, E. Şimşek, and M. Papila, "Stabilized electrospinning of heat stimuli/in situ crosslinkable nanofibers and their self-same nanocomposites," *Journal of Applied Polymer Science*, vol. 133, no. 43, 2016/11/15 2016.
- [78] E. T. Nicknejad, S. M. Ghoreishi, and N. Habibi, "Electrospinning of Cross-Linked Magnetic Chitosan Nanofibers for Protein Release," (in eng), *AAPS PharmSciTech*, vol. 16, no. 6, pp. 1480-1486, 2015.
- [79] I. Harsini, M. Sadiq, P. Soroushian, and A. Balachandra, "Polymer nanocomposites processed via self-assembly through introduction of nanoparticles, nanosheets, and nanofibers," *Journal of Materials Science*, vol. 52, 02/01 2017.
- [80] W. Qi, X. Zhang, and H. Wang, "Self-assembled polymer nanocomposites for biomedical application," *Current Opinion in Colloid & Interface Science*, vol. 35, pp. 36-41, 2018/05/01/ 2018.
- [81] A. Harrison, T. T. Vuong, M. P. Zeevi, B. J. Hittel, S. Wi, and C. Tang, "Rapid Self-Assembly of Metal/Polymer Nanocomposite Particles as Nanoreactors and Their Kinetic Characterization," (in eng), *Nanomaterials (Basel, Switzerland)*, vol. 9, no. 3, p. 318, 2019.
- [82] D. Zhang and T. Cui, "Tunable mechanical properties of layer-by-layer self-assembled carbon nanotube/polymer nanocomposite membranes for M/NEMS," *Sensors and Actuators A: Physical*, vol. 185, pp. 101-108, 2012/10/01/ 2012.
- [83] S. Kumar, N. Jouault, B. Benicewicz, and T. Neely, "Nanocomposites with Polymer Grafted Nanoparticles," *Macromolecules*, vol. 46, pp. 3199-3214, 05/01 2013.

- [84] X. Cao, Y. Habibi, and L. Lucia, "One-pot polymerization, surface grafting, and processing of waterborne polyurethane-cellulose nanocrystal nanocomposites," *Journal of Materials Chemistry - J MATER CHEM*, vol. 19, 09/22 2009.
- [85] C. D. Jones, M. Fidalgo, M. R. Wiesner, and A. R. Barron, "Alumina ultrafiltration membranes derived from carboxylate–alumoxane nanoparticles," *Journal of Membrane Science*, vol. 193, no. 2, pp. 175-184, 2001/11/15/ 2001.
- [86] Z.-H. Huang, Y.-N. Yin, G.-l.-m.-l. Aikebaier, and Y. Zhang, "Preparation of a novel positively charged nanofiltration composite membrane incorporated with silver nanoparticles for pharmaceuticals and personal care product rejection and antibacterial properties," *Water Science and Technology*, vol. 73, no. 8, pp. 1910-1919, 2016.
- [87] J. W. Jeong, H. S. Hwang, D. Choi, B. C. Ma, J. Jung, and M. Chang, "Hybrid Polymer/Metal Oxide Thin Films for High Performance, Flexible Transistors," (in eng), *Micromachines*, vol. 11, no. 3, p. 264, 2020.
- [88] A. Yaqoob, T. Parveen, K. Umar, M. Nasir, and M. Ibrahim, "Role of Nanomaterials in the Treatment of Wastewater: A Review," *Water*, vol. 12, p. 495, 02/11 2020.
- [89] V. Moghimifar, A. Raisi, and A. Aroujalian, "Surface modification of polyethersulfone ultrafiltration membranes by corona plasma-assisted coating TiO<sub>2</sub> nanoparticles," *Journal of Membrane Science*, vol. 461, pp. 69-80, 2014/07/01/ 2014.
- [90] S. S. Madaeni and N. Ghaemi, "Characterization of Self-Cleaning RO Membranes Coated with TiO<sub>2</sub> Particles Under UV Irradiation," *Journal of Membrane Science*, vol. 303, pp. 221-233, 10/01 2007.

- [91] H. Wu, J. Mansouri, and V. Chen, "Silica nanoparticles as carriers of antifouling ligands for PVDF ultrafiltration membranes," *Journal of Membrane Science*, vol. 433, pp. 135-151, 2013/04/15/ 2013.
- [92] T.-S. Chung, L. Y. Jiang, Y. Li, and S. Kulprathipanja, "Mixed matrix membranes (MMMs) comprising organic polymers with dispersed inorganic fillers for gas separation," *Progress in Polymer Science*, vol. 32, pp. 483-507, 04/01 2007.
- [93] D. Qadir, H. Mukhtar, and L. K. Keong, "Mixed Matrix Membranes for Water Purification Applications," *Separation & Purification Reviews*, vol. 46, no. 1, pp. 62-80, 2017/01/02 2017.
- [94] X.-L. Li, L.-P. Zhu, B.-K. Zhu, and Y.-Y. Xu, "High-flux and anti-fouling cellulose nanofiltration membranes prepared via phase inversion with ionic liquid as solvent," *Separation and Purification Technology*, vol. 83, pp. 66-73, 2011/11/15/ 2011.
- [95] B. Medronho, A. Romano, M. Miguel, L. Stigsson, and B. Lindman, "Rationalizing cellulose (in)solubility: Reviewing basic physicochemical aspects and role of hydrophobic interactions," *Cellulose*, vol. 19, pp. 581-587, 06/01 2012.
- [96] A. Sagie and B. Freeman, "Fundamentals of Membranes for Water Treatment," *The Future of Desalination in Texas*, vol. 2, 01/01 2004.
- [97] H. A. G. a. U. B. Pelin Onsekizoglu Bagci, "Surface modification of commercial cellulose acetate membranes via low pressure plasma for improved reverse osmosis performance: A case study of pomegranate juice concentration," 2017.

- [98] F. Liu, N. A. Hashim, Y. Liu, M. R. M. Abed, and K. Li, "Progress in the production and modification of PVDF membranes," *Journal of Membrane Science*, vol. 375, no. 1, pp. 1-27, 2011/06/15/ 2011.
- [99] H. Karimnezhad, A. H. Navarchian, T. Tavakoli Gheinani, and S. Zinadini, "Incorporation of iron oxyhydroxide nanoparticles in polyacrylonitrile nanofiltration membrane for improving water permeability and antifouling property," *Reactive and Functional Polymers*, vol. 135, pp. 77-93, 2019/02/01/ 2019.
- [100] M. T. Tsehay, J. Wang, J. Zhu, S. Velizarov, and B. Van der Bruggen, "Development and characterization of polyethersulfone-based nanofiltration membrane with stability to hydrogen peroxide," *Journal of Membrane Science*, vol. 550, pp. 462-469, 2018/03/15/ 2018.
- [101] C. Wei *et al.*, "Negatively charged polyimide nanofiltration membranes with high selectivity and performance stability by optimization of synergistic imidization," *Journal of Membrane Science*, vol. 563, pp. 752-761, 2018/10/01/ 2018.
- [102] S. Yang, Q. Zou, T. Wang, and L. Zhang, "Effects of GO and MOF@GO on the permeation and antifouling properties of cellulose acetate ultrafiltration membrane," *J. Membr. Sci.*, vol. 569, pp. 48-59, 2019/01/01/ 2019.
- [103] B. Han, D. Zhang, Z. Shao, L. Kong, and S. Lv, "Preparation and characterization of cellulose acetate/carboxymethyl cellulose acetate blend ultrafiltration membranes," *Desalination*, vol. 311, pp. 80-89, 2013/02/15/ 2013.

- [104] S.-s. Shen, H. Chen, R.-h. Wang, W. Ji, Y. Zhang, and R. Bai, "Preparation of antifouling cellulose acetate membranes with good hydrophilic and oleophobic surface properties," *Materials Letters*, vol. 252, pp. 1-4, 2019/10/01/ 2019.
- [105] C. S. Ong, P. S. Goh, W. J. Lau, N. Misdan, and A. F. Ismail, "Nanomaterials for biofouling and scaling mitigation of thin film composite membrane: A review," *Desalination*, vol. 393, pp. 2-15, 2016/09/01/ 2016.
- [106] J. Zhu *et al.*, "Polymeric antimicrobial membranes enabled by nanomaterials for water treatment," *Journal of Membrane Science*, vol. 550, pp. 173-197, 2018/03/15/ 2018.
- [107] S. Beisl *et al.*, "Synthesis and bactericide activity of nanofiltration composite membranes – Cellulose acetate/silver nanoparticles and cellulose acetate/silver ion exchanged zeolites," *Water Research*, vol. 149, pp. 225-231, 2019/02/01/ 2019.
- [108] S. M. Ghaseminezhad, M. Barikani, and M. Salehirad, "Development of graphene oxide-cellulose acetate nanocomposite reverse osmosis membrane for seawater desalination," *Composites Part B: Engineering*, vol. 161, pp. 320-327, 2019/03/15/ 2019.
- [109] b. Sanchuan Yu a, c,n, Qibo Cheng a,b, Chuanmin Huang a,b, Jia Liu a,b, Xiangyang Peng a,b, Meihong Liu b,c, Congjie Gao d, "Cellulose acetate hollow fiber nanofiltration membrane with improved permselectivity prepared through hydrolysis followed by carboxymethylation," *ScienceDirect*, 2013.
- [110] H.-C. Y. Jing-Jing Wang, Ming-Bang Wu, Xi Zhang and Zhi-Kang Xu, " Nanofiltration membranes with cellulose nanocrystals as an interlayer for unprecedented performance†," *Journal of Materials Chemistry A*, 2017.

- [111] S. L. Shi Li†, Fang Huang†, Shan Lin†, Hui Zhang†, Shilin Cao†, Lihui Chen†, Zhibin He‡, Ryan Lutes‡, "Preparation and Characterization of Cellulose-Based Nanofiltration Membranes by Interfacial Polymerization with Piperazine and Trimesoyl Chloride," *ACS Sustainable Chemistry & Engineering* 2018.
- [112] S. L. Shi Li, Fang Huang, Shan Lin, Hui Zhang, Shilin Cao, Lihui Chen, Zhibin He, Ryan Lutes, junhui Yang, Yonghao Ni, and Liulian Huang, "Preparation and characterization of cellulose-based nanofiltration membranes by interfacial polymerization with piperazine and trimesoyl chloride," *ACS Sustainable Chemistry Engineering*, 2018.
- [113] L.-P. Z. Xiao-Lin Li, Bao-Ku Zhu, You-Yi Xu, "High-flux and anti-fouling cellulose nanofiltration membranes prepared via phase inversion with ionic liquid as solvent," *ScienceDirect*, 2011.
- [114] A. Karimi, A. Khataee, V. Vatanpour, and M. Safarpour, "High-flux PVDF mixed matrix membranes embedded with size-controlled ZIF-8 nanoparticles," *Separation and Purification Technology*, vol. 229, p. 115838, 2019/12/15/ 2019.
- [115] c. Seyedeh Masumeh Ghaseminezhada, Mehdi Barikanib,\*, Mehdi Salehirad, "Development of graphene oxide-cellulose acetate nanocomposite reverse T osmosis membrane for seawater desalination " *Science Direct*
- [116] H. Zarrabi, m. e. Yekavalangi, V. Vatanpour, A. Shockravi, and M. Safarpour, "Improvement in desalination performance of thin film nanocomposite nanofiltration membrane using amine-functionalized multiwalled carbon nanotube," *Desalination*, vol. 394, pp. 83-90, 09/01 2016.
- [117] S. Zinadini, A. A. Zinatizadeh, M. Rahimi, V. Vatanpour, and H. Zangeneh, "Preparation of a novel antifouling mixed matrix PES membrane by embedding



- graphene oxide nanoplates," *Journal of Membrane Science*, vol. 453, pp. 292-301, 2014/03/01/ 2014.
- [118] R. Abedini, S. M. Mousavi, and R. Aminzadeh, "A novel cellulose acetate (CA) membrane using TiO<sub>2</sub> nanoparticles: Preparation, characterization and permeation study," *Desalination*, vol. 277, no. 1, pp. 40-45, 2011/08/15/ 2011.
- [119] A. Ahmad *et al.*, "Effect of silica on the properties of cellulose acetate/polyethylene glycol membranes for reverse osmosis," *Desalination*, vol. 355, pp. 1–10, 01/01 2015.
- [120] R. Kabiri and H. Namazi, "Nanocrystalline cellulose acetate (NCCA)/graphene oxide (GO) nanocomposites with enhanced mechanical properties and barrier against water vapor," *cellulose*, vol. 21, 07/20 2014.
- [121] W. Choi, J. Choi, J. Bang, and J.-H. Lee, "Layer-by-Layer Assembly of Graphene Oxide Nanosheets on Polyamide Membranes for Durable Reverse-Osmosis Applications," *ACS Applied Materials & Interfaces*, vol. 5, no. 23, pp. 12510-12519, 2013/12/11 2013.
- [122] J.-J. Wang, H.-C. Yang, M.-B. Wu, X. Zhang, and Z.-K. Xu, "Nanofiltration membranes with cellulose nanocrystals as an interlayer for unprecedented performance," *Journal of Materials Chemistry A*, 10.1039/C7TA00501F vol. 5, no. 31, pp. 16289-16295, 2017.
- [123] Y. Shi, C. Li, D. He, L. Shen, and N. Bao, "Preparation of graphene oxide–cellulose acetate nanocomposite membrane for high-flux desalination," *Journal of Materials Science*, vol. 52, 11/01 2017.
- [124] R. Han, X. Ma, Y. Xie, D. Teng, and S. Zhang, "Preparation of a new 2D MXene/PES composite membrane with excellent hydrophilicity and high flux," *RSC Advances*, 10.1039/C7RA10318B vol. 7, no. 89, pp. 56204-56210, 2017.

- [125] C. E. R. Zheng Linga, Meng-Qiang Zhaoa, Jian Yanga, James M. Giammarcoa, Jieshan Qiuc, Michel W. Barsouma, and Yury Gogotsia, "Flexible and conductive MXene films and nanocomposites with high capacitance," 2014.
- [126] H. Zhang *et al.*, "Preparation, mechanical and anti-friction performance of MXene/polymer composites," *Materials & Design*, vol. 92, pp. 682-689, 2016/02/15/ 2016.
- [127] C. Xinxin, W. Mengqi, Z. Aiguo, W. You, H. Xiaofang, and W. Libo, "Non-isothermal crystallization and thermal degradation kinetics of MXene/linear low-density polyethylene nanocomposites," (in English), *e-Polymers*, vol. 17, no. 5, pp. 373-381, 2017.
- [128] M. Naguib *et al.*, "Ti<sub>3</sub>C<sub>2</sub>T<sub>x</sub> (MXene)–polyacrylamide nanocomposite films," *RSC Advances*, 10.1039/C6RA10384G vol. 6, no. 76, pp. 72069-72073, 2016.
- [129] R. P. Pandey, P. A. Rasheed, T. Gomez, R. S. Azam, and K. A. Mahmoud, "A fouling-resistant mixed-matrix nanofiltration membrane based on covalently cross-linked Ti<sub>3</sub>C<sub>2</sub>TX (MXene)/cellulose acetate," *Journal of Membrane Science*, p. 118139, 2020/04/16/ 2020.
- [130] M. Hu and B. Mi, "Enabling Graphene Oxide Nanosheets as Water Separation Membranes," *Environmental Science & Technology*, vol. 47, no. 8, pp. 3715-3723, 2013/04/16 2013.
- [131] Y. Han, Y. Jiang, and C. Gao, "High-Flux Graphene Oxide Nanofiltration Membrane Intercalated by Carbon Nanotubes," *ACS Applied Materials & Interfaces*, vol. 7, no. 15, pp. 8147-8155, 2015/04/22 2015.

- [132] Y. Yuan *et al.*, "Enhanced desalination performance of carboxyl functionalized graphene oxide nanofiltration membranes," *Desalination*, vol. 405, pp. 29-39, 2017/03/01/ 2017.
- [133] Z. Luo, Q. Fang, X. Xu, D. V. Raj, X. Zhou, and Z. Liu, "Attapulgite nanofibers and graphene oxide composite membrane for high-performance molecular separation," *Journal of Colloid and Interface Science*, vol. 545, pp. 276-281, 2019/06/01/ 2019.
- [134] J. Lv, G. Zhang, H. Zhang, and F. Yang, "Exploration of permeability and antifouling performance on modified cellulose acetate ultrafiltration membrane with cellulose nanocrystals," *Carbohydrate Polymers*, vol. 174, pp. 190-199, 2017/10/15/ 2017.
- [135] S. Vetrivel, M. S. A. Saraswathi, D. Rana, and A. Nagendran, "Fabrication of cellulose acetate nanocomposite membranes using 2D layered nanomaterials for macromolecular separation," *International Journal of Biological Macromolecules*, vol. 107, pp. 1607-1612, 2018/02/01/ 2018.
- [136] Y. Zhang, K. Su, and Z. Li, "Graphene oxide composite membranes cross-linked with urea for enhanced desalting properties," *Journal of Membrane Science*, vol. 563, pp. 718-725, 2018/10/01/ 2018.
- [137] Y. Jiang, Q. Zeng, P. Biswas, and J. D. Fortner, "Graphene oxides as nanofillers in polysulfone ultrafiltration membranes: Shape matters," *Journal of Membrane Science*, vol. 581, pp. 453-461, 2019/07/01/ 2019.
- [138] L. Ding, Y. Wei, Y. Wang, H. Chen, J. Caro, and H. Wang, "A Two-Dimensional Lamellar Membrane: MXene Nanosheet Stacks," *Angewandte Chemie International Edition*, vol. 56, no. 7, pp. 1825-1829, 2017/02/06 2017.

- [139] R. P. Pandey, K. Rasool, V. E. Madhavan, B. Aïssa, Y. Gogotsi, and K. A. Mahmoud, "Ultrahigh-flux and fouling-resistant membranes based on layered silver/MXene (Ti<sub>3</sub>C<sub>2</sub>T<sub>x</sub>) nanosheets," *J. Mater. Chem. A*, 10.1039/C7TA10888E vol. 6, no. 8, pp. 3522-3533, 2018.
- [140] M. Naguib *et al.*, "Two-Dimensional Nanocrystals Produced by Exfoliation of Ti<sub>3</sub>AlC<sub>2</sub>," *Advanced Materials*, vol. 23, no. 37, pp. 4248-4253, 2011/08/22 2011.
- [141] N. Tzenov and M. Barsoum, "Synthesis and Characterization of Ti<sub>3</sub>AlC<sub>2</sub>," *Journal of the American Ceramic Society*, vol. 83, pp. 825-832, 04/01 2000.
- [142] R. Alfahel *et al.*, "Fabrication of fouling resistant Ti<sub>3</sub>C<sub>2</sub>T<sub>x</sub> (MXene)/cellulose acetate nanocomposite membrane for forward osmosis application," *Journal of Water Process Engineering*, vol. 38, p. 101551, 2020/12/01/ 2020.
- [143] M. Naguib *et al.*, "Two-Dimensional Nanocrystals Produced by Exfoliation of Ti<sub>3</sub>AlC<sub>2</sub>," *Adv. Mater.*, vol. 23, no. 37, pp. 4248-4253, 2011.
- [144] M. Ghidui, M. R. Lukatskaya, M.-Q. Zhao, Y. Gogotsi, and M. W. Barsoum, "Conductive two-dimensional titanium carbide 'clay' with high volumetric capacitance," *Nature*, vol. 516, p. 78, 11/26/online 2014.
- [145] L. Dong, C. Ye, L. Zheng, Z. F. Gao, and F. Xia, "Two-dimensional metal carbides and nitrides (MXenes): preparation, property, and applications in cancer therapy," *Nanophotonics*, 04/13 2020.
- [146] K. Rasool, R. P. Pandey, P. A. Rasheed, S. Buczek, Y. Gogotsi, and K. A. Mahmoud, "Water treatment and environmental remediation applications of two-dimensional metal carbides (MXenes)," *Materials Today*, vol. 30, pp. 80-102, 2019/11/01/ 2019.

- [147] S. Li *et al.*, "Highly selective sodium alginate mixed-matrix membrane incorporating multi-layered MXene for ethanol dehydration," *Separation and Purification Technology*, vol. 235, p. 116206, 2020/03/18/ 2020.
- [148] G. Liu *et al.*, "Ultrathin two-dimensional MXene membrane for pervaporation desalination," *Journal of Membrane Science*, vol. 548, pp. 548-558, 2018/02/15/ 2018.
- [149] J. Wang *et al.*, "Confined Self-Assembly in Two-Dimensional Interlayer Space: Monolayered Mesoporous Carbon Nanosheets with In-Plane Orderly Arranged Mesopores and a Highly Graphitized Framework," *Angewandte Chemie International Edition*, vol. 57, no. 11, pp. 2894-2898, 2018/03/05 2018.
- [150] K. Rasool, K. Mahmoud, D. Johnson, M. I Helal, G. Berdiyrov, and Y. Gogotsi, "Efficient Antibacterial Membrane based on Two-Dimensional Ti<sub>3</sub>C<sub>2</sub>Tx (MXene) Nanosheets," *Scientific Reports*, vol. 7, 12/01 2017.
- [151] K. Rasool, M. Helal, A. Ali, C. E. Ren, Y. Gogotsi, and K. A. Mahmoud, "Antibacterial Activity of Ti<sub>3</sub>C<sub>2</sub>Tx MXene," *ACS Nano*, vol. 10, no. 3, pp. 3674-3684, 2016/03/22 2016.
- [152] Z. Ling *et al.*, "Flexible and conductive MXene films and nanocomposites with high capacitance," *Proceedings of the National Academy of Sciences*, vol. 111, no. 47, p. 16676, 2014.
- [153] J. Saththasivam, K. Wang, W. Yiming, Z. Liu, and K. A. Mahmoud, "A flexible Ti<sub>3</sub>C<sub>2</sub>Tx (MXene)/paper membrane for efficient oil/water separation," *RSC Advances*, 10.1039/C9RA02129A vol. 9, no. 29, pp. 16296-16304, 2019.
- [154] J.-Y. Si *et al.*, "Functionalization of MXene Nanosheets for Polystyrene towards High Thermal Stability and Flame Retardant Properties," *Polymers*, vol. 11, p. 976, 06/03 2019.

- [155] W. Zhi *et al.*, "Study of MXene-filled polyurethane nanocomposites prepared via an emulsion method," *Composites Science and Technology*, vol. 168, 10/01 2018.
- [156] H. Zhang, Z. Wang, Y. Shen, P. Mu, Q. Wang, and J. Li, "Ultrathin 2D Ti<sub>3</sub>C<sub>2</sub>T<sub>x</sub> MXene membrane for effective separation of oil-in-water emulsions in acidic, alkaline, and salty environment," *Journal of Colloid and Interface Science*, vol. 561, pp. 861-869, 2020/03/01/ 2020.
- [157] C. E. Ren, K. B. Hatzell, M. Alhabeb, Z. Ling, K. A. Mahmoud, and Y. Gogotsi, "Charge- and Size-Selective Ion Sieving Through Ti<sub>3</sub>C<sub>2</sub>T<sub>x</sub> MXene Membranes," *J. Phys. Chem. Lett.*, vol. 6, no. 20, pp. 4026-4031, 2015/10/15 2015.
- [158] K. Rasool, K. A. Mahmoud, D. J. Johnson, M. Helal, G. R. Berdiyrov, and Y. Gogotsi, "Efficient Antibacterial Membrane based on Two-Dimensional Ti<sub>3</sub>C<sub>2</sub>T<sub>x</sub> (MXene) Nanosheets," *Sci. Rep.*, vol. 7, no. 1, p. 1598, 2017/05/09 2017.
- [159] X. Wu, L. Hao, J. Zhang, X. Zhang, J. Wang, and J. Liu, "Polymer-Ti<sub>3</sub>C<sub>2</sub>T<sub>x</sub> composite membranes to overcome the trade-off in solvent resistant nanofiltration for alcohol-based system," *J. Membr. Sci.*, vol. 515, pp. 175-188, 2016/10/01/ 2016.
- [160] K. M. Kang *et al.*, "Selective Molecular Separation on Ti<sub>3</sub>C<sub>2</sub>T<sub>x</sub>-Graphene Oxide Membranes during Pressure-Driven Filtration: Comparison with Graphene Oxide and MXenes," *ACS Appl. Mater. Interfaces*, vol. 9, no. 51, pp. 44687-44694, 2017/12/27 2017.

- [161] S. Wei *et al.*, "Two-dimensional graphene Oxide/MXene composite lamellar membranes for efficient solvent permeation and molecular separation," *Journal of Membrane Science*, vol. 582, pp. 414-422, 2019/07/15/ 2019.
- [162] G. Liu *et al.*, "Ultrathin two-dimensional MXene membrane for pervaporation desalination," *J. Membr. Sci.*, vol. 548, pp. 548-558, 2018/02/15/ 2018.
- [163] R. Han, Y. Xie, and X. Ma, "Crosslinked P84 copolyimide/MXene mixed matrix membrane with excellent solvent resistance and permselectivity," *Chinese Journal of Chemical Engineering*, vol. 27, no. 4, pp. 877-883, 2019/04/01/ 2019.
- [164] Z. Xu, G. Liu, H. Ye, W. Jin, and Z. Cui, "Two-dimensional MXene incorporated chitosan mixed-matrix membranes for efficient solvent dehydration," *Journal of Membrane Science*, vol. 563, pp. 625-632, 2018/10/01/ 2018.
- [165] J. Li, X. Li, and B. Bruggen, "MXene based membrane for molecular separation," *Environmental Science: Nano*, 03/06 2020.
- [166] X. Jin *et al.*, "Effects of Thermal Cross-Linking on the Structure and Property of Asymmetric Membrane Prepared from the Polyacrylonitrile," (in eng), *Polymers*, vol. 10, no. 5, p. 539, 2018.
- [167] B. Bolto, T. Tran, M. Hoang, and Z. Xie, "Crosslinked poly(vinyl alcohol) membranes," *Progress in Polymer Science*, vol. 34, pp. 969-981, 09/01 2009.
- [168] T.-T. Dong, G.-H. Chen, and C.-J. Gao, "Preparation of chitin xanthate/polyacrylonitrile NF composite membrane with cross-linking agent hydrogen peroxide and its characterization," *Journal of Membrane Science*, vol. 304, no. 1, pp. 33-39, 2007/11/01/ 2007.

- [169] Q. Guo, P. N. Pintauro, H. Tang, and S. O'Connor, "Sulfonated and crosslinked polyphosphazene-based proton-exchange membranes," *Journal of Membrane Science*, vol. 154, no. 2, pp. 175-181, 1999/03/17/ 1999.
- [170] Y.-L. Liu, Y.-H. Su, and J.-Y. Lai, "In situ crosslinking of chitosan and formation of chitosan-silica hybrid membranes with using  $\gamma$ -glycidoxypropyltrimethoxysilane as a crosslinking agent," *Polymer*, vol. 45, no. 20, pp. 6831-6837, 2004/09/16/ 2004.
- [171] T. Puspasari, N. Pradeep, and K.-V. Peinemann, "Crosslinked cellulose thin film composite nanofiltration membranes with zero salt rejection," *Journal of Membrane Science*, vol. 491, pp. 132-137, 2015/10/01/ 2015.
- [172] J.-W. Rhim, H. B. Park, C.-S. Lee, J.-H. Jun, D. S. Kim, and Y. M. Lee, "Crosslinked poly(vinyl alcohol) membranes containing sulfonic acid group: proton and methanol transport through membranes," *Journal of Membrane Science*, vol. 238, no. 1, pp. 143-151, 2004/07/15/ 2004.
- [173] M. Heydari, A. Moheb, M. Ghiaci, and M. Masoomi, "Effect of cross-linking time on the thermal and mechanical properties and pervaporation performance of poly(vinyl alcohol) membrane cross-linked with fumaric acid used for dehydration of isopropanol," *Journal of Applied Polymer Science*, vol. 128, no. 3, pp. 1640-1651, 2013/05/05 2013.
- [174] M. Beppu, R. Vieira, C. Aimoli, and C. Santana, "Crosslinking of chitosan membranes using glutaraldehyde: Effect on ion permeability and water absorption," *Journal of Membrane Science - J MEMBRANE SCI*, vol. 301, pp. 126-130, 09/01 2007.



- [175] S. Shenvi, A. F. Ismail, and A. M. Isloor, "Preparation and characterization study of PPEES/chitosan composite membrane crosslinked with tripolyphosphate," *Desalination*, vol. 344, pp. 90-96, 2014/07/01/ 2014.
- [176] "Phase inversion," ed, 2018.
- [177] K. Ebert, D. Fritsch, J. Koll, and C. Tjahjajawiguna, "Influence of inorganic fillers on the compaction behaviour of porous polymer based membranes," *Journal of Membrane Science*, vol. 233, pp. 71-78, 04/01 2004.
- [178] J. María Arsuaga *et al.*, "Influence of the type, size, and distribution of metal oxide particles on the properties of nanocomposite ultrafiltration membranes," *Journal of Membrane Science*, vol. 428, pp. 131-141, 2013/02/01/ 2013.
- [179] Y. Yang, P. Wang, and Q. Zheng, "Preparation and properties of polysulfone/TiO<sub>2</sub> composite ultrafiltration membranes," *Journal of Polymer Science Part B: Polymer Physics*, vol. 44, no. 5, pp. 879-887, 2006/03/01 2006.
- [180] X. Cao, J. Ma, X. Shi, and Z. Ren, "Effect of TiO<sub>2</sub> nanoparticle size on the performance of PVDF membrane," *Applied Surface Science*, vol. 253, pp. 2003-2010, 12/01 2006.
- [181] Y. Xiao, K. Wang, T.-S. Chung, and J. Tan, "Evolution of nano-particle distribution during the fabrication of mixed matrix TiO<sub>2</sub>-polyimide hollow fiber membranes," *Chemical Engineering Science - CHEM ENG SCI*, vol. 61, pp. 6228-6233, 09/01 2006.
- [182] J.-B. Li, J.-W. Zhu, and M.-S. Zheng, "Morphologies and properties of poly(phthalazinone ether sulfone ketone) matrix ultrafiltration membranes with entrapped TiO<sub>2</sub> nanoparticles," *Journal of Applied Polymer Science*, vol. 103, no. 6, pp. 3623-3629, 2007/03/15 2007.

- [183] Y. Yang, H. Zhang, P. Wang, Q. Zheng, and J. Li, "The influence of nano-sized TiO<sub>2</sub> fillers on the morphologies and properties of PSF UF membrane," *Journal of Membrane Science*, vol. 288, no. 1, pp. 231-238, 2007/02/01/ 2007.
- [184] X. Fu, H. Matsuyama, and H. Nagai, "Structure control of asymmetric poly(vinyl butyral)-TiO<sub>2</sub> composite membrane prepared by nonsolvent induced phase separation," *Journal of Applied Polymer Science*, vol. 108, no. 2, pp. 713-723, 2008/04/15 2008.
- [185] G. Wu, S. Gan, L. Cui, and Y. Xu, "Preparation and characterization of PES/TiO<sub>2</sub> composite membranes," *Applied Surface Science*, vol. 254, no. 21, pp. 7080-7086, 2008/08/30/ 2008.
- [186] L.-Y. Yu, H.-M. Shen, and Z.-L. Xu, "PVDF-TiO<sub>2</sub> composite hollow fiber ultrafiltration membranes prepared by TiO<sub>2</sub> sol-gel method and blending method," *Journal of Applied Polymer Science*, vol. 113, no. 3, pp. 1763-1772, 2009/08/05 2009.
- [187] J.-F. Li, Z.-L. Xu, H. Yang, L.-Y. Yu, and M. Liu, "Effect of TiO<sub>2</sub> nanoparticles on the surface morphology and performance of microporous PES membrane," *Applied Surface Science*, vol. 255, no. 9, pp. 4725-4732, 2009/02/15/ 2009.
- [188] S. J. Oh, N. Kim, and Y. T. Lee, "Preparation and characterization of PVDF/TiO<sub>2</sub> organic-inorganic composite membranes for fouling resistance improvement," *Journal of Membrane Science*, vol. 345, no. 1, pp. 13-20, 2009/12/01/ 2009.
- [189] A. Razmjou, J. Mansouri, and V. Chen, "The effects of mechanical and chemical modification of TiO<sub>2</sub> nanoparticles on the surface chemistry, structure and fouling performance of PES ultrafiltration membranes," *Journal of Membrane Science*, vol. 378, no. 1, pp. 73-84, 2011/08/15/ 2011.

- [190] S. S. Madaeni, S. Zinadini, and V. Vatanpour, "A new approach to improve antifouling property of PVDF membrane using in situ polymerization of PAA functionalized TiO<sub>2</sub> nanoparticles," *Journal of Membrane Science*, vol. 380, pp. 155-162, 09/01 2011.
- [191] A. Sotto, A. Boromand, S. Balta, J. Kim, and B. Van der Bruggen, "Doping of polyethersulfone nanofiltration membranes: antifouling effect observed at ultralow concentrations of TiO<sub>2</sub> nanoparticles," *Journal of Materials Chemistry*, 10.1039/C1JM11040C vol. 21, no. 28, pp. 10311-10320, 2011.
- [192] N. A. A. Hamid *et al.*, "Morphological and separation performance study of polysulfone/titanium dioxide (PSF/TiO<sub>2</sub>) ultrafiltration membranes for humic acid removal," *Desalination*, vol. 273, no. 1, pp. 85-92, 2011/06/01/ 2011.
- [193] E. Yuliwati and A. Ismail, "Effect of additives concentration on the surface properties and performance of PVDF ultrafiltration membranes for refinery produced wastewater treatment," *Desalination*, vol. 273, pp. 226-234, 06/01 2011.
- [194] A. Rahimpour, M. Jahanshahi, B. Rajaeian, and M. Rahimnejad, "TiO<sub>2</sub> entrapped nano-composite PVDF/SPES membranes: Preparation, characterization, antifouling and antibacterial properties," *Desalination*, 09/01 2011.
- [195] A. Sotto *et al.*, "Effect of nanoparticle aggregation at low concentrations of TiO<sub>2</sub> on the hydrophilicity, morphology, and fouling resistance of PES–TiO<sub>2</sub> membranes," *Journal of Colloid and Interface Science*, vol. 363, no. 2, pp. 540-550, 2011/11/15/ 2011.
- [196] V. Vatanpour, S. Madaeni, A. Khataee, E. Salehi, S. Zinadini, and H. Monfared, "TiO<sub>2</sub> embedded mixed matrix PES nanocomposite membranes: Influence of

- different sizes and types of nanoparticles on antifouling and performance," *Desalination*, vol. 292, pp. 19–29, 04/01 2012.
- [197] A. Razmjou, A. Resosudarmo, R. L. Holmes, H. Li, J. Mansouri, and V. Chen, "The effect of modified TiO<sub>2</sub> nanoparticles on the polyethersulfone ultrafiltration hollow fiber membranes," *Desalination*, vol. 287, pp. 271-280, 2012/02/15/ 2012.
- [198] S. S. Homaeigohar, H. Mahdavi, and M. Elbahri, "Extraordinarily water permeable sol–gel formed nanocomposite nanofibrous membranes," *Journal of Colloid and Interface Science*, vol. 366, no. 1, pp. 51-56, 2012/01/15/ 2012.
- [199] S. Zhao, P. Wang, C. Wang, X. Sun, and L. Zhang, "Thermostable PPESK/TiO<sub>2</sub> nanocomposite ultrafiltration membrane for high temperature condensed water treatment," *Desalination*, vol. 299, pp. 35-43, 2012/08/01/ 2012.
- [200] R. Abedini, S. Mousavi, and R. Aminzadeh, "Effect of Sonochemical Synthesized TiO<sub>2</sub> nanoparticles and Coagulation Bath Temperature on Morphology, Thermal Stability and Pure Water Flux of Asymmetric Cellulose Acetate Nanocomposite Membranes Prepared via Phase Inversion Method," *Chemical Industry and Chemical Engineering Quarterly*, vol. 18, 01/06 2012.
- [201] V. Vatanpour, S. Madaeni, R. Moradian, S. Zinadini, and B. Astinchap, "Novel antibifouling nanofiltration polyethersulfone membrane fabricated from embedding TiO<sub>2</sub> coated multiwalled carbon nanotubes," *Separation and Purification Technology*, vol. 90, pp. 69–82, 04/01 2012.
- [202] N. Huey Ping, A. L. Ahmad, S. C. Low, and O. Seng, "Preparation of mixed-matrix membranes for micellar enhanced ultrafiltration based on response surface methodology," *Desalination*, vol. 293, pp. 7–20, 05/01 2012.

- [203] G. Zhang, S. Lu, L. Zhang, Q. Meng, C. Shen, and J. Zhang, "Novel polysulfone hybrid ultrafiltration membrane prepared with TiO<sub>2</sub>-g-HEMA and its antifouling characteristics," *Journal of Membrane Science*, vol. 436, pp. 163-173, 2013/06/01/ 2013.
- [204] F. Zhang, W. Zhang, Y. Yu, B. Deng, J. Li, and J. Jin, "Sol-gel preparation of PAA-g-PVDF/TiO<sub>2</sub> nanocomposite hollow fiber membranes with extremely high water flux and improved antifouling property," *Journal of Membrane Science*, vol. 432, pp. 25-32, 2013/04/01/ 2013.
- [205] S. B. Teli, S. Molina, A. Sotto, E. G. Calvo, and J. d. Abajob, "Fouling Resistant Polysulfone-PANI/TiO<sub>2</sub> Ultrafiltration Nanocomposite Membranes," *Industrial & Engineering Chemistry Research*, vol. 52, no. 27, pp. 9470-9479, 2013/07/10 2013.
- [206] Y. H. Teow, A. L. Ahmad, J. K. Lim, and B. S. Ooi, "Studies on the surface properties of mixed-matrix membrane and its antifouling properties for humic acid removal," *Journal of Applied Polymer Science*, vol. 128, no. 5, pp. 3184-3192, 2013/06/05 2013.
- [207] H. Kim, H. Pant, J. Kim, N. Choi, and C. Kim, "Fabrication of multifunctional TiO<sub>2</sub>-fly ash/polyurethane nanocomposite membrane via electrospinning," *Ceramics International*, vol. 40, pp. 3023-3029, 03/01 2014.
- [208] M. Sun, Y. Su, C. Mu, and Z. Jiang, "Improved Antifouling Property of PES Ultrafiltration Membranes Using Additive of Silica-PVP Nanocomposite," *Industrial & Engineering Chemistry Research*, vol. 49, no. 2, pp. 790-796, 2010/01/20 2010.
- [209] E. M. V. Hoek, A. K. Ghosh, X. Huang, M. Liang, and J. I. Zink, "Physical-chemical properties, separation performance, and fouling resistance of mixed-

- matrix ultrafiltration membranes," *Desalination*, vol. 283, pp. 89-99, 2011/12/01/ 2011.
- [210] A. Jomekian, S. Mansoori, and N. Monirimanesh, "Synthesis and characterization of novel PEO–MCM-41/PVDC nanocomposite membrane," *Desalination*, vol. 276, 05/08 2011.
- [211] C. Klaysom, S.-H. Moon, B. P. Ladewig, G. Q. M. Lu, and L. Wang, "The Influence of Inorganic Filler Particle Size on Composite Ion-Exchange Membranes for Desalination," *The Journal of Physical Chemistry C*, vol. 115, no. 31, pp. 15124-15132, 2011/08/11 2011.
- [212] J.-n. Shen, H.-m. Ruan, L.-g. Wu, and C.-j. Gao, "Preparation and characterization of PES–SiO<sub>2</sub> organic–inorganic composite ultrafiltration membrane for raw water pretreatment," *Chemical Engineering Journal*, vol. 168, no. 3, pp. 1272-1278, 2011/04/15/ 2011.
- [213] B. Muriithi and D. A. Loy, "Processing, Morphology, and Water Uptake of Nafion/Ex situ Stöber Silica Nanocomposite Membranes As a Function of Particle Size," *ACS Applied Materials & Interfaces*, vol. 4, no. 12, pp. 6766-6773, 2012/12/26 2012.
- [214] J. Huang, K. Zhang, K. Wang, Z. Xie, B. Ladewig, and H. Wang, "Fabrication of polyethersulfone-mesoporous silica nanocomposite ultrafiltration membranes with antifouling properties," *Journal of Membrane Science*, vol. 423, 12/01 2012.
- [215] M. Pakizeh, A. Moghadam, M. Omidkhah, and M. Namvar-Mahboub, "Preparation and characterization of dimethyldichlorosilane modified SiO<sub>2</sub>/PSf nanocomposite membrane," *Korean Journal of Chemical Engineering*, vol. 30, 03/01 2013.

- [216] H. Wu, B. Tang, and P. Wu, "Development of novel SiO<sub>2</sub>–GO nanohybrid/polysulfone membrane with enhanced performance," *Journal of Membrane Science*, vol. 451, pp. 94-102, 2014/02/01/ 2014.
- [217] I. Yan, S. Hong, M. Li, and Y. Li, "Application of the Al<sub>2</sub>O<sub>3</sub>–PVDF nanocomposite tubular ultrafiltration (UF) membrane for oily wastewater treatment and its antifouling research," *Separation and Purification Technology - SEP PURIF TECHNOL*, vol. 66, pp. 347-352, 04/01 2009.
- [218] N. Maximous, G. Nakhla, W. Wan, and K. Wong, "Preparation, characterization and performance of Al<sub>2</sub>O<sub>3</sub>/PES membrane for wastewater filtration," *Journal of Membrane Science*, vol. 341, no. 1, pp. 67-75, 2009/09/30/ 2009.
- [219] N. Maximous, G. Nakhla, K. Wong, and W. Wan, "Optimization of Al<sub>2</sub>O<sub>3</sub>/PES membranes for wastewater filtration," *Separation and Purification Technology*, vol. 73, no. 2, pp. 294-301, 2010/06/18/ 2010.
- [220] N. Maximous, G. Nakhla, W. Wan, and K. Wong, "Effect of the metal oxide particle distributions on modified PES membranes characteristics and performance," *Journal of Membrane Science*, vol. 361, no. 1, pp. 213-222, 2010/09/30/ 2010.
- [221] I. Csetneki, G. Filipcsei, and M. Zrínyi, "Smart Nanocomposite Polymer Membranes with On/Off Switching Control," *Macromolecules*, vol. 39, no. 5, pp. 1939-1942, 2006/03/01 2006.
- [222] P. Daraei *et al.*, "Novel polyethersulfone nanocomposite membrane prepared by PANI/Fe<sub>3</sub>O<sub>4</sub> nanoparticles with enhanced performance for Cu(II) removal from water," *Journal of Membrane Science*, vol. 415–416, pp. 250-259, 05/18 2012.

- [223] A. Gholami, A. Moghadassi, S. M. Hosseini, S. Shabani, and F. Gholami, "Preparation and characterization of polyvinyl chloride based nanocomposite nanofiltration-membrane modified by iron oxide nanoparticles for lead removal from water," *Journal of Industrial and Engineering Chemistry*, vol. 20, pp. 1517-1522, 07/01 2014.
- [224] J. Alam, L. A. Dass, M. Ghasemi, and M. Alhoshan, "Synthesis and optimization of PES-Fe<sub>3</sub>O<sub>4</sub> mixed matrix nanocomposite membrane: Application studies in water purification," *Polymer Composites*, vol. 34, no. 11, pp. 1870-1877, 2013/11/01 2013.
- [225] P. Daraei, S. Madaeni, N. Ghaemi, M. A. Khadivi, B. Astinchap, and R. Moradian, "Fouling resistant mixed matrix polyethersulfone membranes blended with magnetic nanoparticles: Study of magnetic field induced casting," *Separation and Purification Technology*, vol. 109, pp. 111-121, 05/09 2013.
- [226] R. Gohari, W. J. Lau, T. Matsuura, E. Halakoo, and A. Ismail, "Adsorptive removal of Pb(II) from aqueous solution by novel PES/HMO ultrafiltration mixed matrix membrane," *Separation and Purification Technology*, vol. 120, pp. 59–68, 12/01 2013.
- [227] R. Jamshidi Gohari, E. Halakoo, N. A. M. Nazri, W. J. Lau, T. Matsuura, and A. F. Ismail, "Improving performance and antifouling capability of PES UF membranes via blending with highly hydrophilic hydrous manganese dioxide nanoparticles," *Desalination*, vol. 335, no. 1, pp. 87-95, 2014/02/17/ 2014.
- [228] M. Alhoshan, J. Alam, L. A. Dass, and N. Al-Homaidi, "Fabrication of Polysulfone/ZnO Membrane: Influence of ZnO Nanoparticles on Membrane Characteristics," *Advances in Polymer Technology*, vol. 32, no. 4, 2013/12/01 2013.



- [229] W.-L. Chou, D.-G. Yu, and M.-C. Yang, "The preparation and characterization of silver-loading cellulose acetate hollow fiber membrane for water treatment," *Polymers for Advanced Technologies*, vol. 16, no. 8, pp. 600-607, 2005/08/01 2005.
- [230] Y. Deng, G. Dang, H. Zhou, X. Rao, and C. Chen, "Preparation and characterization of polyimide membranes containing Ag nanoparticles in pores distributing on one side," *Materials Letters - MATER LETT*, vol. 62, pp. 1143-1146, 03/01 2008.
- [231] K. Zodrow *et al.*, "Polysulfone ultrafiltration membranes impregnated with silver nanoparticles show improved biofouling resistance and virus removal," *Water Research*, vol. 43, no. 3, pp. 715-723, 2009/02/01/ 2009.
- [232] H. Basri *et al.*, "Silver-filled polyethersulfone membranes for antibacterial applications — Effect of PVP and TAP addition on silver dispersion," *Desalination*, vol. 261, no. 3, pp. 264-271, 2010/10/31/ 2010.
- [233] S. Kar *et al.*, "Potential of nanoparticles for water purification: A case study on anti-biofouling behaviour of metal based polymeric nanocomposite membrane," *Desalination and Water Treatment - DESALIN WATER TREAT*, vol. 27, pp. 224-230, 03/01 2011.
- [234] H. Basri, A. Ismail, and M. Aziz, "Polyethersulfone (PES)–silver composite UF membrane: Effect of silver loading and PVP molecular weight on membrane morphology and antibacterial activity," *Desalination*, vol. 273, pp. 72-80, 06/01 2011.
- [235] H. Basri, A. Ismail, and M. Aziz, "Polyethersulfone (PES) ultrafiltration (UF) membranes loaded with silver nitrate for bacteria removal," *Membrane Water Treatment*, vol. 2, 01/25 2011.

- [236] S. K. Jewrajka and S. Haldar, "Amphiphilic poly(acrylonitrile-co-acrylic acid)/silver nanocomposite additives for the preparation of antibiofouling membranes with improved properties," *Polymer Composites*, vol. 32, no. 11, pp. 1851-1861, 2011/11/01 2011.
- [237] A. Dasari, J. Quirós, B. Herrero, K. Boltes, E. García-Calvo, and R. Rosal, "Antifouling membranes prepared by electrospinning polylactic acid containing biocidal nanoparticles," *Journal of Membrane Science*, vol. 405-406, pp. 134-140, 2012/07/01/ 2012.
- [238] M. Zhang, R. Field, and K. Zhang, "Biogenic silver nanocomposite polyethersulfone UF membranes with antifouling properties," *Journal of Membrane Science*, vol. 471, pp. 274–284, 12/01 2014.
- [239] Y. Liu, E. Rosenfield, M. Hu, and B. Mi, "Direct observation of bacterial deposition on and detachment from nanocomposite membranes embedded with silver nanoparticles," *Water research*, vol. 47, 03/14 2013.
- [240] A. Alpatova, E.-S. Kim, X. Sun, G. Hwang, Y. Liu, and M. Gamal El-Din, "Fabrication of porous polymeric nanocomposite membranes with enhanced anti-fouling properties: Effect of casting composition," *Journal of Membrane Science*, vol. 444, pp. 449-460, 2013/10/01/ 2013.
- [241] H. Pant *et al.*, "One-step fabrication of multifunctional composite polyurethane spider-web-like nanofibrous membrane for water purification," *Journal of hazardous materials*, vol. 264C, pp. 25-33, 11/04 2013.
- [242] N. Akar, B. Asar, N. Dizge, and I. Koyuncu, "Investigation of characterization and biofouling properties of PES membrane containing selenium and copper nanoparticles," *Journal of Membrane Science*, vol. 437, pp. 216–226, 06/01 2013.

- [243] G. Ciobanu, G. Carja, and O. Ciobanu, "Preparation and characterization of polymer–zeolite nanocomposite membranes," *Materials Science and Engineering: C*, vol. 27, no. 5, pp. 1138-1140, 2007/09/01/ 2007.
- [244] S. Husain and W. J. Koros, "Macrovoids in Hybrid Organic/Inorganic Hollow Fiber Membranes," *Industrial & Engineering Chemistry Research*, vol. 48, no. 5, pp. 2372-2379, 2009/03/04 2009.
- [245] M. U. M. Junaidi, C. Leo, S. Kamal, and A. L. Ahmad, "Fouling mitigation in humic acid ultrafiltration using polysulfone/SAPO-34 mixed matrix membrane," *Water science and technology : a journal of the International Association on Water Pollution Research*, vol. 67, pp. 2102-9, 05/01 2013.
- [246] C. P. Leo, N. Kamil, M. U. M. Junaidi, S. N. M. Kamal, and A. L. Ahmad, "The potential of SAPO-44 zeolite filler in fouling mitigation of polysulfone ultrafiltration membrane," *Separation and Purification Technology*, vol. 103, pp. 84–91, 01/15 2013.
- [247] F. Liu, B.-R. Ma, D. Zhou, Y.-h. Xiang, and L. Xue, "Breaking through tradeoff of Polysulfone ultrafiltration membranes by zeolite 4A," *Microporous and Mesoporous Materials*, vol. 186, pp. 113–120, 03/01 2014.
- [248] G. Mago, D. Kalyon, and F. Fisher, "Membranes of Polyvinylidene Fluoride and PVDF Nanocomposites with Carbon Nanotubes via Immersion Precipitation," *Journal of Nanomaterials*, 04/15 2008.
- [249] H. Wu, B. Tang, and P. Wu, "Novel ultrafiltration membranes prepared from a multi-walled carbon nanotubes/polymer composite," *Journal of Membrane Science*, vol. 362, no. 1, pp. 374-383, 2010/10/15/ 2010.
- [250] P. S. Goh, B. C. Ng, A. F. Ismail, M. Aziz, and S. M. Sanip, "Surfactant dispersed multi-walled carbon nanotube/polyetherimide nanocomposite

- membrane," *Solid State Sciences*, vol. 12, no. 12, pp. 2155-2162, 2010/12/01/ 2010.
- [251] H. Shawky, S.-R. Chae, S. Lin, and M. Wiesner, "Synthesis and characterization of a carbon nanotube/polymer nanocomposite membrane for water treatment," *Desalination*, vol. 272, pp. 46-50, 05/03 2011.
- [252] Y. Mansourpanah, S. S. Madaeni, A. Rahimpour, M. Adeli, M. Hashemi, and M. R. Moradian, "Fabrication new PES-based mixed matrix nanocomposite membranes using polycaprolactone modified carbon nanotubes as the additive: Property changes and morphological studies," *Desalination*, vol. 277, pp. 171-177, 08/01 2011.
- [253] V. Vatanpour, S. S. Madaeni, R. Moradian, S. Zinadini, and B. Astinchap, "Fabrication and characterization of novel antifouling nanofiltration membrane prepared from oxidized multiwalled carbon nanotube/polyethersulfone nanocomposite," *Journal of Membrane Science*, vol. 375, no. 1, pp. 284-294, 2011/06/15/ 2011.
- [254] S. Majeed *et al.*, "Multi-walled carbon nanotubes (MWCNTs) mixed polyacrylonitrile (PAN) ultrafiltration membranes," *Journal of Membrane Science*, vol. 403-404, pp. 101-109, 2012/06/01/ 2012.
- [255] X. Zhao *et al.*, "Hyperbranched-polymer functionalized multi-walled carbon nanotubes for poly (vinylidene fluoride) membranes: From dispersion to blended fouling-control membrane," *Desalination*, vol. 303, pp. 29-38, 2012/10/01/ 2012.
- [256] C. F. de Lannoy, D. Jassby, D. D. Davis, and M. R. Wiesner, "A highly electrically conductive polymer–multiwalled carbon nanotube nanocomposite

- membrane," *Journal of Membrane Science*, vol. 415-416, pp. 718-724, 2012/10/01/ 2012.
- [257] P. Daraei, S. Madaeni, N. Ghaemi, H. Monfared, and M. A. Khadivi, "Fabrication of PES nanofiltration membrane by simultaneous use of multi-walled carbon nanotube and surface graft polymerization method: Comparison of MWCNT and PAA modified MWCNT," *Separation and Purification Technology*, vol. 104, pp. 32-44, 11/24 2013.
- [258] P. Daraei, S. Madaeni, N. Ghaemi, M. A. Khadivi, B. Astinchap, and R. Moradian, "Enhancing antifouling capability of PES membrane via mixing with various types of polymer modified multi-walled carbon nanotube," *Journal of Membrane Science*, vol. 444, pp. 184-191, 05/21 2013.
- [259] C.-F. De Lannoy, E. Soyer, and M. Wiesner, "Optimizing carbon nanotube-reinforced polysulfone ultrafiltration membranes through carboxylic acid functionalization," *Journal of Membrane Science*, vol. 447, pp. 395-402, 11/01 2013.
- [260] J. Yin, G. Zhu, and B. Deng, "Multi-walled carbon nanotubes (MWNTS)/polysulfone (PSU) mixed matrix hollow fiber membranes for enhanced water treatment," *Journal of Membrane Science*, vol. 437, pp. 237–248, 06/01 2013.
- [261] N. Phao, E. Nxumalo, B. Mamba, and S. Mhlanga, "A nitrogen-doped carbon nanotube enhanced polyethersulfone membrane system for water treatment," *Physics and Chemistry of the Earth, Parts A/B/C*, vol. 66, pp. 148–156, 12/31 2013.

- [262] E.-S. Kim, Y. Liu, and M. El-Din, "An in-situ integrated system of carbon nanotubes nanocomposite membrane for oil sands process-affected water treatment," *Journal of Membrane Science*, vol. 429, pp. 418-427, 02/01 2013.
- [263] A. Zirehpour, A. Rahimpour, M. Jahanshahi, and M. Peyravi, "Mixed matrix membrane application for olive oil wastewater treatment: Process optimization based on Taguchi design method," *Journal of Environmental Management*, vol. 132, pp. 113-120, 2014/01/01/ 2014.
- [264] R. Saranya, G. Arthanareeswaran, and D. Dionysiou, "Treatment of paper mill effluent using Polyethersulfone/functionalised multiwalled carbon nanotubes based nanocomposite membranes," *Chemical Engineering Journal*, vol. 236, pp. 369-377, 01/15 2014.
- [265] B. M. Ganesh, A. M. Isloor, and A. F. Ismail, "Enhanced hydrophilicity and salt rejection study of graphene oxide-polysulfone mixed matrix membrane," *Desalination*, vol. 313, pp. 199-207, 2013/03/15/ 2013.
- [266] H. Zhao, L. Wu, Z. Zhou, L. Zhang, and H. Chen, "Improving the antifouling property of polysulfone ultrafiltration membrane by incorporation of isocyanate-treated graphene oxide," *Physical Chemistry Chemical Physics*, 10.1039/C3CP50955A vol. 15, no. 23, pp. 9084-9092, 2013.
- [267] C. Crock, A. Rogensues, W. Shan, and V. Tarabara, "Polymer nanocomposites with graphene-based hierarchical fillers as materials for multifunctional water treatment membranes," *Water research*, vol. 47, 03/29 2013.
- [268] Z. Fan, Z. Wang, N. Sun, J. Wang, and S. Wang, "Performance improvement of polysulfone ultrafiltration membrane by blending with polyaniline nanofibers," *Journal of Membrane Science*, vol. 320, pp. 363-371, 07/01 2008.

- [269] M. Sankır, S. Bozkır, and B. Aran, "Preparation and performance analysis of novel nanocomposite copolymer membranes for Cr(VI) removal from aqueous solutions," *Desalination*, vol. 251, no. 1, pp. 131-136, 2010/02/01/ 2010.
- [270] S. Zhao *et al.*, "Comparison study of the effect of PVP and PANI nanofibers additives on membrane formation mechanism, structure and performance," *Journal of Membrane Science*, vol. 385-386, pp. 110-122, 2011/12/01/ 2011.
- [271] S. Zhao, Z. Wang, J. Wang, S. Yang, and S. Wang, "PSf/PANI nanocomposite membrane prepared by in situ blending of PSf and PANI/NMP," *Journal of Membrane Science*, vol. 376, no. 1, pp. 83-95, 2011/07/01/ 2011.
- [272] S. B. Teli, S. Molina, E. G. Calvo, A. E. Lozano, and J. de Abajo, "Preparation, characterization and antifouling property of polyethersulfone–PANI/PMA ultrafiltration membranes," *Desalination*, vol. 299, pp. 113-122, 2012/08/01/ 2012.
- [273] S. Zhao *et al.*, "Performance Improvement of Polysulfone Ultrafiltration Membrane Using Well-Dispersed Polyaniline–Poly(vinylpyrrolidone) Nanocomposite as the Additive," *Industrial & Engineering Chemistry Research*, vol. 51, no. 12, pp. 4661-4672, 2012/03/28 2012.
- [274] Y. Liao, X. Wang, W. Qian, Y. Li, X. Li, and D.-G. Yu, "Bulk synthesis, optimization, and characterization of highly dispersible polypyrrole nanoparticles toward protein separation using nanocomposite membranes," *Journal of Colloid and Interface Science*, vol. 386, no. 1, pp. 148-157, 2012/11/15/ 2012.
- [275] C. H. Worthley, K. T. Constantopoulos, M. Ginic-Markovic, E. Markovic, and S. Clarke, "A study into the effect of POSS nanoparticles on cellulose acetate

- membranes," *Journal of Membrane Science*, vol. 431, pp. 62-71, 2013/03/15/ 2013.
- [276] R. Gohari, W. J. Lau, T. Matsuura, and A. Ismail, "Fabrication and characterization of novel PES/Fe–Mn binary oxide UF mixed matrix membrane for adsorptive removal of As(III) from contaminated water solution," *Separation and Purification Technology*, vol. 118, pp. 64-72, 10/01 2013.
- [277] a. K. R. Ravi P. Pandey, a Vinod E. Madhavan, a Brahim A ïssa, a Yury Gogotsi b and Khaled A. Mahmoud \*ac, "Ultra-high-flux and fouling-resistant membranes based on layered silver/MXene (Ti<sub>3</sub>C<sub>2</sub>T<sub>x</sub>) nanosheets†," *Royal society of chemistry* 2018.
- [278] X. Wu, L. Hao, J. Zhang, X. Zhang, J. Wang, and J. Liu, "Polymer-Ti<sub>3</sub>C<sub>2</sub>T<sub>x</sub> composite membranes to overcome the trade-off in solvent resistant nanofiltration for alcohol-based system," *Journal of Membrane Science*, vol. 515, pp. 175-188, 2016/10/01/ 2016.
- [279] R. P. Pandey, A. K. Thakur, and V. K. Shahi, "Stable and efficient composite anion-exchange membranes based on silica modified poly(ethyleneimine)–poly(vinyl alcohol) for electrodialysis," *J. Membr. Sci.*, vol. 469, pp. 478-487, 2014/11/01/ 2014.
- [280] A. K. Singh, R. P. Pandey, A. Jasti, and V. K. Shahi, "Self-assembled silica nanocrystal-based anti-biofouling nanofilter membranes," *RSC Adv.*, 10.1039/C2RA21135A vol. 3, no. 2, pp. 458-467, 2013.
- [281] FEI. Quanta™ 650 FEG Discover the “any sample, all data” solution for ultimate versatility and high resolution SEM [Online]. Available: <http://emcfiles.missouri.edu/pdf/Quanta650FEG.pdf>



- [282] E. ZURich. Scanning Electron Microscopy (SEM) [Online]. Available: <https://www.microscopy.ethz.ch/sem.htm>
- [283] L. S. U. Barbara L Dutrow, Christine M. Clark, Eastern Michigan University, "X-ray Powder Diffraction (XRD)," ed.
- [284] B. D. CULLITY, *Elements of X-RAY DIFFRACTION SECOND EDITION*. Menlo Park, California London - Amsterdam - Don Mills, Ontario - Sydney: Addison-Wesley Publishing Company, Inc., 1978.
- [285] M. Rosillo-Lopez, "Preparation, Chemistry and Applications of Novel Carbon Nanomaterials," Doctor of Philosophy, University College London (UCL), 2018.
- [286] A. paar. Electrokinetic Analyzer: SurPASS [Online]. Available: <https://www.anton-paar.com/corp-en/products/details/electrokinetic-analyzer-for-solid-surface-analysis-surpasstm-3/>
- [287] micromeritics. (1996-2020). *Surface Area Instruments* Available: <https://www.micromeritics.com/product-showcase/Surface-Area.aspx>
- [288] S. Kertész, T. Freitas, and C. Hodúr, "Characterization of polymer membranes by contact angle goniometer," *Analecta Technica Szegedinensia*, vol. 8, pp. 18-22, 05/12 2014.
- [289] krUss. *DROP SHAPE ANALYZER – DSA25*. Available: [https://www.kruss-scientific.com/fileadmin/user\\_upload/website/brochures/kruss-bro-dsa25-en.pdf](https://www.kruss-scientific.com/fileadmin/user_upload/website/brochures/kruss-bro-dsa25-en.pdf)
- [290] parksystems, "How AFM Works," 2020.
- [291] N.-G. GmbH. *Thermal Characterization of Polymers*. Available: [https://d2brmtk65c6tyc.cloudfront.net/media/thermal-analysis/brochures/Thermal\\_Characterization\\_of\\_Polymers\\_en\\_web.pdf?1586](https://d2brmtk65c6tyc.cloudfront.net/media/thermal-analysis/brochures/Thermal_Characterization_of_Polymers_en_web.pdf?1586)

152194&Policy=eyJTdGF0ZW11bnQiOlt7IIJlc291cmNIIjoiaHR0cHM6XC9cL2QyYnJtdGs2NWM2dHIjLmNsb3VkZnJvbnQubmV0XC9tZWRpYVwvdGhlcm1hbC1hbmFseXNpc1wvYnJvY2h1cmVzXC9UaGVybWFsX0NoYXJhY3Rlcml6YXRpb25fb2ZfUG9seW1lcuNfZW5fd2ViLnBkZj8xNTg2MTUyMTk0IiwuQ29uZGI0aW9uIjp7IkRhZGVmZXNzVGhhbiI6eyJBV1M6RXBvY2hUaW1IjoXNTg4MzI2MTIzfx19XX0\_&Signature=R0oyIZLpSqhWLJ4EA8rjbPiahDQ81Sxlzkj-~e2a6UDuY02s8wwfRY5xR7TBopJZCAyTm~79NiS2MaZKQvCDlooBCw8PxXt28G3tea~gHtScpWKCih44KcKKIhQt6K5wnmpjKYFJzQ~HB0ZuyMlZhGpAYJa1RhLAKa-Eps661L8\_&Key-Pair-Id=APKAIBNUHYIJDHQEJVRQ

[292]

[293] E. T. Igunnu and G. Z. Chen, "Produced water treatment technologies," *International Journal of Low-Carbon Technologies*, vol. 9, no. 3, pp. 157-177, 2012.

[294] J. Su, J. Teo, and T.-S. Chung, "Cellulose acetate nanofiltration hollow fiber membranes for forward osmosis processes," *Journal of Membrane Science*, vol. 355, pp. 36-44, 06/15 2010.

[295] V. Vatanpour, A. Shockravi, H. Zarrabi, Z. Nikjavan, and A. Javadi, "Fabrication and characterization of anti-fouling and anti-bacterial Ag-loaded graphene oxide/polyethersulfone mixed matrix membrane," *Journal of Industrial and Engineering Chemistry*, vol. 30, pp. 342-352, 2015/10/25/ 2015.

[296] B. J. Halim, *Synthesis and transport properties of 2D transition metal carbides (MXenes)*. 2018.

- [297] Y. Cao *et al.*, "Enhanced thermal properties of poly(vinylidene fluoride) composites with ultrathin nanosheets of MXene," *RSC Advances*, 10.1039/C7RA00184C vol. 7, no. 33, pp. 20494-20501, 2017.
- [298] D. Wu *et al.*, "Delaminated Ti<sub>3</sub>C<sub>2</sub>T<sub>x</sub> (MXene) for electrochemical carbendazim sensing," *Materials Letters*, vol. 236, pp. 412-415, 2019/02/01/ 2019.
- [299] T. Zhang *et al.*, "Synthesis of two-dimensional Ti<sub>3</sub>C<sub>2</sub>T<sub>x</sub> MXene using HCl+LiF etchant: Enhanced exfoliation and delamination," *Journal of Alloys and Compounds*, vol. 695, pp. 818-826, 2017/02/25/ 2017.
- [300] R. Liu and W. Li, "High-Thermal-Stability and High-Thermal-Conductivity Ti<sub>3</sub>C<sub>2</sub>T<sub>x</sub> MXene/Poly(vinyl alcohol) (PVA) Composites," *ACS Omega*, vol. 3, no. 3, pp. 2609-2617, 2018/03/31 2018.
- [301] M. Mohiuddin, K. K. Sadasivuni, S. Mun, and J. Kim, "Flexible cellulose acetate/graphene blueprints for vibrotactile actuator," *RSC Advances*, 10.1039/C5RA03043A vol. 5, no. 43, pp. 34432-34438, 2015.
- [302] B. P. Tripathi and V. K. Shahi, "Organic–inorganic nanocomposite polymer electrolyte membranes for fuel cell applications," *Progress in Polymer Science*, vol. 36, no. 7, pp. 945-979, 2011/07/01/ 2011.
- [303] R. P. Pandey, P. A. Rasheed, T. Gomez, R. S. Azam, and K. A. Mahmoud, "A fouling-resistant mixed-matrix nanofiltration membrane based on covalently cross-linked Ti<sub>3</sub>C<sub>2</sub>T<sub>x</sub> (MXene)/cellulose acetate," *Journal of Membrane Science*, vol. 607, p. 118139, 2020/07/15/ 2020.
- [304] b. Xiaojing Changa, 1, Zhenxing Wanga,1, Shuai Quana,1, Yanchao Xua,1, Zaixing Jianga,1, Lu Shaoa,\*,1, " Exploring the synergetic effects of graphene oxide (GO) and polyvinylpyrrolidone (PVP) on poly(vinylidene fluoride) (PVDF) ultrafiltration membrane performance," *Applied Surface Science*, 2014.

- [305] J. Wang, P. Chen, B. Shi, W. Guo, M. Jaroniec, and S.-Z. Qiao, "A Regularly Channeled Lamellar Membrane for Unparalleled Water and Organics Permeation," *Angewandte Chemie International Edition*, vol. 57, no. 23, pp. 6814-6818, 2018/06/04 2018.
- [306] J. Li, X. Li, and B. Van der Bruggen, "An MXene-based membrane for molecular separation," *Environmental Science: Nano*, 10.1039/C9EN01478K vol. 7, no. 5, pp. 1289-1304, 2020.
- [307] K. Chen, C. Xiao, Q. Huang, H. Liu, and Y. Tang, "Fabrication and properties of graphene oxide-embedded cellulose triacetate RO composite membrane via melting method," *Desalination*, vol. 425, pp. 175-184, 2018/01/01/ 2018.
- [308] S. Neelapala, A. Nair, and J. PonnannEttiappan, "Synthesis and characterisation of TiO<sub>2</sub> nanofibre/cellulose acetate nanocomposite ultrafiltration membrane," *Journal of Experimental Nanoscience*, vol. 12, pp. 1-14, 02/06 2017.
- [309] Z. Shen *et al.*, "Fabrication of a Novel Antifouling Polysulfone Membrane with in Situ Embedment of Mxene Nanosheets," *International Journal of Environmental Research and Public Health*, vol. 16, p. 4659, 11/22 2019.
- [310] S. Chatterjee and S. De, "Adsorptive removal of arsenic from groundwater using a novel high flux polyacrylonitrile (PAN)–laterite mixed matrix ultrafiltration membrane," *Environmental Science: Water Research & Technology*, 10.1039/C4EW00075G vol. 1, no. 2, pp. 227-243, 2015.
- [311] I. Corp. (2007-2020). *Applications of the nGauge AFM*. Available: <https://www.icspicorp.com/applications>
- [312] J. H. Alberto Figoli, Sacide Alsoy Altinkaya, Jochen Bundschuh, "Application of Nanotechnology in Membranes for Water Treatment," CRC Press, 2020.

- [313] X. Wang *et al.*, "Preparation, characterisation, and desalination performance study of cellulose acetate membranes with MIL-53(Fe) additive," *Journal of Membrane Science*, vol. 590, p. 117057, 2019/11/15/ 2019.
- [314] M. A. Kamal, S. Bibi, S. W. Bokhari, A. H. Siddique, and T. Yasin, "Synthesis and adsorptive characteristics of novel chitosan/graphene oxide nanocomposite for dye uptake," *Reactive and Functional Polymers*, vol. 110, pp. 21-29, 2017/01/01/ 2017.
- [315] P. W. COMPANY, "dead-end filtration."
- [316] Z. F. Cui, Y. Jiang, and R. W. Field, "Chapter 1 - Fundamentals of Pressure-Driven Membrane Separation Processes," in *Membrane Technology*, Z. F. Cui and H. S. Muralidhara, Eds. Oxford: Butterworth-Heinemann, 2010, pp. 1-18.
- [317] S. Filtration, "Cross Flow Membrane Operations " 2020.
- [318] Z. Xie, N. Li, Q. Wang, and B. Bolto, "6 - Desalination by pervaporation," in *Emerging Technologies for Sustainable Desalination Handbook*, V. G. Gude, Ed.: Butterworth-Heinemann, 2018, pp. 205-226.
- [319] E. Mahmoudi, L. Y. Ng, W. L. Ang, Y. T. Chung, R. Rohani, and A. Mohammad, "Enhancing Morphology and Separation Performance of Polyamide 6,6 Membranes By Minimal Incorporation of Silver Decorated Graphene Oxide Nanoparticles," *Scientific Reports*, vol. 9, 12/01 2019.
- [320] M. Kumar, D. McGlade, M. Ulbricht, and J. Lawler, "Quaternized polysulfone and graphene oxide nanosheet derived low fouling novel positively charged hybrid ultrafiltration membranes for protein separation," *RSC Advances*, 10.1039/C5RA06893B vol. 5, no. 63, pp. 51208-51219, 2015.

- [321] A. Kayvani Fard *et al.*, "Inorganic Membranes: Preparation and Application for Water Treatment and Desalination," (in eng), *Materials (Basel, Switzerland)*, vol. 11, no. 1, p. 74, 2018.
- [322] Z. He, K. S. Kumar Reddy, G. Karanikolos, and K. Wang, "Chapter 5 - CO<sub>2</sub>/CH<sub>4</sub> Separation (Natural Gas Purification) by Using Mixed Matrix Membranes," in *Current Trends and Future Developments on (Bio-) Membranes*, A. Basile and E. P. Favvas, Eds.: Elsevier, 2018, pp. 155-181.

## APPENDIXES


### Appendix A: Poster Awards and Presentation

A poster was presented at The Annual Research Forum & Exhibition 2019, arranged by Qatar University. A contribution was made from this thesis work by This poster contribution, which came from the work of this thesis, won first place among all the graduate studies posters.



A. A snapshot of the poster award is shown below.



B. A snapshot of the poster is presented below.



## Enhancing the fouling resistance and flux of CAM/Xene ( $Ti_3C_2Tx$ ) nanocomposite membrane

Presented by: Reem Azam, Radwan Alfahel and Mhd Ammar Hafiz.  
Supervised by: Dr.Khaled A.Mahmoud, Dr.Mohamed Hassan and Dr.Alaa AlHawari

Graduate Student  
Energy, Environment & Resource  
Sustainability

---

### Introduction

Limited water resources motivate researches to focus on efficient water purification technologies such as nano filtration technologies. However, the major obstacles in membrane based separation process is the membrane fouling, which is responsible for continuous flux reduction [1]. It is desired to synthesis a membrane that is able to enhance the fouling properties of the material while maintaining a good flux and rejection. This can be achieved by using cellulose acetate membrane that is environmentally attractive polymer with regards to its cheap price and to its good resistance to chlorine [2]. Loading MXene into cellulose acetate membrane is necessary to improve the antifouling properties of the membrane, as it has been investigated as a membrane material for water purification applications: [3],[4].

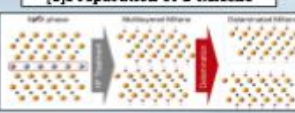

### Objectives

- To enhance the anti-fouling properties of the composite membrane.
- Maintain a high flux and rejection for the composite membrane.
- Evaluate MXene/CA membrane performance through FO.

---


### Preparation and Membrane Synthesis Method

#### [1] Preparation of d-MXene


Ti<sub>3</sub>AlC<sub>2</sub> MAX phase

HF etching



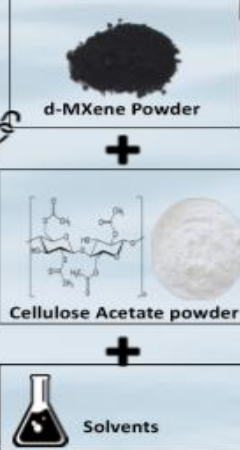
M-Ti<sub>3</sub>AlC<sub>2</sub>

Sonication



d-Ti<sub>3</sub>AlC<sub>2</sub>

#### [2] Preparation CAM-M% solution



d-MXene Powder

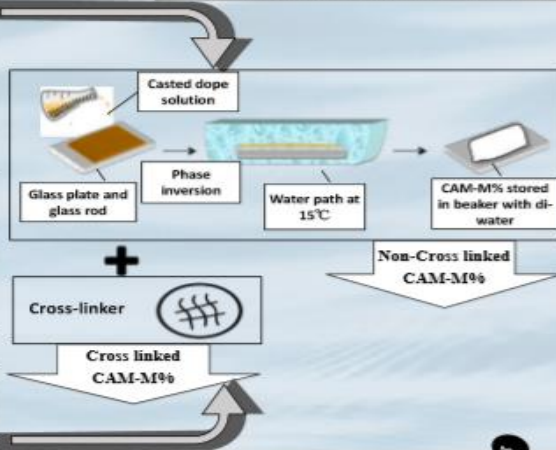
+

Cellulose Acetate powder

+

Solvents

#### [3] Casting of CAM-M% membrane by Phase inversion Method then chemical cross-linking



Casted dope solution

Phase inversion

Glass plate and glass rod

Water path at 15°C

CAM-M% stored in beaker with di-water

Non-Cross linked CAM-M%

+


Cross-linker

Cross linked CAM-M%

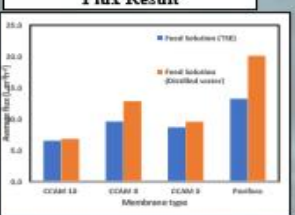
---

### Performance

#### Forward osmosis Setup



#### Flux Result




Membrane type	Average Flux (L/m <sup>2</sup> h)
CCAM 10	~1.5
CCAM 8	~2.5
CCAM 5	~1.8
Porifera	~1.2

### Forward osmosis


#### SEM results

##### Before TSE Experiment




CCAM-10%

##### Porifera




##### After TSE Experiment



CCAM-10%

##### Porifera



### Future work

- Evaluate the MXene/Cellulose acetate membranes under different pressure.
- To scale up the CCA-M% membrane
- Evaluate the performance of the membrane through cross-flow filtration set up.

---

### Conclusion

- CCAM-8% FO membrane has resulted in higher resistance to fouling compared to the commercial membranes.
- CCAM-8% FO membrane has resulted in highest average membrane flux of 13 Lm<sup>-2</sup> h<sup>-1</sup>.

---

### References

[1] Fang L.L, Chunhui Deng, L. \*, DaIV, C., Be Yang, L., & Qing Tian, I. (2015, July). Fouling mechanism and cleanability of ultrafiltration membranes modified with polydopamine-graft-PEG. *article south africa*.

[2] Trademark of The Dow Chemical Company. (n.d.). Retrieved from [http://materialsearch.dow.com/PublishedLiteratureDOW/CCAM\\_dh\\_0042.0901b00300\\_002196.pdf?filepath=liquidscape/pdfs/noreg\\_009](http://materialsearch.dow.com/PublishedLiteratureDOW/CCAM_dh_0042.0901b00300_002196.pdf?filepath=liquidscape/pdfs/noreg_009)

[3] Shuangjie Sun, C. L. (2017). Two-dimensional MXenes for energy storage. *Chemical Engineering Journal*.

[4] Khashif Raseed, T. M. (2016). Antibacterial Activity of Ti3C2Tx MXene. *ACS Nano*.



## Appendix B: Research Outcomes (Publications)

R.P. Pandey, P.A. Rasheed, T. Gomez, R.S. Azam, K.A. Mahmoud, A fouling-resistant mixed-matrix nanofiltration membrane based on covalently cross-linked Ti<sub>3</sub>C<sub>2</sub>T<sub>x</sub> (MXene)/cellulose acetate, *Journal of Membrane Science*, (2020) 118139.



A. A snapshot of the first page of the first published paper is shown below.

Journal of Membrane Science 607 (2020) 118139

Contents lists available at ScienceDirect

**Journal of Membrane Science**

journal homepage: <http://www.elsevier.com/locate/memsci>



**A fouling-resistant mixed-matrix nanofiltration membrane based on covalently cross-linked Ti<sub>3</sub>C<sub>2</sub>T<sub>x</sub> (MXene)/cellulose acetate**

Ravi P. Pandey<sup>a</sup>, P. Abdul Rasheed<sup>a</sup>, Tricia Gomez<sup>a</sup>, Reem S. Azam<sup>a,b</sup>, Khaled A. Mahmoud<sup>a,\*</sup>

<sup>a</sup> Qatar Environment and Energy Research Institute (QEERI), Hamad Bin Khalifa University (HBKU), P.O. Box 34110, Doha, Qatar  
<sup>b</sup> Materials Science and Technology Program, College of Arts and Sciences, Qatar University, Doha, 2713, Qatar

---

**ARTICLE INFO**

**Keywords:**  
Ti<sub>3</sub>C<sub>2</sub>T<sub>x</sub> MXene  
Cellulose acetate  
Mixed-matrix  
Nanofiltration membrane  
Antifouling

**ABSTRACT**

A new fouling-resistant mixed-matrix nanofiltration membrane based on a covalently cross-linked Ti<sub>3</sub>C<sub>2</sub>T<sub>x</sub> (MXene)/cellulose acetate (MXene@CA) composite was fabricated by phase inversion followed by formaldehyde cross-linking. The physicochemical properties of the prepared MXene@CA composite membranes were studied by field emission scanning electron microscopy (FESEM), energy dispersive spectroscopy (EDS), X-ray diffraction (XRD), and water contact angle techniques. The performance of the prepared membranes was evaluated with respect to the water flux, bacterial growth inhibition, and rejection properties. The 10%MXene@CA (10:90 wt % of MXene:CA) composite membrane shows high pure water flux of ~256.85 L m<sup>-2</sup> h<sup>-1</sup> bar<sup>-1</sup>, 123.28% water uptake, and 69.7% porosity. The 10%MXene@CA membrane, exhibited more than 92% and 98% rejection of rhodamine B (RhB) and methyl green (MG), respectively. Furthermore, 10%MXene@CA membrane exhibited more than 98% and 96% growth inhibition for *E. coli* and *B. subtilis*, respectively. Also, the optimal membrane showed a significantly improved hydrophilicity (water contact angle = 60.8°), which has favored good antifouling properties. The reported nanofiltration membrane, especially 10%MXene@CA, can be suggested for water purification and biomedical applications.

---

**1. Introduction**

Nowadays, nanofiltration (NF) has become one of the cutting-edge pressure-driven membrane separation techniques used for water softening, wastewater treatment, chemical, and pharmaceutical industries, etc. [1–4]. NF has been efficiently used in the selective rejection of multivalent ions and charged organic molecules due to their unique separation mechanisms such as steric hindrance and Donnan exclusion [3,5,6]. High selectivity, (chemical and mechanical) stability, and fouling resistance are crucial criteria for developing functional NF membranes [1,7–11]. To minimize fouling and improve the properties of NF membranes various strategies have been proposed such as modification with highly hydrophilic polymers [12–14], and incorporation of nanomaterials [15,16]. Among these strategies, incorporation of hydrophilic nanomaterials into polymeric membranes leads to tremendous enhancement of the membrane stability, hydrophilicity and antifouling properties [17–20]. However, mixed-matrix hybrid membranes prepared by physical blending can agglomerate or leach out, thus possible loss to homogeneity, which might decrease the membrane separation performance [21].

Among other hydrophilic polymers being used to fabricate NF membranes [22–25], cellulose acetate (CA) was considered as a promising alternative because of their good water affinity, biodegradability, excellent film-forming capability, high toughness, hydrophilic, excellent biocompatibility, easy chemical modification, and relatively low cost [26–28]. However, CA membranes are highly susceptible to fouling by biological and organic contaminants leads to deterioration in its overall separation performances [29,30]. These challenges encouraged researchers to improve the antifouling properties of CA membranes by the incorporation of nanomaterials, especially 2D nanosheets, to achieve improved separation performances [29–32].

Recently, the 2D MXenes have attracted extensive attention for diverse applications including water treatment membranes, due to their excellent flexibility, mechanical stability, chemical tunability, hydrophilic surfaces, and most significantly their nanometer thin 2D structure with excellent antibacterial activity [33–38]. Particularly, Ti<sub>3</sub>C<sub>2</sub>T<sub>x</sub> has been the most explored MXene for various applications such as efficient removal of ions, heavy metals, dyes, and radionuclides [39–41]. Ti<sub>3</sub>C<sub>2</sub>T<sub>x</sub> is typically prepared by selective etching of the Al layer from MAX (Ti<sub>3</sub>AlC<sub>2</sub>) through either direct HF etching or *in situ* HCl/LiF acid

---

\* Corresponding author.  
E-mail address: [kmahmood@hbku.edu.qa](mailto:kmahmood@hbku.edu.qa) (K.A. Mahmoud).

<https://doi.org/10.1016/j.memsci.2020.118139>  
Received 9 March 2020; Accepted 2 April 2020  
Available online 16 April 2020  
0376-7388/© 2020 The Author(s). Published by Elsevier B.V. This is an open access article under the CC BY license (<http://creativecommons.org/licenses/by/4.0/>).

R. Alfahel, R.S. Azzam, M. Hafiz, A.H. Hawari, R.P. Pandey, K.A. Mahmoud, M.K. Hassan, A.A. Elzatahry, Fabrication of fouling resistant Ti<sub>3</sub>C<sub>2</sub>T<sub>x</sub> (MXene)/cellulose acetate nanocomposite membrane for forward osmosis application, Journal of Water Process Engineering, 38 (2020) 10155.

B. A snapshot of the first page of the second published paper is shown below.

Journal of Water Process Engineering 38 (2020) 101551

Contents lists available at ScienceDirect

**Journal of Water Process Engineering**

journal homepage: [www.elsevier.com/locate/jwpe](http://www.elsevier.com/locate/jwpe)



**Fabrication of fouling resistant Ti<sub>3</sub>C<sub>2</sub>T<sub>x</sub> (MXene)/cellulose acetate nanocomposite membrane for forward osmosis application**

Radwan Alfahel<sup>a</sup>, Reem S. Azzam<sup>b,c</sup>, MhdAmmar Hafiz<sup>a</sup>, Alaa H. Hawari<sup>a,\*</sup>, Ravi P. Pandey<sup>c</sup>, Khaled A. Mahmoud<sup>c,\*\*</sup>, Mohammad K. Hassan<sup>d</sup>, Ahmed A. Elzatahry<sup>b</sup>

<sup>a</sup> Department of Civil and Architectural Engineering, Qatar University, P.O. Box 2713, Doha, Qatar  
<sup>b</sup> Materials Science and Technology Program, College of Arts and Sciences, Qatar University, Doha, 2713, Qatar  
<sup>c</sup> Qatar Environment and Energy Research Institute (QEERI), Hamad Bin Khalifa University (HBKU), Qatar Foundation, P.O. Box 34110, Doha, Qatar  
<sup>d</sup> Center for Advanced Materials, Qatar University P.O. Box 2713, Doha, Qatar

---

**ARTICLE INFO**

**Keywords:**  
Forward Osmosis  
MXene  
Thin-film nanocomposite  
Cellulose acetate  
Fouling

**ABSTRACT**

In this study, Ti<sub>3</sub>C<sub>2</sub>T<sub>x</sub> (MXene) was used to enhance the fouling resistance of FO flat-film membranes. Mixed-matrix Ti<sub>3</sub>C<sub>2</sub>T<sub>x</sub> (MXene)/ cellulose acetate (CA) membranes with different (wt%) loading of MXene were fabricated by covalent crosslinking followed by phase inversion protocol. The fabricated membranes were characterized by scanning electron microscopy (SEM), energy-dispersive X-ray spectroscopy (EDS), X-ray powder diffraction (XRD) and contact angle measurement. The performance of the fabricated FO membranes was evaluated using seawater as draw solution (DS) and two feed solutions (FS) namely; distilled water (DW) and treated sewage effluent (TSE). The water flux, reverse solute flux and the rejection of dissolved solids were evaluated in the FO process. It was found that the cross-linked cellulose acetate membrane with 8 wt% MXene (CCAM-8%) showed higher resistance to fouling when compared with commercial thin-film composite (TFC) FO membrane, the water flux of CCAM-8% decreased by only 10.7% using TSE as FS compared to DW, where the water flux of the TFC commercial membrane decreased by 32.2% when using TSE as FS compared to DW.

---

**1. Introduction**

Forward Osmosis (FO) is a membrane-based separation process that utilizes the osmotic pressure gradient between a feed solution (FS) and a draw solution (DS) as the driving force instead of the hydraulic pressure [1]. Therefore, the operating cost of FO is lower than other membrane separation processes. The FO process has attracted significant attention in recent years due to the low energy consumption, low membrane fouling and high water flux [2–4]. Although FO has shown lower membrane fouling when compared to other membrane separation technologies, resistance to fouling is yet to be improved. Extensive development of FO membranes have been made during the last decade. Li et al. developed polyethylene terephthalate mesh (PET) enhanced cellulose acetate (CA) FO membranes via a phase inversion process [5]. The optimal FO membrane displayed a water flux of 4.74 L/m<sup>2</sup>/h and salt rejection of 96.03% using 0.2 mol/L NaCl as the FS and 1.5 mol/L glucose as the DS in a pressure retarded osmosis (PRO) mode. It was found that the PET modified CA membrane was able to reduce the effect of the internal concentration polarization (ICP) phenomenon. Ohland et al. developed a new FO membrane using hydroxyapatite particles (Hapf) functionalized by plasma treatment added to CA substrate and a selective polyimide layer of nanocomposite membrane [6]. The addition of hydroxyapatite particles (Hapf) to the CA-substrate has enhanced the FO water flux from 13.8 to 18.0 L/m<sup>2</sup>/h. This was due to lower diffusion resistance and higher hydrophilicity of the modified membrane. Shakeri et al. enhanced the performance of thin-film nanocomposite (TFN) FO membranes by incorporating super hydrophilic modified silica nanoparticles [7]. The TFN membrane with 0.2 wt% nanoparticles showed higher water flux of 31 L/m<sup>2</sup>/h compared to 18 L/m<sup>2</sup>/h using TFC membrane with no nanoparticles. Wang et al. studied the performance of CA membranes with MIL-53(Fe) additive in FO process [8]. MIL-53 (Fe) was used to improve the selectivity and permeability performance of FO membranes. Using distilled water (DW) as FS and 1 M NaCl as DS, the modified membrane showed higher water flux of 34.0 L/m<sup>2</sup>/h

---

\* Corresponding author at: Department of Civil and Architectural Engineering, College of Engineering, Qatar University, 2713 Doha, Qatar.  
\*\* Corresponding author at: Qatar Environment and Energy Research Institute (QEERI), Hamad Bin Khalifa University (HBKU), Qatar Foundation, 34110, Doha, Qatar.  
E-mail addresses: [a.hawari@qu.edu.qa](mailto:a.hawari@qu.edu.qa) (A.H. Hawari), [kmahmoud@hbku.edu.qa](mailto:kmahmoud@hbku.edu.qa) (K.A. Mahmoud).

<https://doi.org/10.1016/j.jwpe.2020.101551>  
Received 29 March 2020; Received in revised form 16 July 2020; Accepted 19 July 2020  
Available online 27 July 2020  
2214-7144/© 2020 Elsevier Ltd. All rights reserved.